UNIVERSITY OF NAPLES "FEDERICO II"

PhD in Computational Biology and Bioinformatics

XXVI CYCLE

COMPUTATIONAL STRATEGIES TO INVESTIGATE TRANSCRIPTIONAL EFFECTS OF THE UPREGULATION OF GENES MAPPING TO CHROMOSOME 21

Coordinator:

Prof. Sergio Cocozza

PhD student:

Ferdinando Bonfiglio

Tutor:

Prof. Lucio Nitsch

Co-tutor:

Prof. Diego Di Bernardo

ACADEMIC YEAR 2012/2013

TABLE OF CONTENTS

LIST OF PUBLICATIONS

1) Piccoli C, Izzo A, Scrima R, **Bonfiglio F**, Manco R, Negri R, Quarato G, Cela O, Ripoli M, Prisco M, Gentile F, Calì G, Pinton P, Conti A, Nitsch L, Capitanio N. Chronic pro-oxidative state and mitochondrial dysfunctions are more pronounced in fibroblasts from Down syndrome foeti with congenital heart defects. (2013) *Hum. Mol. Genet*. Mar 15;22(6):1218-32.

2) Izzo A*, Manco R*, **Bonfiglio F***, Calì G, de Cristofaro T, Patergnani S, Cicatiello R, Scrima R, Pinton P, Conti A, Nitsch L. NRIP1/RIP140 siRNA-mediated attenuation counteracts mitochondrial dysfunction in Down syndrome. (2014) *Hum. Mol. Genet*. Accepted in print.

*Co-first Authors.

ABSTRACT

Down Syndrome (DS) is the most frequent autosomal aneuploidy compatible with post-natal life. Few meta-analyses of DS gene expression data have been conducted to date even though comprehensive comparative studies would be pivotal to understand genetic hallmarks of DS and molecular mechanisms responsible for DS phenotypes.

For this reason, aim of this study was to provide new insights into the transcriptional changes influencing the molecular mechanisms associated with DS using computational strategies. We first performed a comprehensive computational analysis of expression feature-level extraction output (FLEO) files from transcriptome studies on different tissues from human DS subjects, with Affymetrix microarray technology. The non-biological experimental variation was adjusted with a recently developed algorithm, called ComBat. Comparative analysis of 44 DS samples versus 40 controls from 9 experiments identified 178 genes consistently dysregulated in DS. Functional class scoring of these genes revealed that Gene Ontology categories related to cellular morphogenesis, development, defects in synapsis and apoptosis were enriched among dysregulated genes. Hsa21 genes were globally upregulated and the pathway of *PGC-1α*, a key regulator of mitochondrial biogenesis, was altered.

A second computational strategy was applied to identify Hsa21 genes likely responsible for 2 specific traits of DS, highlighted by a previous experiment of expression profiling performed on heart tissues from DS subjects, i.e. the downregulation of nuclear encoded mitochondrial genes (NEMGs), and the upregulation of genes encoding extracellular matrix (ECM) proteins. We speculated that most of the under-expressed NEMGs might be under the same regulatory control, as well as the overexpressed ECM genes and that these controls might be affected by the trisomy of Hsa21.

Therefore, to investigate whether the overexpression of individual Hsa21 genes might alter either NEMG or ECM gene expression, we analyzed expression data, retrieved from public repositories. With this strategy we identified *NRIP1*, a repressor of *PGC-1α* activity, as a good candidate gene for NEMG downregulation, and *RUNX1* for the upregulation of ECM genes. These predictions agree with the result of our comprehensive meta-analysis and are supported by literature and by the analysis of the promoter regions of the NEMGs and ECM genes dysregulated in DS.

Finally, we successfully validated the predicted *NRIP1* repressive role on both NEMG regulation and mitochondrial function, by modulating its expression in human fibroblasts from DS fetuses.

1. BACKGROUND

1.1. Down syndrome (DS)

Down Syndrome (DS) is the most frequent autosomal aneuploidy that is compatible with post-natal life. It results from complete or partial trisomy of chromosome 21 (Hsa21) and is characterized by a complex phenotype in which over 80 features occur with various degrees of expression and frequency [Epstein et al. 1991]. Constant features in trisomic subjects are mental retardation, hypotonia, developmental delay, a partial immune deficiency, especially of thymus dependent system, and an increased risk of leukemia. DS is a major cause of congenital heart defects (CHD). It is associated mostly with endocardial cushion defects [Ferencz et al. 1989, Park et al. 1977], the most frequent being atrio-ventricular canal defects (AVCD) followed by ventricular septal defects (VSD) and tetralogy of Fallot [Park et al. 1977].

1.2. Gene expression in DS

It has been postulated that a triplicated Hsa21 causes an increase in the expression of trisomic genes as a primary dosage effect. This primary dysregulation produces, as secondary effect, the dysregulation of genes mapping on different chromosomes and consequently the DS phenotype (**Fig. 1**). In agreement with the above hypothesis, several studies have reported a generalized overexpression of triplicated genes at the mRNA level in mouse models of DS and human DS tissues [Amano et al, 2004; Lyle et al, 2004; Kahlem et al, 2004; Dauphinot et al, 2005]. Interestingly, these studies indicated that only a subset of Hsa21 genes is consistently over-expressed in comparison to euploid controls and that the increase in expression may slightly differ from the expected ~1.5-fold [FitzPatrick et al. 2002; Mao et al. 2005, Conti et al, 2007]. Also, the set of over-expressed Hsa21 genes differs across the trisomic cell types [Li et al. 2006]. These findings indicate that other factors (e.g. developmental stage, tissue-specific differences) also affect gene expression [Sommer and Henrique-Silva, 2008].

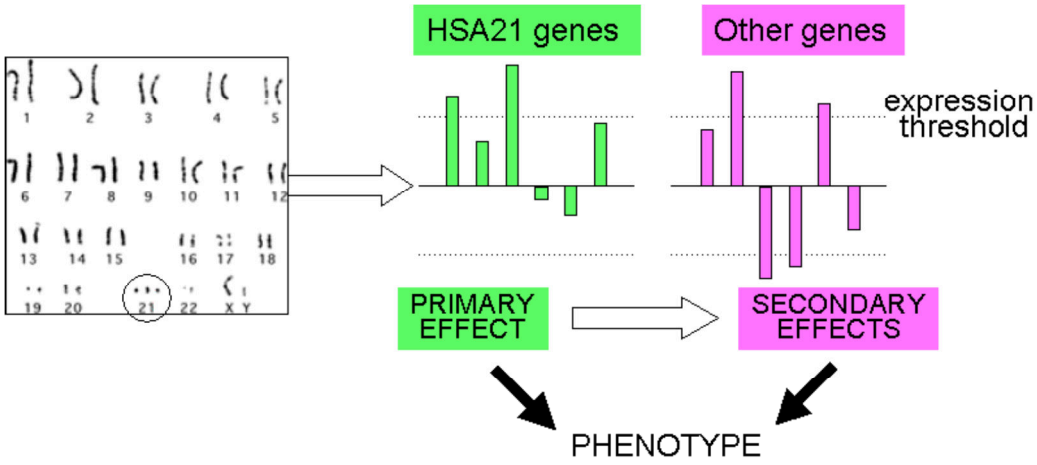

Figure 1. Primary and secondary effects of trisomy 21. Three copies of Hsa21 may cause a 50% increase in the expression of trisomic genes as primary dosage effect. The abnormal mRNA levels of Hsa21 genes may cause alteration of disomic gene expression as secondary effects. Both primary and secondary effects will finally result in developmental defects and phenotypic alterations.

Vilardell et al. (2011) performed a comprehensive meta-analysis from 45 different human and mouse DS studies at transcriptomic and proteomic levels including quantitative data such as Affymetrix microarrays, qRT-PCR and MALDI studies as well as qualitative data such as SAGE and Western blot analyses. By using a computed score and an entropy criterion, they identified 324 genes with consistent dosage effects in many of these studies. As expected, they observed a high fraction of Hsa21 genes (N = 77) but also a large amount of non-Hsa21 genes (N = 247). Besides well investigated genes in the context of DS, they also detected a significant proportion of novel ones (N = 62) mostly associated with neurodegenerative disorders including Alzheimer's disease and age-related degeneration. The 324 genes were further investigated using functional information, molecular interactions and promoter analysis revealing overrepresented motifs of four transcription factors: *RUNX1*, *E2F1*, *STAF*/*PAX2* and *STAT3*. Since the meta-analysis was enriched with brain experiments, a high fraction of genes related to neurodevelopment, synapsis and neurodegeneration (**Tab. 1**) was detected.

TABLE 1. ENRICHED NEUROPATHOLOGICAL PATHWAYS IN VILARDELL'S META-ANALYSIS WITH ADJ.P.VAL < 0.01

PATHWAY	Pathway size	Genes on HSA21	HSA21 Interactors	Others
HUNTINGTONS DISEASE (KEGG)	159	SOD1; DONSON	REST	BDNF; SOD2
ALZHEIMERS DISEASE (KEGG)	147	APP; BACE2; DONSON	PPP3CA; GSK3B	CAPN2
SIGNALLING BY NGF (REACTOME)	209	ITSN1; TIAM1	PIK3R1; GSK3B	RPS6KA2; RAP1A; KRAS
AXON GUIDANCE (REACTOME)	256	COL6A2	GSK3B;COL1A1; COL1A2; COL4A1; COL4A2	COL5A2; DPYSL3; RPS6KA2; LAMB1; COL3A1; COL5A1; ALCAM; KRAS
PARKINSONS DISEASE (KEGG)	105	DONSON		UBE2G2
P75(NTR)-MEDIATED SIGNALING (PID)	68	APP	PIK3R1	BDNF
NOTCH (NETPATH)	61	APP	PIK3R1; GSK3B	
NEUROTROPHIN SIGNALING PATHWAY (KEGG)	121		PIK3R1; GSK3B	BDNF; RPS6KA2; RAP1A; KRAS
NGF SIGNALLING VIA TRKA FROM THE PLASMA MEMBRANE (REACTOME)	127		PIK3R1; GSK3B	RPS6KA2; RAP1A; KRAS
MEMBRANE TRAFFICKING (REACTOME)	87		TJP1	GJA1; COPG
NEUROTROPHIC FACTOR-MEDIATED TRK RECEPTOR SIGNALING (PID)	60	TIAM1	PIK3R1	BDNF; RAP1A; KRAS
EPO SIGNALING (INOH)	180		PIK3R1; GSK3B	
CDC42 SIGNALING EVENTS (PID)	68	TIAM1	PIK3R1; GSK3B	EPS8; YES1
L1CAM INTERACTIONS (REACTOME)	93			LAMB1; ALCAM1; RPS6KA2

1.2.1. Gene expression profiling in DS heart tissue

A transcriptome study of DS fetal heart tissue was performed in our laboratory [Conti et al, 2007]. Gene expression profile of 15 fetal hearts (10 with DS versus 5 euploid controls) was determined by DNA microarray analysis using Affymetrix HG-U133A oligonucleotide arrays. The 22,283 probe sets represented on the Affymetrix chip corresponded to ~14,500 genes and 500 expressed sequence tags and clones.

Genes were considered differentially expressed with FC < -0.8 and FC > 0.8 with Adj.P.val < 0.05 after Benjamini and Hochberg correction for multiple comparisons. Approximately half of the genes examined (87 of the 168 genes on Hsa21) were expressed in the heart at 18-22 weeks of gestation. Hsa21 gene expression was globally upregulated 1.5 fold in trisomic samples. However, not all genes were equally dysregulated and 25 genes were not upregulated at all. Genes located on other chromosomes were also significantly dysregulated. Functional class scoring and gene set enrichment analyses (GSEA) of 473 genes, differentially expressed between trisomic and non-trisomic hearts, showed that the downregulation of nuclear encoded mitochondrial genes (NEMGs) and the upregulation of genes encoding extracellular matrix (ECM) proteins, appeared to be a hallmark of trisomy 21 (TS21) in fetal heart samples (**Fig. 2 and Tab. 2-3**).

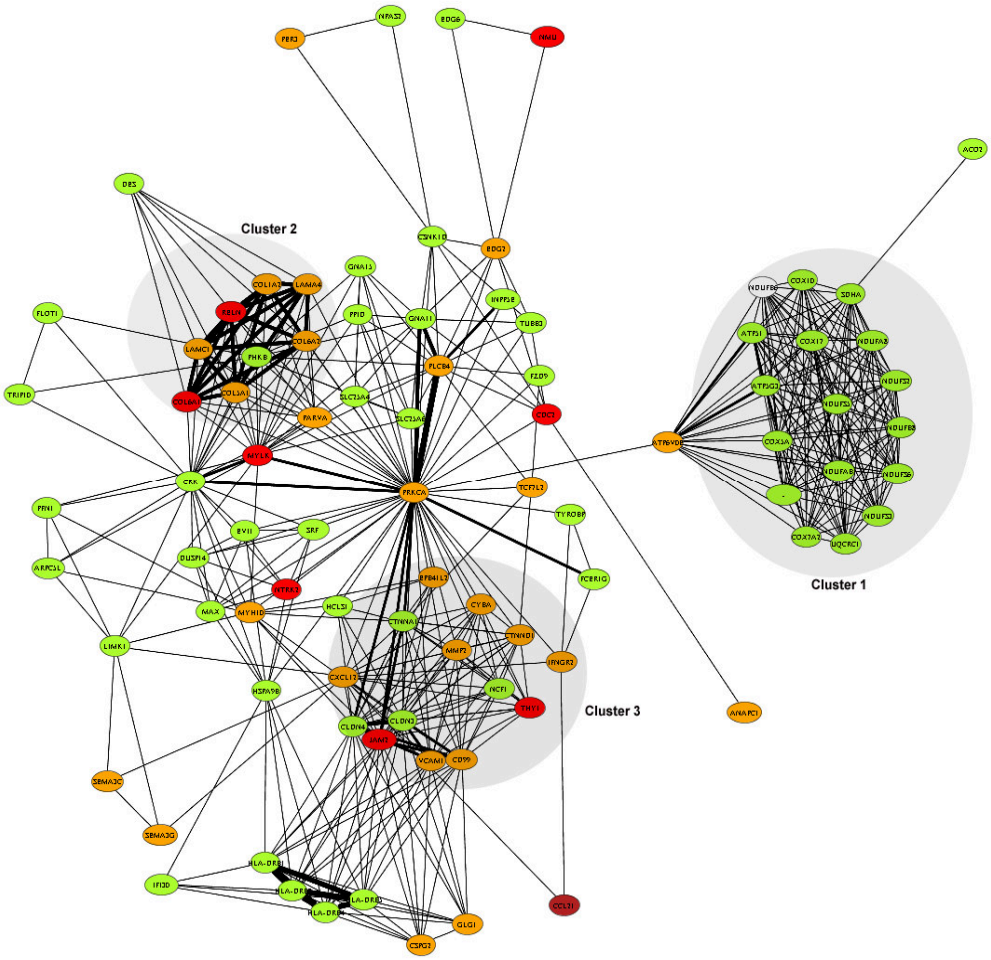

Figure 2. Genes and gene pathways affected by Hsa21 trisomy. Pathway analysis performed with Pathway Miner software (http://www.biorag.org/pathway.html) showed one cluster of downregulated genes, including 16 genes involved in oxidative phosphorylation pathway. Two clusters of upregulated genes included ECM genes: cluster 2 (Focal adhesion) and cluster 3 (Cell adhesion). Green indicates downregulated genes (darker green = more downregulated); red indicates upregulated genes (darker red = more upregulated).

TABLE 2. SIGNIFICANTLY DOWNREGULATED GENES IN DS FETAL HEARTS ENCODING NEMGs

Probe_ID	Gene_Name	FC (DSH/NH) ratio
214274_s_at	ACAA1	0,647
215210_s_at	ACADM	0,548
205412_at	ACAT1	0,756
208967_s_at	AK2	0,757
201322_at	ATP5B	0,739
208972_s_at	ATP5G1	0,739
211715_s_at	BDH1	0,554
205295_at	CKMT2	0,699
209746_s_at	COQ7	0,721
203858_s_at	COX10	0,74
218057_x_at	COX4NB	0,738
201597_at	COX7A2	0,764

201633_s_at	CYB5B	0,727
208905_at	CYCS	0,702
209759_s_at	DCI	0,729
211150_s_at	DLAT	0,568
204824_at	ENDOG	0,638
201931_at	ETFA	0,698
202942_at	ETFB	0,692
213133_s_at	GCSH	0,713
221415_s_at	GJA10	0,545
200947_s_at	GLUD1	0,758
208813_at	GOT1	0,671
203745_at	HCCS	0,678
200691_s_at	HSPA9B	0,645
210046_s_at	IDH2	0,743
202070_s_at	IDH3A	0,709
210418_s_at	IDH3B	0,751
200955_at	IMMT	0,704
36830_at	MIPEP	0,711
219527_at	MOSC2	0,701
218027_at	MRPL15	0,716
203781_at	MRPL33	0,741
218890_x_at	MRPL35	0,745
204331_s_at	MRPS12	0,735
220864_s_at	NDUFA13	0,638
202077_at	NDUFAB1	0,748
218201_at	NDUFB2	0,669
201226_at	NDUFB8	0,663
201966_at	NDUFS2	0,62
201740_at	NDUFS3	0,72
201757_at	NDUFS5	0,763
202941_at	NDUFV2	0,76
218455_at	NFS1	0,712
202780_at	OXCT1	0,705
200980_s_at	PDHA1	0,598
214225_at	PIN4	0,677
203649_s_at	PLA2G2A	0,657
205241_at	SCO2	0,724
201093_x_at	SDHA	0,591
202675_at	SDHB	0,744
202004_x_at	SDHC	0,722
203340_s_at	SLC25A12	0,688
217961_at	SLC25A38	0,705
202825_at	SLC25A4	0,607
216841_s_at	SOD2	0,734
218119_at	TIMM23	0,634
203092_at	TIMM44	0,612

220415_at	TNNI3K	0,635
209077_at	TXN2	0,74
201903_at	UQCRC1	0,75
200883_at	UQCRC2	0,716
208909_at	UQCRFS1	0,744
217140_s_at	VDAC1	0,637
217249_x_at	WUGSC:H_RG162B04.1	0,68

TABLE 3. SIGNIFICANTLY UPREGULATED GENES IN DS FETAL HEARTS ENCODING ECM PROTEINS.

Probe_ID	Gene_Name	FC (DSH/NH) ratio
222162_s_at	ADAMTS1	1,93
219935_at	ADAMTS5	1,5
220706_at	ADAMTS7	2,24
214953_s_at	APP	1,668
219087_at	ASPN	1,829
220988_s_at	C1QTNF3	1,466
219025_at	CD248	1,342
211809_x_at	COL13A1	1,721
203477_at	COL15A1	1,413
209081_s_at	COL18A1	1,57
202310_s_at	COL1A1	1,546
202403_s_at	COL1A2	1,596
212489_at	COL5A1	1,595
212091_s_at	COL6A1	1,927
209156_s_at	COL6A2	2,391
213622_at	COL9A2	1,434
204724_s_at	COL9A3	1,6
207420_at	COLEC10	4,268
209335_at	DCN	1,73
213661_at	DKFZP586H2123	1,516
206101_at	ECM2	1,554
202994_s_at	FBLN1	1,716
204359_at	FLRT2	1,522
209220_at	GPC3	1,685
206766_at	ITGA10	1,378
204989_s_at	ITGB4	2,269
221462_x_at	KLK15	3,113
202202_s_at	LAMA4	1,591
203417_at	MFAP2	1,434
203877_at	MMP11	1,673
201069_at	MMP2	1,586
205907_s_at	OMD	1,961
202465_at	PCOLCE	1,482
218585_s_at	RAMP	1,48
218452_at	SMARCAL1	1,859

205236_x_at	SOD3	1,372
208606_s_at	WNT4	2,534

In agreement with these findings, functional studies performed by other authors suggest that multiple Hsa21 genes affect mitochondrial function and reactive oxygen species production, one-carbon metabolism and cell adhesion [Gardiner, 2003]. It is plausible to hypothesize that NEMG dysregulation might be a cause of the mitochondrial dysfunction in DS [Conti et al, 2007].

1.3. Mitochondrial dysfunction in DS

TS21 has been associated to mitochondrial dysfunction, in several DS cell [Busciglio et al, 1995; Roat et al, 2007] and mouse models [Shuchman et al, 2000; Shukkur et al, 2006], suggesting that a mitochondrial dysfunction contributes to DS phenotype. It has been hypothesized that the pathogenetic mechanisms may be ascribed to oxidative stress caused by reactive oxygen species (ROS) formation, to altered intracellular calcium homeostasis and to apoptosis [Valenti et al, 2011]

To test the hypothesis that NEMG dysregulation is associated to mitochondrial dysfunction, we have performed molecular, morphological and functional analyses of mitochondria in primary cultures of human fetal fibroblasts (HFFs). With these experiments we demonstrated that TS21, while perturbing the expression of genes involved in mitochondrial pathways, disrupts the mitochondrial morphology, decreases oxygen consumption, and increases mitochondrial Ca^{2+} load and ROS production [Piccoli et al, 2013]. A more severe mitochondrial dysfunction was observed in TS21 fibroblasts derived from fetuses with cardiopathy, thus suggesting that mitochondrial dysfunction contributes to generating a more severe phenotype.

In the same study, peroxisome proliferator-activated receptor gamma, co-activator 1 alpha (*PGC-1α*) was found hypo-expressed at the transcriptional and protein levels [Piccoli et al, 2013]. PGC-1α is known to play a central role in regulating mitochondrial biogenesis and respiratory function through the interaction with transcriptional partners, like *NRF1*, *ERRα*, *PPARs*, and *YY1* [Scarpulla et al, 2011].

Several Hsa21 genes have been proposed as possible candidates for mitochondrial abnormalities, such as *APP* [Askanas et al, 1996], the transcription factor *GABPA* [O'Leary et al, 2004], the copper-zinc superoxide dismutase *SOD1* [Shin et al, 2004], the kinase *DYRK1A*, and the transcriptional regulator *DSCR1/RCAN1* [Bushdid et al, 2003]. The last two genes control *PGC-1α* via the *calcineurin/NFAT* pathway largely through the binding of *NFATc* to the *PGC-1α* promoter [Handschin et al, 2003].

It is so far unknown to what extent these genes affect *PGC-1α* expression and whether other Hsa21 genes play a key role in mitochondrial pathways.

1.4. Upregulation of extracellular matrix (ECM) genes in DS

Functional analysis of differentially expressed genes in DS hearts also demonstrates global upregulation of ECM protein genes. This group includes genes encoding adhesion and ECM proteins that map to Hsa21 such as *ADAMTS1*, *ADAMTS5*, *APP*, *JAM2*, *COL6A1*, *COL6A2* and *COL18A1*, which are dose-dependently upregulated in trisomic samples, and genes that do not map on Hsa21 such as fibronectin, fibulin, collagen type I, type III, type V, type XV, metalloproteases (*MMPs*) and several adhesion molecule genes (**Tab. 3**) Overexpression of this gene family is likely to affect cell adhesion properties, possibly determining an increase in adhesiveness. Cells explanted from endocardial cushion derived structures of fetuses with Hsa21 trisomy are more adhesive in vitro than those from controls [Wright et al, 1984]. A stochastic model has been proposed for septal defects in DS by which higher values of adhesiveness result in deficiencies of the atrio-ventricular (AV) canal development associated with clinical variability among individuals based on chance alone [Kurnit et al, 1985].

About 50% of the subjects with DS is affected by CHD. This high incidence suggests that the overexpression of genes mapping to Hsa21 alters the normal developmental process of the heart either directly or influencing the expression of genes mapping to other chromosomes.

Many authors have either compared human subjects with partial Hsa21 trisomies [Korenberg et al, 1990] or designed mouse models [Barlow et al, 2001; Liu C et al, 2011; Liu C et al, 2013] to identify the smallest critical region for DS-CHD (Down Syndrome Congenital Heart Disease) with conflicting results. The genomic regions on Hsa21 are syntenically distributed in three regions of the mouse genome (Mmu), which are located on Mmu16, Mmu10 and Mmu17. Many mouse models of DS (**Fig. 3**) have been used to identify critical regions for specific phenotypical traits, including a critical region for cardiac defects. The smallest critical region so far identified spans from *D21S3* to *PFKL* and it is included in the 21q22.2 and 21q22.3 cytobands [Barlow et al, 2001]. No Hsa21 ECM proteins are included in this region.

It is also interesting that DNA microarray analysis from right ventricular biopsies of patients with tetralogy of Fallot demonstrated that genes encoding ECM proteins, such as collagen type I, III, IX, XV and fibronectin, were upregulated versus age-matched controls [Sharma et al, 2006], suggesting that the increase of these ECM proteins has a potential role in CHD.

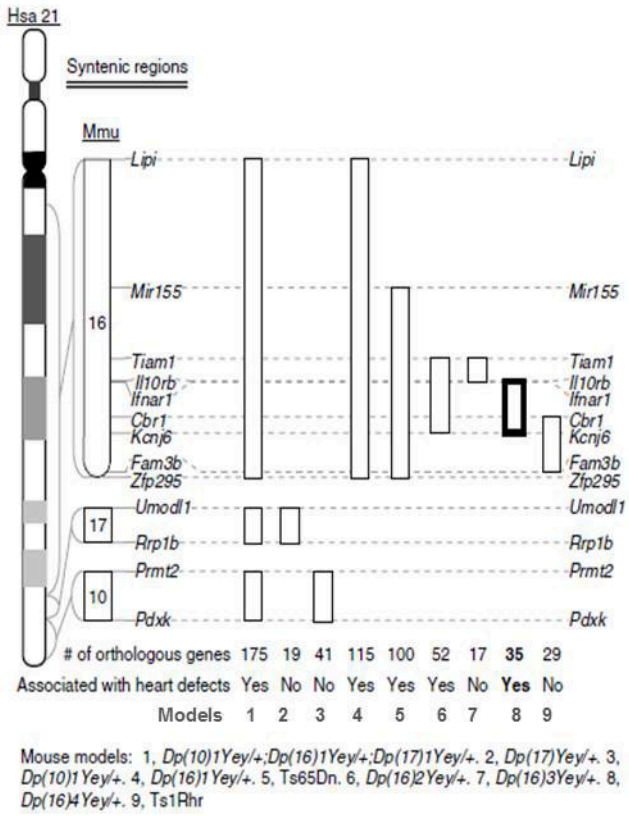

Figure 3. Synteny of the different DS mouse models.

A recently published paper [Vilardell et al, 2013] ascribed a key role in DS-CHD pathogenesis to a large extracellular matrix glycoprotein, the *Fibrillin 1* (*FBN1*). A study reported, indeed, a case of a person affected by DS who carried mutations in *FBN1*, the gene causative for a connective tissue disorder called Marfan Syndrome (MFS). The fact that the person did not have any cardiac alterations suggested compensation effects due to DS. The hypothesis was reinforced by a computational analysis [Vilardell et al, 2013] aimed to identify genes potentially related to *FBN1* and to test their relevance in DS hearts. The analysis proposes a new list of candidate genes related to DS, some of them display similar molecular mechanism affected in DS and in MFS mostly related to the extracellular matrix alteration. Deregulation of genes like *VCAN* [Hatano et al, 2012], *LOX*, *ACTA2* and *MMP2*, related with heart development [Hinton and Yutzey, 2011], are good candidates to explain the higher risk of heart abnormalities in DS. The alteration of *FBN1*-associated network could be crucial to understand the cardiovascular characteristics associated with DS.

This background evokes the interest in speculating which Hsa21 gene or genes might affect ECM upregulation in DS.

1.5. Meta-analysis of expression data from microarray analysis

Many researchers have embraced microarray technology. Due to extensive usage of microarray technology, in recent years there has been an explosion in publicly available datasets. Examples of such repositories include Gene Expression Omnibus (GEO, http://www.ncbi.nlm.nih.gov/geo/), ArrayExpress (http://www.ebi.ac.uk/arrayexpress/) and Stanford Microarray Database (SMD, http://smd.princeton.edu/), as well as researchers' and institutions' websites. The use of these datasets is not exhausted, when used wisely they may yield a depth of information. Demand has increased to effectively utilize these datasets in current research as additional data for analysis and verification.

Combining information from multiple existing studies can increase the reliability and generalizability of results. The use of statistical techniques to combine results from independent but related studies is called “meta-analysis” [Normand, 1999]. Meta-analysis has ranging benefits. Statistical power can be added to an analysis, obtained by the increase in sample size of the study. This aids the ability of the analysis to find effects that exist and is termed “integration-driven discovery” [Choi et al, 2003]. Meta-analysis can also be important when studies have conflicting conclusions as they may estimate an average effect or highlight an important subtle variation [Normand, 1999; Hong and Breitling, 2008].

Through meta-analysis, we can increase the statistical power to obtain a more precise estimate of gene expression differentials, and assess the heterogeneity of the overall estimate. Meta-analysis is relatively inexpensive, since it makes comprehensive use of already available data. Indeed, the advantages of meta-analysis of gene expression microarray datasets have not gone unnoticed by researchers in various fields [Grützmann et al, 2005; Bianchi et al, 2007; Vilardell et al, 2011].

There are a number of issues associated with applying meta-analysis in gene expression studies. These include problems common to traditional meta-analysis such as overcoming different aims, design and populations of interest. There are also concerns specific to gene expression data including challenges with probes and probe sets, differing platforms being compared and laboratory effects. As different microarray platforms contain probes pertaining to different genes, platform comparisons are made difficult when comparing these differing gene lists. Often the intersection of these lists are the only probes to be retained for further analysis. Moreover, when probes are mapped to their “Entrez IDs” [Maglott et al, 2007] for cross platform comparisons often multiple probes pertain to the same gene. Due to reasons ranging from alternative splicing to probe location these probes may produce different expression results [Ramasamy et al, 2008]. Ideal methods for aggregating these probe results in a meaningful and powerful way is currently the topic of much discussion. Laboratory effects are important because array hybridization is a sensitive

procedure. Influences that may affect the array hybridization include different experimental procedures and laboratory protocols [Irizarry et al, 2005], sample preparation and ozone level [Fare et al, 2003].

In conclusion, the main objectives of a meta-analysis are to [Walker et al, 2008]:

- Summarize and integrate results from a number of individual studies;
- Analyze differences in the results among studies;
- Overcome small sample sizes of individual studies to detect effects of interest, and analyze end points that require larger sample sizes;
- Increase precision in estimating effects;
- Evaluate effects in subsets of patients or tissue dependent/independent processes;
- Determine if new studies are needed to further investigate an issue;
- Generate new hypotheses for future studies.

For all these reasons, this kind of integrative and comparative study is pivotal for the analysis of such complex nature of gene expression and regulation in DS at a more general level [Antonarakis et al, 2006; Amano et al, 2004].

2. AIMS OF THE STUDY

High genome variability was observed in gene expression profiling of human DS samples and mouse models [Chou et al, 2009; FitzPatrick et al, 2002; Mao et al, 2003; Chrast et al, 2000; Saran et al, 2003]. Different experimental platforms, specific tissues, developmental stages or imperfect models introduce a high variation to the assessment of genome-wide effects. Few DS-related meta-analysis studies have been conducted to date even though comprehensive comparative studies, aimed to attenuate experimental influences and increase the number of compared samples, would be pivotal to understand genetic hallmarks of DS and molecular mechanisms responsible for DS phenotypes.

For this reason, this study was designed to provide new insights into the transcriptional changes influencing the molecular mechanisms associated with DS using meta-analysis and other computational strategies. A comprehensive computational analysis of expression feature-level extraction output (FLEO) files from independent transcriptome studies performed with Affymetrix technology on different tissues from human DS subjects was carried out. We merged data from heterogeneous platforms and adjusted the non-biological experimental variation with a recently developed algorithm, called ComBat in order to identify genes consistently dysregulated in DS. These genes were further classified in functional categories to discover pathways possibly affected by Hsa21 trisomy.

Aim of this study was to find Hsa21 genes likely responsible for pathways classified as dysregulated in DS based on previous experiments and meta-analysis results.

A computational strategy was therefore applied to identify Hsa21 candidate genes for the impairment of two Gene Ontology categories, i.e. the nuclear encoded mitochondrial genes (NEMGs) and the extracellular matrix (ECM) genes [Conti et al, 2007]. We speculated that most of the under-expressed NEMGs, as well as the overexpressed ECM genes, might be under the control of specific transcriptional regulators through molecular mechanisms influenced by the trisomy of Hsa21.

We combined the analysis of expression data retrieved from public repositories with the study of the promoter regions of dysregulated genes to identify candidate Hsa21 genes to be validated in a biological system.

.

3. MATERIALS AND METHODS

3.1. Meta-analysis procedures

The meta-analysis strategies are summarized in **Figure 4**.

Data collection

One-hundred-nine Affymetrix CEL files (FLEO files) from 9 different data sets were collected from the GEO (http://www.ncbi.nlm.nih.gov/geo/) and ArrayExpress (http://www.ebi.ac.uk/arrayexpress/) databases or retrieved from the author's web pages. Expression data concerned human cell lines or tissues from DS subjects at different developmental stages, analyzed prior to Sept. 2013, using the Affymetrix chipsets Human Genome U133 Plus 2.0, Human Gene 1.0 ST Array or Human Genome HG-U133A. The inclusion criteria for the current meta-analysis were as follows:

i) Affymetrix technology;
ii) human samples studies;
iii) DS condition/control studies;
iv) complete raw data (CEL files) publicly available for download;
v) experiments performed and documented according to the MIAME standard.

TABLE 4. DATA SETS INCLUDED IN THE META-ANALYSIS

ACCESSION	TISSUE	ASSAYS	AFFYMETRIX CHIP	RELEASE DATE	PMID
GSE6283	CV cells/ amniocytes	15	Human Genome U133 Plus 2.0	2008-06-14	18253026
E-MTAB-1238	limphoblastoid cells	12	Human Genome U133 Plus 2.0	2013-08-06	23830204
GSE48611	iPS cells	18	Human Genome U133 Plus 2.0	2013-07-09	23716668
GSE35561	iPS cells	6	Human Gene 1.0 ST Array	2012-09-24	23045704
GSE16176	amniocytes	14	Human Genome U133 Plus 2.0	2009-05-21	19474297
GSE9762	skin fibroblasts	10	Human Genome U133 Plus 2.0	2008-06-16	not published
GSE5390	brain	15	Human Genome HG-U133A	2009-04-23	20138973
GSE1789	fetal heart	15	Human Genome HG-U133A	2008-06-11	17683628
GSE1397	fetal heart	4	Human Genome HG-U133A	2005-05-10	16420667

Overview of the different sources of data, including different cells or tissues (brain, heart and others), different stages of development (adult, postnatal, embryonic) and different versions of Affymetrix GeneChips.

Data quality control

Extensive quality control of the raw microarray data has been carried out using the methods implemented in the BioConductor packages "affy" [Gautier et al, 2004], "affyQCReport" [Parman et al, 2008], "AffyPLM" [Bolstad et al, 2005; Brettschneider et al, 2007], "simpleaffy" [Wilson et al, 2005] and "arrayQualityMetrics" [Kauffmann et al, 2009]. In brief, all arrays were scanned for the overall sample quality (array image check, RNA degradation plots), signal distribution, intensity-dependent bias, and probe-set homogeneity (Normalized Unscaled Standard Error, NUSE, and Relative Log Expression, RLE). In addition, correlation plots and PCA analyses have been carried out in order to evaluate correlations between arrays. For each parameter a numerical score has been calculated and the values distribution plotted. Samples that showed more than two quality parameters out of the interquartile range of the distribution, were excluded from the analysis. Eighty-four out of 109 microarrays showed excellent quality according to the standards and, thus, considered for further analysis.

Affymetrix probes re-annotation

Although Affymetrix GeneChip design is very well documented, tremendous progress in genome sequencing and annotation in recent years renders existing probe set information suboptimal [Dai et al, 2005]. Since, chip sequence-based re-annotation has been shown to improve the cross-platform reproducibility and analysis of independent experiments [Carter et al, 2005], all probes were re-annotated according to the latest release of the Ensembl Gene database (http://www.ensembl.org/index.html). Mapping information and merging were done using R and the BioConductor package software. The custom cdf files (v. 17.1.0, ENSG) R packages for the re-annotated Affymetrix chipset are available for download at http://brainarray.mbni.med.umich.edu/Brainarray/Database/CustomCDF/17.1.0/ensg.asp.

Data Pre-processing

CEL files were imported into R (R Development Core Team, 2008) and preprocessed using the robust multiarray average algorithm, RMA (Irizarry et al, 2003), implemented in the Bioconductor (Gentleman et al, 2004) package "affy". In particular, the background correction and the summarization algorithms were firstly applied to individual series of data (see flow chart in **Fig. 4**); then, after merging data from the three different GenChips by the common Ensembl gene ID, the "quantile normalization" algorithm was

implemented to the resulting data frame consisting of 11547 Ensembl IDs in 84 assays.

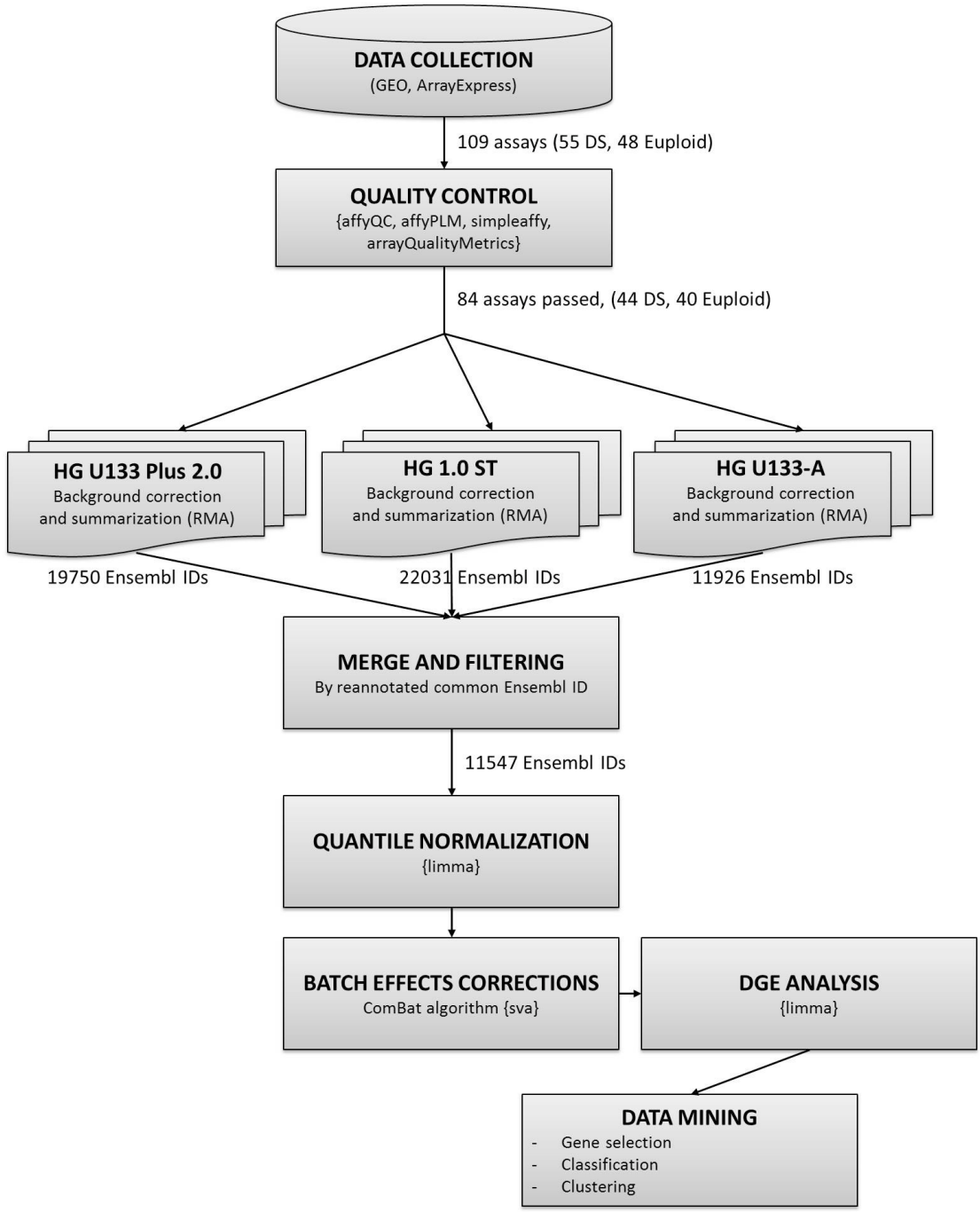

Figure 4. Flowchart of the pipeline followed for the meta-analysis.

Batch effects correction

In order to correct the non-biological experimental variation or "batch effects", normalized data were processed by the ComBat algorithm [Johnson et al, 2007] from the "sva" Bioconductor package. ComBat allows users to adjust for batch effects in datasets where the batch covariate is known, using methodology described in Johnson et al. 2007. It uses either parametric or non-parametric

empirical Bayes frameworks for adjusting data for batch effects. Users are returned an expression matrix that has been corrected for batch effects. In particular, the algorithm has been used with the nine different series as "batch" argument (GSE6283, E-MTAB-1238, GSE48611, GSE35561, GSE16176, GSE9762, GSE5390, GSE1789, GSE1397) and with the two types of karyotype as "covariate" argument (trisomic and euploid), keeping the other settings as default.

Differentially expressed genes and gene set enrichment analysis

Analysis of variance and moderated t-test were carried out for identifying the differentially expressed genes (DEG) in DS vs euploid samples, using the methods implemented into the Limma package [Smyth et al, 2005]. Benjamini and Hochberg method [Benjamini and Hochberg, 1995] was adopted for multiple test correction. We considered genes differentially expressed with a logarithmic Fold change (logFC) < -0.2 and > 0.2 with p-value ≤ 0.01.

The list of significantly dysregulated genes was analyzed for functional class scoring using Fisher's exact test with DAVID (http://david.abcc.ncifcrf.gov/, [Huang et al, 2009]) and Web-based Gene Set Analysis Toolkit V2 (http://bioinfo.vanderbilt.edu/webgestalt/ [Wang et al, 2013]) using GO term (biological process, cellular component, molecular function), Interpro domain and KEGG pathway enrichment with default settings. We considered enriched pathways with a significance threshold FDR $< 5\%$ and fold enrichment $\geq 1.5\%$. Gene Set Enrichment Analysis of the dysregulated genes was also performed with respect to pre-defined human pathways agglomerated from 22 pathway resources from the ConsensusPathDB (http://cpdb.molgen.mpg.de, [Kamburov et al, 2009]).

Related GO terms found enriched among the dysregulated genes were then, summarized using REVIGO software (http://revigo.irb.hr, [Supek et al, 2011]). REVIGO is a web server that summarizes long, often unintelligible lists of GO terms by finding a representative subset of the terms using a simple clustering algorithm that relies on semantic similarity measures. Furthermore, REVIGO visualizes this non-redundant GO term set in multiple ways to assist in interpretation: multidimensional scaling and graph-based visualizations accurately render the subdivisions and the semantic relationships in the data, while tree maps and tag clouds are also offered as alternative views.

GSEA analysis [Subramanian et al, 2005; Mootha et al, 2003] of pathways and gene-sets was performed running the java application (downloaded from the Broad Institute website, http://www.broadinstitute.org/gsea/index.jsp) on the normalized matrix of expression data obtained after RMA processing. We used all the seven collections of gene-sets downloaded from The Molecular

Signatures Database (MSigDB), including positional, curated, motif gene sets and GO terms. A total of 10,925 categories were screened in the analysis (MSigDB release v4.0). In order to assess the statistical significance, a permutation technique was applied to generate the null distribution of the enrichment score. Using a permutation test 1,000 times, the cut-off of the significance level p-values was chosen as 0.01 for the most significant pathways. The annotation of significant genes in each pathway was performed by using the biomaRt package (http://www.biomart.org/). Next, clustering on groups or genes was performed based on the identified genes' expression in each significant pathway using the method of hierarchical clustering with Euclidean distance.

Transcription factors binding analysis of co-regulated genes

In order to scan promoter sequences from our input lists of upregulated or downexpressed genes, we used a web server called Pscan (http://www.beaconlab.it/pscan, [Zambelli et al, 2009]), looking for over-represented TF motifs. This software provides hints on which factors could be responsible for the patterns of expression observed, or vice versa seem to be avoided (with P-values nearing 1). We considered enriched in targets, TF with adjusted P-values < 0.05.

Gene network inference

String 9.1 software [Franceschini et al, 2013] and the R/Bioconductor package minet [Meyer et al, 2008], which provides a set of functions to infer mutual information networks from a dataset were used. Once fed with a microarray dataset, the minet package returns a network where nodes denote genes, edges model statistical dependencies between genes and the weight of an edge quantifies the statistical evidence of a specific (e.g. transcriptional) gene-to-gene interaction. Four different entropy estimators are made available in the package minet (empirical, Miller-Madow, Schurmann-Grassberger and shrink) as well as four different inference methods, namely relevance networks, ARACNE, CLR and MRNET. In addition, the package integrates accuracy assessment tools, like F-scores, PR-curves and ROC-curves in order to compare the inferred network with a reference one.

3.2. Procedures to identify and validate single Hsa21 genes responsible for DS phenotypes

Public data expression analysis

A set of expression data from GSE 19836 series [De Cegli et al, 2010] was obtained from Gene Expression Omnibus repository GEO (http://www.ncbi.nlm.nih.gov/geo). This set of data, derived from the analysis of a mouse embryonic stem cell bank in which 32 orthologs of human chromosome 21 genes, including transcription factors and protein kinases, were individually overexpressed in an inducible manner. A set of clones individually overexpressing 20 of the 32 genes, namely 13 transcription factors (*Aire*, *Bach1*, *Erg*, *Ets2*, *Gabpa*, *Nrip1*, *Olig1*, *Olig2*, *Pknox1*, *Runx1*, *Sim2*, *ZFP295*, *1810007M14Rik*), one transcriptional activator (*Dscr1-Rcan1*) and 6 protein kinases (*DYRK1A*, *SNF1LK*, *Hunk*, *Pdxk*, *Pfkl*, *Ripk4*), was transcriptionally profiled under inducing and non-inducing conditions with Affymetrix Gene Chip Mouse 430_2. Specifically, RNAs from 3 induced mouse ESCs and 3 controls were profiled for each inducible Hsa21 gene [De Cegli et al, 2010]. In our analysis, we used R software vers. 3.0.2. We considered genes differentially expressed with a Fold change (LogFC) > 0.3 and < −0.3 with $p < 0.05$. Gene ontology (GO) functional class scoring of all the lists of significantly upregulated or downregulated genes was performed using the Web−based Gene Set Analysis Toolkit V2 (http://bioinfo.vanderbilt.edu/webgestalt/, [Wang et al, 2013]). Special attention was given to mitochondria-related categories and pathways for downregulated genes and ECM for upregulated genes.

Comparison of lists of differentially expressed NEMGs

We compared 3 sets of gene expression data from different experiments, to identify genes consistently dysregulated across the 3 studies. The first set, SET 1, included genes dysregulated by Nrip1 modulation in mouse adipocytes [Powelka et al, 2006]. The second set, SET2, included genes upregulated after PGC-1α induction in SAOS2 cells (human osteoblast like cells) [Schreiber et al, 2004]. The third set included mitochondria-related genes, downregulated in DS fetal heart tissue [Conti et al, 2007]. The 3 sets were filtered according to the GO cell component category "mitochondrion" with the above mentioned Web−based Gene Set Analysis Toolkit V2. The resulting genes – 123 genes in SET1, 129 in SET2 and 70 in SET3 – were intersected using the “suma2venn” package [Conesa and Nueda, R package]. A Venn Diagram was built, which shows overlapping genes across the 3 sets.

3.3. Methods for the validation of NRIP1 role in DS mitochondrial dysfunction

Samples for validation of NRIP1 role

Human primary lines of fetal fibroblasts (HFFs) were obtained from the "Telethon Bank of Fetal Biological Samples" at the University of Naples. All experimental protocols were approved by the local Institutional Ethics Committee. Eight skin biopsies were explanted from human fetuses with trisomy of Hsa21 (DS-HFF) after therapeutic abortion at 18-22 gestational weeks. Fibroblasts from biopsies were cultured in T25 flasks (BD Falcon) with Chang medium B+C (Irvine Scientific) supplemented with 1% penicillin/streptomycin (Gibco) at 37°C in 5% CO_2 atmosphere; all the analyses described throughout this study were carried out at cell culture passages 4-5.

Transfection protocol

NRIP1 was transiently silenced in 8 DS-HFF lines using a pool of specific NRIP1-siRNAs (ON-TARGETplus SMARTpool, Dharmacon), with negative (ON-TARGETplus SMARTpool Non targeting siRNAs control, Dharmacon) and positive controls (ON-TARGETplus SMARTpool, GAPDH siRNAs, Dharmacon). Interferin transfection reagent (Polyplus transfection) was used. Cells were plated on 12-well plates (50000 cells/well) for RNA collection, on 35 mm plates with 20 mm slides (Delchimica) (50000 cells/well) for ROS production analysis and on 24-well plates (30000 cells/well) (BD Falcon) for immunofluorescence and mitochondrial activity assays. DS-HFFs were transfected with 5nM and 20nM siRNA according to the manufacturer's protocol (Polyplus transfection). Seventy-two hours after transfection, the effects of *NRIP1* silencing were evaluated.

NRIP1 immunofluorescence

For the evaluation of NRIP1 protein by immunofluorescence, 30,000 cells were plated in 24-well plates on 12 mm diameter round glass coverslips. Cells were fixed in 3:1 methanol: acetic acid for 15 min, washed twice with PBS, and then incubated twice in 0.1M Borate Buffer pH 8.5 for 10 minutes to neutralize the pH. After two washes with PBS, the cells were incubated with DNase 1:10 in RDD Buffer (Qiagen) at 37°C for 1h and then treated with 2% BSA in PBS to block non-specific protein-protein interactions. The cells were then incubated with the antibody anti-NRIP1 (30µg/ml, ab42126 Abcam, Cambridge Science Park, Cambridge, UK) overnight at +4°C. The secondary antibody (green) was Alexa Fluor® 488 goat anti-rabbit IgG (H+L) used at a 1/200 dilution for 1h.

Cells were finally mounted in 50% glycerol in PBS. Immunofluorescence analysis was performed at a confocal laser-scanning microscope LSM 510 (Zeiss, Gottingen, Germany) equipped with an Argon ionic laser whose λ was set at 488nm, and a HeNe laser whose λ was set at 633nm. Emission of fluorescence was revealed by a BP 505-530 band pass filter for Alexa Fluor 488 and by a 615 long pass filter for DRAQ5. Images were acquired at a resolution of 1024x1024 pixels. Analysis of data was performed with ImageJ software, version 1.37. Fifty random single cells were analyzed for each imaging analysis.

Laser scanning confocal microscopy (LSCM) live cell imaging of ROS production

For the evaluation of ROS production after NRIP1 siRNA transfection, 50,000 cells were plated on 25 mm diameter round glass coverslips in an Attofluor cell chamber (Molecular Probe, Leiden, NL). Seventy-two hours later, the cells were incubated for 15 minutes at 37°C with 10 μM of 2,7-di-chloro-fluorescin di-acetate (DCF-DA) which is converted to di-chloro-fluorescein by intracellular esterases, for detection of H_2O_2, or with 5 μM of MitoSOX™ Red reagent (Life Technologies, Molecular Probes), which is a live-cell permeant which is rapidly and selectively targeted to the mitochondria. Once in the mitochondria, MitoSOX™ Red reagent is oxidized by superoxide and exhibits red fluorescence. After incubation cells were washed three times with medium w/o serum. To maintain the cells alive during observation and to create the proper environmental conditions, the specimen was placed in an Oko Lab (Na, Italy) Water Jacket Top Stage Incubator, kept at 37°C, under humidified condition of 5% CO_2 and 95% air by means of temperature controllers, gas mixers, and humidifiers right on the microscope. The analysis of immunofluorescence was performed with a confocal laser scanner microscopy Zeiss LSM 510 (Carl Zeiss, Gottingen, Germany), equipped with Argon ionic laser whose λ was set at 488 nm, an HeNe laser whose λ was set at 546 nm, and an immersion oil objective 63x/1.4f. Emission of fluorescence was revealed by BP 505-530 band pass filter for DCF and 560 Long Pass for MitoSOX™ Red. Images were acquired in the green or in the red channels and then saved in LSM format to prevent the loss of information. They were acquired with a resolution of 1024x1024 pixel with the confocal pinhole set to one Airy unit. Analysis of data was performed with ImageJ software, version 1.37. Fifty random single cells were analyzed for each imaging analysis.

Mitotracker immunofluorescence

For the evaluation of mitochondrial activity MitoTracker® Red CMXRos (Molecular Probes) was chosen. MitoTracker® probes passively diffuse across the plasma membrane and accumulate in actively respiring mitochondria. Thirty-thousand cells were plated on 24-well plates on 12 mm diameter round glass coverslips and then incubated with 150nM of Mitotracker Red for 30 minutes. After incubation cells were fixed for 20 minutes in PBS containing 4% paraformaldehyde (Sigma) and then washed once with PBS 1X. Nuclei were stained with the DNA intercalant DRAQ5 (Bio status, Alexis Corporation). Cells were finally mounted in 50% glycerol in PBS. Immunofluorescence analysis was performed with a confocal laser-scanning microscope LSM 510 (Zeiss, Gottingen, Germany). The lambda of the two HeNe lasers was set at 546 nm and at 633 nm. Fluorescence emission was revealed by BP 560–615 band pass filter for Mitotracker Red and by 615 long pass filter for DRAQ5. Double staining immunofluorescence images were acquired separately in the red and infrared channels at a resolution of 1024x1024 pixels, with the confocal pinhole set to one Airy unit, and then saved in LSM format. Fifty random single cells were analyzed for each imaging analysis using the ImageJ version 1.37.

RNA extraction and Quantitative Real-time PCR

Total RNA from each sample was extracted using TRIzol reagent (Gibco/BRL Life Technologies, Inc., Gaithersburg, MD) and was reverse transcribed using the iScript cDNA Synthesis kit (Bio-Rad Laboratories Inc., Hercules, CA, USA). Real-time PCR was performed using iQ Supermix SYBR Green 2X on a Bio-Rad iCycler according to the manufacturer's protocols. PCR reactions were performed in triplicate. Primer pairs (MWG Biotech, Ebersberg, Germany) were designed using the Primer 3 software (http://frodo.wi.mit.edu/primer3) to obtain amplicons ranging from 100 to 150 base pairs. In order to obtain correct amplifications, each primer pair was tested for its specificity and its thermodynamics parameters with Blast (http://blast.ncbi.nlm.nih.gov/Blast.cgi), mFold (http://mfold.rit.albany.edu/?q=mfold) and OligoAnalyzer (http://eu.idtdna.com/analyzer/Applications/OligoAnalyzer/) software. Expression values were normalized either versus scrambled transfected cells or versus scrambled transfected euploid cells. ABELSON and GAPDH housekeeping genes were chosen as reference genes. To quantify the mtDNA content, we selected two genes: D-loop as the mitochondrial target and ACTIN as the nuclear target. Both targets were quantified by qRT-PCR using cDNA reverse-transcribed from RNA of 3 NRIP1-silenced trisomic samples and scrambled control. Normalization of gene expression was obtained using ABL

gene as housekeeping. The ratio between D-loop and ACTIN expression under each condition (NRIP1-silenced or scrambled trisomic cells) was calculated.

Immunoblotting

For immunoblotting, cells were scraped into ice cold phosphate-buffered saline and lysed in a modified 10 mM Tris buffer pH 7.4 containing 150 mM NaCl, 1% Triton X-100, 10% glycerol, 10 mM EDTA and protease inhibitor cocktail. After 30 min of incubation on ice, the lysates were cleared via centrifugation at 12,000 xg at 4°C for 10 min. Protein concentrations were determined by the Lowry procedure. Protein extracts (18 μg) were separated on 4–12% Bis-Tris acrylamide Gel (Life Technologies, NP0323) and electron-transferred to PVDF or nitrocellulose membrane according to standard procedures. Unspecific binding sites were saturated by incubating membranes with TBS-Tween 20 (0.05%) supplemented with 5% non-fat powdered milk for 1 h. Next, the membranes were incubated overnight with primary antibodies [GAPDH (Cell Signaling, 2118); LUCIFERASE (Invitrogen, 356700)] and the detection was assessed by appropriate HRP-labeled secondary antibodies [Santa Cruz, sc-2004 (goat anti-rabbit) and sc-2005 (goat anti-mouse)] plus a chemiluminescent substrate (Thermo Scientific, 34080). Equal loading of lanes was confirmed by incubation with an anti-GAPDH antibody.

Luciferase measurements

Cells were seeded on glass coverslips (13 mm diameter) for single sample luminescence measurements and allowed to grow until 50% confluence. The cells were then transfected with a cytosolic (untargeted) firefly luciferase (cytLuc) and a mitochondrially targeted luciferase (mtLuc). Cell luminescence was measured in the same purpose-built luminometer used for the aequorin measurements, constantly perfused with KRB, supplemented with 1 mM $CaCl_2$ and 20 mM luciferin. The light output of a coverslip of infected cells was in the range of 1,000 –10,000 counts per second (cps) versus a background lower than 10 cps. All compounds employed in the experiments were tested for non-specific effects on the luminescence, but none was observed.

Statistics

The analyses applied to the microarray data have been described above. For all other experiments, analysis of variance was carried out, followed by post hoc comparison (ANOVA, F-test). Data were expressed as mean +/− SEM.

4. RESULTS

4.1. Data integration of microarray experiments shows genes consistently dysregulated in DS.

Genome-wide dosage effects were computed with the approach described in Materials and Methods. In total, nine case-control experiments performed using three different Affymetrix GeneChips (Affymetrix Human Genome HG-U133A, Affymetrix Human Genome U133 Plus 2.0, Affymetrix Human Gene 1.0 ST Array) were interrogated and 44 DS vs 40 euploid samples were compared (**Tab. 4**). All assays were quality checked and ~80% of them passed the defined cut-off thresholds (84 out of 109). Comparison between the DS and the euploid conditions and the statistical significance were calculated with the methods implemented in the limma package [Smyth et al, 2005].

Since gene chip re-annotation has been shown to improve the cross-platform reproducibility and analysis of independent experiments [Carter et al, 2005], all probes were re-annotated according to the last release of the Ensembl gene database (Version 17.1.0, ENSG). In particular all the probe sets initially contained in the three Chipsets analyzed (respectively 22283, 54675 and 241576), were matched to 11926, 19750 and 22031 unique Ensembl gene stable identifiers.

Before data processing, 11547 genes were considered in the meta-analysis corresponding to the Ensembl gene identifiers shared by the GeneChip analyzed. In order to compare expression data deriving from heterogeneous platforms in the correct way, we implemented in our pipeline the ComBat algorithm, developed in order to reduce the non-biological experimental variation or "batch effects". Batch effect deriving from analyzing different GEO series was evident from the first heatmap in **Fig. 5**, in which arrays mostly cluster according to the series. After running ComBat on the matrix of normalized expression data, we removed, or at least reduced, this problem as demonstrated by the second heatmap in **Fig. 5** that shows the correlation among the arrays after the ComBat adjustment.

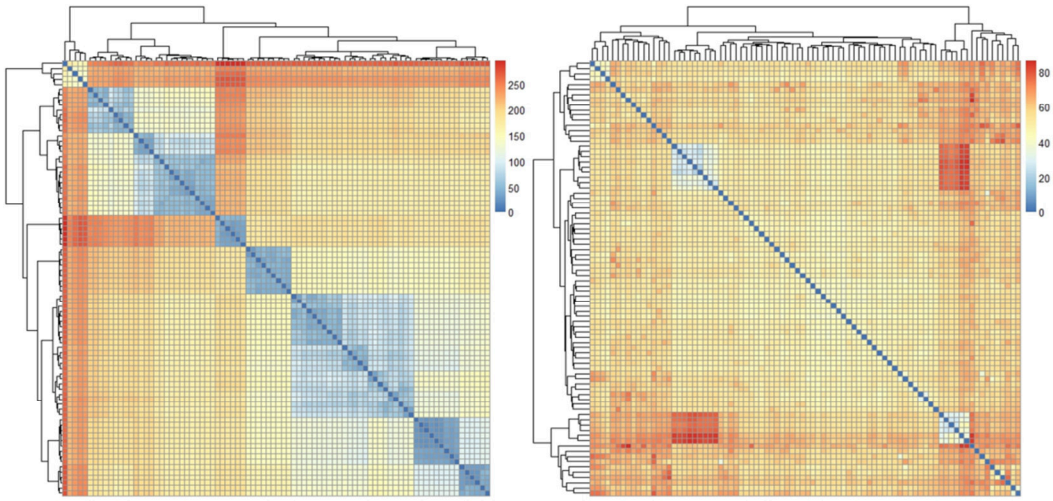

Figure 5. Heatmap of array correlation using Euclidean distances before (left) and after (right) batch effect correction. It is easy to point out the batch effect before the correction, samples mostly cluster according to the different GEO series.

We identified 178 genes consistently dysregulated among the experiments in DS vs controls (**Tab. 5-6**). Proportionally, Hsa21 contributed in great part to the global dysregulation (**Fig. 6**).

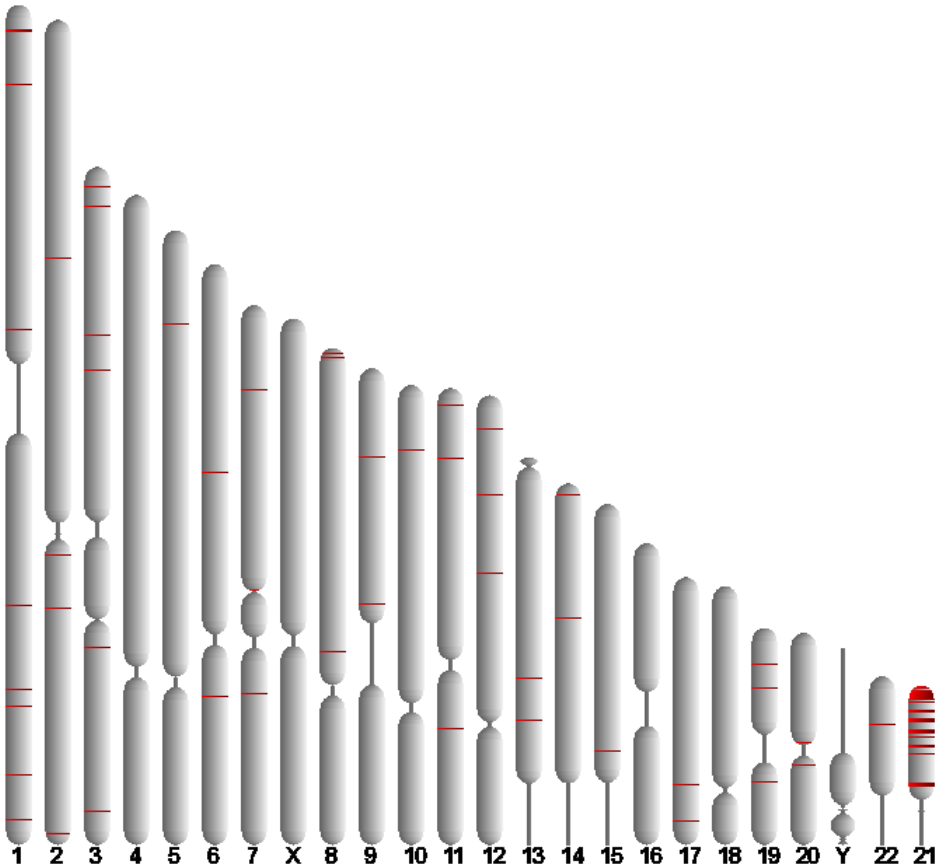

Figure 6. Ideograms showing the position of dysregulated genes on chromosomes. Horizontal bars represent the chromosomal location for the biological database identifiers. The scale is 2 million bases per pixel.

As expected, Hsa21 genes were globally upregulated in gene expression studies. It is remarkable that only 50% of all Hsa21 genes (71 out of 135 studied here using the Ensembl genome annotation [Flicek et al, database]) showed consistent effects across the different experiments, indicating that dosage effects were either compensated or not detected in the selected experimental data.

TABLE 5. LIST OF THE 71 HSA21 GENES UPREGULATED IN THE META-ANALYSIS

ID	LOG_FC	P.VALUE	ADJ.P.VAL	GENE_ID	CHR
ENSG00000184787	0,386204	2,65E-14	3,06E-10	UBE2G2	21
ENSG00000141959	0,393163	2,35E-13	1,36E-09	PFKL	21
ENSG00000159140	0,48527	7,56E-13	2,33E-09	SON	21
ENSG00000184900	0,380755	8,08E-13	2,33E-09	SUMO3	21
ENSG00000185808	0,648185	6,40E-12	1,48E-08	PIGP	21
ENSG00000160221	0,476313	2,83E-11	5,44E-08	C21orf33	21
ENSG00000198862	0,435255	3,54E-11	5,83E-08	LTN1	21
ENSG00000155313	0,53725	1,47E-10	2,12E-07	USP25	21
ENSG00000142207	0,394657	1,86E-10	2,38E-07	URB1	21
ENSG00000154640	0,680346	4,09E-10	4,72E-07	BTG3	21
ENSG00000160209	0,328505	4,61E-10	4,84E-07	PDXK	21
ENSG00000159128	0,369301	7,95E-10	7,65E-07	IFNGR2	21
ENSG00000183527	0,453732	1,17E-09	1,04E-06	PSMG1	21
ENSG00000159131	0,379272	1,31E-09	1,08E-06	GART	21
ENSG00000159147	0,657731	1,57E-09	1,21E-06	DONSON	21
ENSG00000182240	0,547411	1,71E-09	1,23E-06	BACE2	21
ENSG00000154719	0,528216	1,86E-09	1,27E-06	MRPL39	21
ENSG00000159086	0,432171	5,40E-09	3,46E-06	PAXBP1	21
ENSG00000157538	0,407667	6,49E-09	3,95E-06	DSCR3	21
ENSG00000160201	0,399059	7,37E-09	4,26E-06	U2AF1	21
ENSG00000185658	0,288545	1,15E-08	6,32E-06	BRWD1	21
ENSG00000142188	0,642974	1,44E-08	7,55E-06	TMEM50B	21
ENSG00000157617	0,457443	2,61E-08	1,31E-05	C2CD2	21
ENSG00000159256	0,424298	7,95E-08	3,82E-05	MORC3	21
ENSG00000205726	0,248475	1,39E-07	6,43E-05	ITSN1	21
ENSG00000160218	0,362649	1,76E-07	7,82E-05	TRAPPC10	21
ENSG00000156239	0,348446	1,85E-07	7,92E-05	N6AMT1	21
ENSG00000185917	0,348	1,97E-07	8,13E-05	SETD4	21
ENSG00000160213	0,422201	2,25E-07	8,97E-05	CSTB	21
ENSG00000156304	0,287182	2,76E-07	0,000106	SCAF4	21
ENSG00000159228	0,493672	3,65E-07	0,000136	CBR1	21

ENSG00000156256	0,428437	4,23E-07	0,000153	USP16	21
ENSG00000160294	0,235276	6,36E-07	0,000223	MCM3AP	21
ENSG00000182093	0,52092	7,19E-07	0,000239	WRB	21
ENSG00000183255	0,422953	7,25E-07	0,000239	PTTG1IP	21
ENSG00000142166	0,344144	8,56E-07	0,000274	IFNAR1	21
ENSG00000159055	0,538771	3,13E-06	0,000976	MIS18A	21
ENSG00000142168	0,381354	3,26E-06	0,000991	SOD1	21
ENSG00000159231	0,378271	3,39E-06	0,001003	CBR3	21
ENSG00000155304	0,352388	4,97E-06	0,001384	HSPA13	21
ENSG00000156261	0,319143	5,07E-06	0,001384	CCT8	21
ENSG00000159216	0,466797	5,15E-06	0,001384	RUNX1	21
ENSG00000185437	0,488504	5,80E-06	0,001506	SH3BGR	21
ENSG00000160310	0,302425	8,50E-06	0,002135	PRMT2	21
ENSG00000160299	0,311682	1,01E-05	0,002489	PCNT	21
ENSG00000182670	0,544217	1,31E-05	0,003018	TTC3	21
ENSG00000160285	0,399759	2,23E-05	0,00505	LSS	21
ENSG00000142192	0,318108	5,41E-05	0,01157	APP	21
ENSG00000156299	0,429725	5,52E-05	0,011598	TIAM1	21
ENSG00000154727	0,281409	7,76E-05	0,015714	GABPA	21
ENSG00000160208	0,245652	0,000121	0,023762	RRP1B	21
ENSG00000154734	0,485059	0,000175	0,030642	ADAMTS1	21
ENSG00000159259	0,294897	0,000258	0,043193	CHAF1B	21
ENSG00000156253	0,287605	0,000271	0,044023	RWDD2B	21
ENSG00000182871	0,441329	0,000432	0,063924	COL18A1	21
ENSG00000159082	0,285239	0,000471	0,068786	SYNJ1	21
ENSG00000180530	0,501849	0,000636	0,080917	NRIP1	21
ENSG00000154721	0,367926	0,001008	0,109757	JAM2	21
ENSG00000160216	0,21927	0,001666	0,156436	AGPAT3	21
ENSG00000157601	0,494649	0,001911	0,175119	MX1	21
ENSG00000160200	0,349411	0,001977	0,178367	CBS	21
ENSG00000243646	0,322797	0,002116	0,186497	IL10RB	21
ENSG00000142156	0,250492	0,002196	0,189607	COL6A1	21
ENSG00000215424	0,291364	0,002526	0,198737	MCM3AP	21
ENSG00000154639	0,311744	0,003256	0,226523	CXADR	21
ENSG00000156273	0,239164	0,003482	0,235146	BACH1	21
ENSG00000177692	0,212829	0,003991	0,254589	DNAJC28	21
ENSG00000160191	0,260016	0,004398	0,267283	PDE9A	21
ENSG00000157557	0,29883	0,004826	0,279563	ETS2	21
ENSG00000142173	0,3151	0,00493	0,281797	COL6A2	21
ENSG00000160307	0,21962	0,007483	0,334407	S100B	21

TABLE 6. TOP TWENTY NON-HSA21 GENES DYSREGULATED IN THE META-ANALYSIS

ID	LOGFC	P.VALUE	ADJ.P.VAL	GENE_ID	CHR
ENSG00000157014	-0,22981	4,92E-06	0,001384	TATDN2	3
ENSG00000075413	-0,24075	5,87E-06	0,001506	MARK3	14
ENSG00000162931	-0,21856	1,06E-05	0,002544	TRIM17	1
ENSG00000105443	-0,2211	1,21E-05	0,002846	CYTH2	19
ENSG00000123810	-0,20686	3,29E-05	0,007313	B9D2	19
ENSG00000214063	0,359408	0,000111	0,022133	TSPAN4	11
ENSG00000042493	0,53367	0,000136	0,026152	CAPG	2
ENSG00000206549	-0,24367	0,000149	0,02773	PRSS50	3
ENSG00000177731	0,208513	0,000158	0,028891	FLII	17
ENSG00000124587	0,432463	0,000166	0,029978	PEX6	6
ENSG00000141562	-0,26932	0,000173	0,030642	NARF	17
ENSG00000168591	-0,22125	0,000194	0,033444	TMUB2	17
ENSG00000120738	0,32309	0,000199	0,03376	EGR1	5
ENSG00000151746	-0,27399	0,000268	0,044023	BICD1	12
ENSG00000054277	-0,40794	0,000311	0,049848	OPN3	1
ENSG00000198521	0,238111	0,00035	0,054621	ZNF43	19
ENSG00000121691	0,415439	0,000392	0,059045	CAT	11
ENSG00000104522	0,254573	0,00048	0,069353	TSTA3	8
ENSG00000168306	0,335262	0,000532	0,073965	ACOX2	3
ENSG00000256043	0,422635	0,000687	0,085341	CTSO	4

Running GSEA with MSigDB_c1 positional database, two genomic regions on Hsa21 enriched with dysregulated genes have been identified: chr21q22 and chr21q21, (**Fig. 7**); these regions cover almost the entire chromosome 21 and it does not fit well with the hypothesis that a single region could be responsible for the molecular and phenotypic consequences of DS [Belichenko et al, 2007; Ronan et al, 2007].

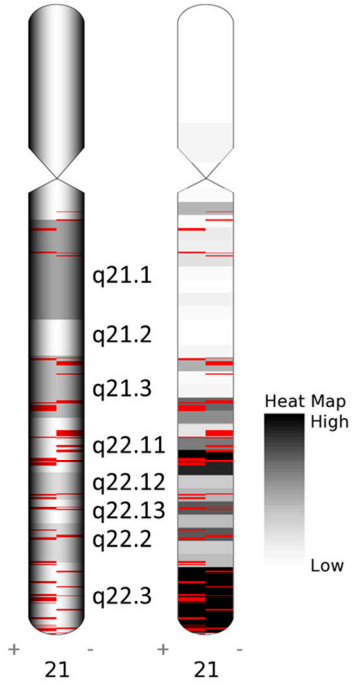

Figure 7. Mapping of the dysregulated genes on chromosome 21. Red bars indicate the genomic mapping of the genes. The two ideograms show also the cytogenetic bands (left ideogram) and the heatmap of the genic density (right ideogram).

4.2. Functional annotation using gene enrichment analysis

Functional classification of dysregulated genes into pathways and Gene Ontology (GO) categories was performed with Fisher's test-based tools such as DAVID, WebGestalt Toolkit and ConsensusPathDb and with GSEA, which uses a running-sum statistics. The first three software showed comparable results and for sake of simplicity we only show results from ConsensusPathDb. The list of 178 dysregulated genes in the meta-analysis was used as input file of the tool and in **Table 7** we reported the complete list of enriched GO biological process (BP3 level) terms obtained. This list of GO terms was then used as input of the REVIGO software [Supek et al, 2011] in order to summarize redundant and/or related terms (**Fig. 8**). The pathways most enriched with dysregulated genes referred mainly to cellular morphogenesis and development, and defects in synapsis (e.g. response to axon injury, dendrite regeneration and regulation of neuronal plasticity). In addition, apoptosis-related gene categories were also enriched.

TABLE 7. ENRICHMENT OF GENE ONTOLOGY BIOLOGICAL PROCESSES AMONG THE DYREGULATED GENES.

TERM_GOID	TERM_NAME	SIZE	P-VALUE	ADJ.P.VAL
GO:0000902	cell morphogenesis	1007	8,68E-06	0,00372
GO:0065003	macromolecular complex assembly	1182	4,26E-05	0,00525
GO:0071453	cellular response to oxygen levels	100	4,52E-05	0,00525
GO:0071822	protein complex subunit organization	1335	4,90E-05	0,00525
GO:0071456	cellular response to hypoxia	91	2,22E-04	0,01903
GO:0012501	programmed cell death	1650	3,40E-04	0,02170
GO:0036293	response to decreased oxygen levels	231	3,55E-04	0,02170
GO:0036296	response to increased oxygen levels	18	6,07E-04	0,03249
GO:0048523	negative regulation of cellular process	3078	6,87E-04	0,03268
GO:0071455	cellular response to hyperoxia	5	8,69E-04	0,03550
GO:0030198	extracellular matrix organization	321	9,68E-04	0,03550
GO:0006921	cellular component disassembly involved in execution phase of apoptosis	82	1,01E-03	0,03550
GO:0048678	response to axon injury	48	1,08E-03	0,03550
GO:0010941	regulation of cell death	1227	1,21E-03	0,03686
GO:0071503	response to heparin	6	1,30E-03	0,03697
GO:0007165	signal transduction	4424	2,84E-03	0,07233
GO:0033273	response to vitamin	63	2,96E-03	0,07233
GO:0014070	response to organic cyclic compound	571	3,04E-03	0,07233
GO:0007157	heterophilic cell-cell adhesion	32	3,35E-03	0,07376
GO:0048858	cell projection morphogenesis	722	3,50E-03	0,07376
GO:0009112	nucleobase metabolic process	67	3,70E-03	0,07376
GO:0008354	germ cell migration	10	3,79E-03	0,07376
GO:0032990	cell part morphogenesis	736	4,18E-03	0,07477
GO:0043094	cellular metabolic compound salvage	35	4,33E-03	0,07477
GO:0044259	multicellular organismal macromolecule metabolic process	113	4,37E-03	0,07477
GO:0046660	female sex differentiation	115	4,70E-03	0,07744
GO:0030574	collagen catabolic process	73	5,03E-03	0,07969
GO:0007611	learning or memory	171	5,72E-03	0,08746
GO:0097305	response to alcohol	231	6,42E-03	0,09131
GO:0070633	transepithelial transport	13	6,45E-03	0,09131
GO:0044243	multicellular organismal catabolic	80	6,94E-03	0,09131
GO:0006066	alcohol metabolic process	358	7,04E-03	0,09131

GO:0097190	apoptotic signaling pathway	426	7,21E-03	0,09131
GO:0030031	cell projection assembly	237	7,35E-03	0,09131
GO:0001967	suckling behavior	14	7,48E-03	0,09131
GO:0048168	regulation of neuronal synaptic plasticity	43	7,73E-03	0,09131
GO:0030705	cytoskeleton-dependent intracellular transport	83	7,89E-03	0,09131
GO:0022617	extracellular matrix disassembly	87	9,29E-03	0,10221
GO:0000096	sulfur amino acid metabolic process	46	9,31E-03	0,10221

List retrieved from ConsensusPathDB. Adjusted P-value cut-off = 0.1.

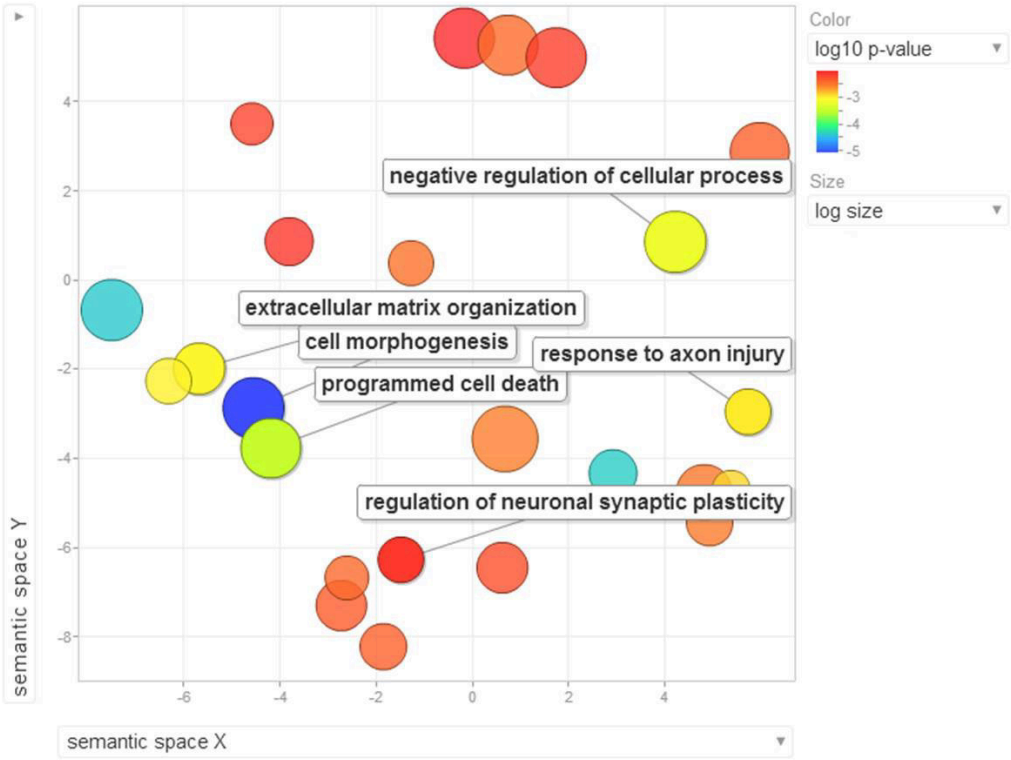

Figure 8. Graphical representation of GO terms found enriched on 178 genes dysregulated in DS samples. Heatmap colors represent the statistical significance of the enriched category. Adj.P.Value cut-off = 0.05. Plot obtained with REVIGO tool (http://revigo.irb.hr).

GSEA (Broad Institute) differs from the other functional class scoring tools used because it adopts a running-sum statistics and it works on the whole expression matrix of normalized data, not on the simple lists of DEG. The analysis with this tool confirmed the enrichment of genes mapping to Hsa21 (**Fig. 9**), as expected, but also revealed the enrichment for genes involved in the

cell cycle, among the upregulated genes, and the targets of *PGC-1α* (P.val < 0.01), among the downregulated genes. This is supported by our previous studies on DS fetal fibroblasts in which we found *PGC-1α* significantly downregulated [Piccoli et al, 2013]. The protein encoded by this gene is a tissue-specific coactivator that enhances the activity of many nuclear receptors and coordinates transcriptional programs important for energy metabolism and energy homeostasis in mitochondria.

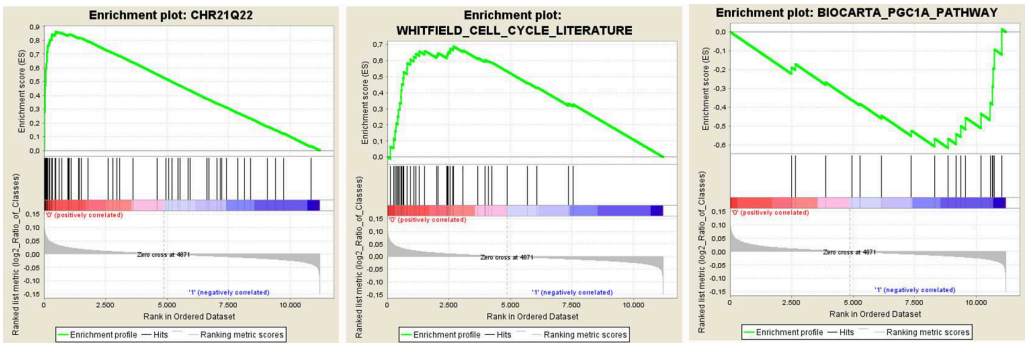

Figure 9. Enrichment plots from the GSEA analysis. Plot retrieved from the GSEA java tool (Broad Institute).

Molecular interactions among the 178 significantly dysregulated genes on Hsa21 and on other chromosomes exhibited a complex and enriched-in-interactions network (111 interactions, instead of 12.8 expected with String 9.1 software [Franceschini et al, 2013]) supporting the important role of physical interactions as transmitter of dosage effects (**Fig. 10**).

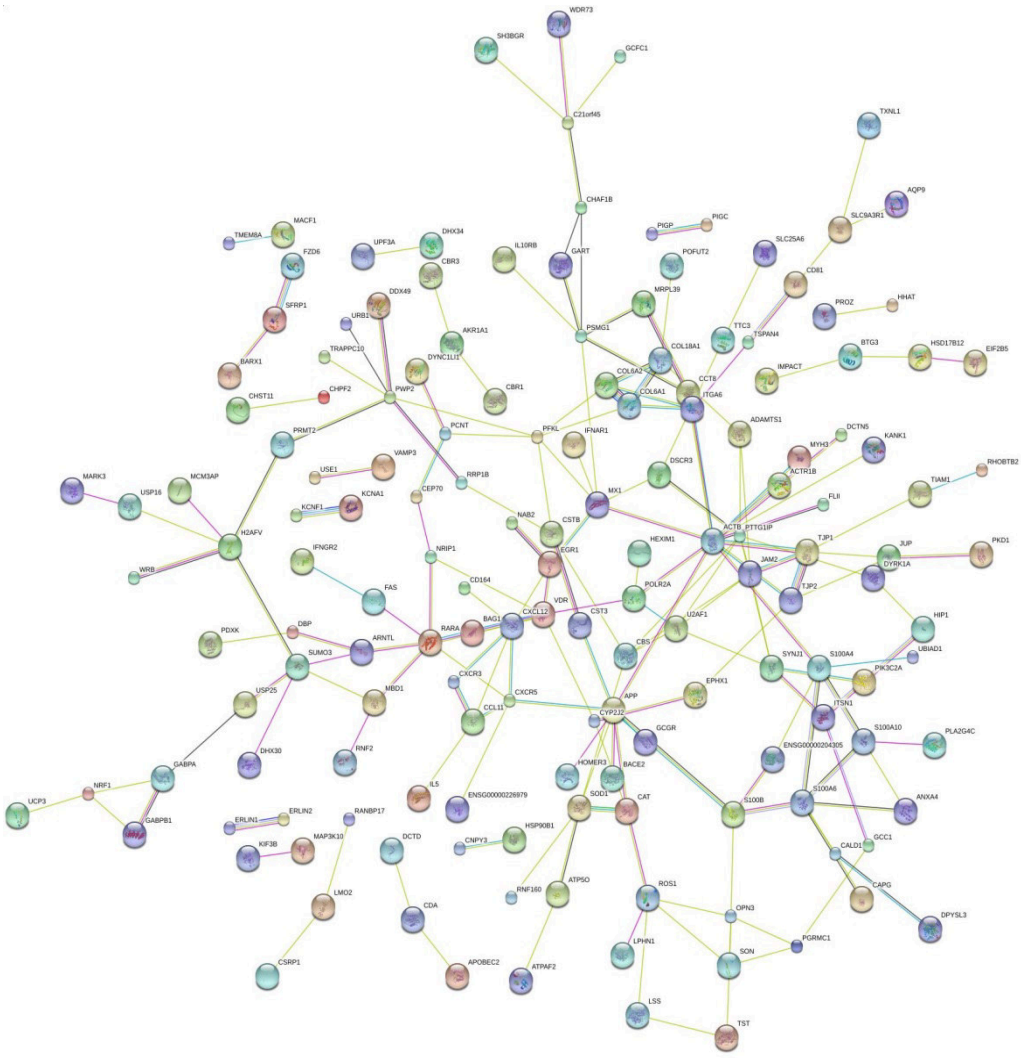

Figure 10. Gene network reconstruction of the 178 genes found dysregulated in the meta-analysis. Connection lines represent the confidence of the physical/genetical interaction between the nodes (genes). Graph obtained with String 9.1 software.

4.3. Enrichment of TF motifs

We further analyzed the promoter sequences of the 107 non-Hsa21 genes dysregulated in the meta-analysis for enrichment of transcription factor (TF) binding sites through the Pscan software [Zambelli et al, 2009] using TF matrices from the Jaspar database. Significant enrichment was computed for the TF motifs showed in **Table 8**. TF enriched for their targets in the differentially expressed list of genes were:

- *EGR1*, an early response transcription factor critical for certain types of memory and learning [Jones et al, 2001; Bozon et al, 2002; Knapska and Kaczmarek, 2004] and its expression is critical for neuronal plasticity and cognition.
- *TFAP2,* which is highly expressed in early neural crest cells, suggesting a key role in their differentiation and development. This is also supported by

the fact that *TFAP2A* knockout mice die perinatally with cranio-abdominoschisis and severe dysmorphogenesis of the face, skull, sensory organs, and cranial ganglia.

- *KLF4,* which regulates the expression of key transcription factors during embryonic development. Plays an important role in maintaining embryonic stem cells and in preventing their differentiation, and is required for establishing the barrier function of the skin and for postnatal maturation and maintenance of the ocular surface. Being involved in the differentiation of epithelial cells, it may also function in skeletal and kidney development. It contributes to the down-regulation of *p53/TP53* transcription.
- *MYCN,* which is a member of the *MYC* family encoding a protein with a basic helix-loop-helix (bHLH) domain. This protein is located in the nucleus and must dimerize with another bHLH protein in order to bind DNA. Amplification of this gene is associated with a variety of tumors, most notably neuroblastomas.
- *NFKB1,* which is a transcription regulator that is activated by various intra- and extra-cellular stimuli such as cytokines, oxidant-free radicals, ultraviolet irradiation, and bacterial or viral products. *NFKB1* is a pleiotropic transcription factor present in almost all cell types. It is the endpoint of signal transduction events initiated by a lot of stimuli related to different biological processes such as inflammation, immunity, differentiation, cell growth, tumorigenesis and apoptosis.
- *GABPA*, a TF mapping to Hsa21 involved in activation of cytochrome oxidase expression and nuclear control of mitochondrial function. It is among the most studied genes involved in DS.

TABLE 8. TRANSCRIPTION FACTORS ENRICHED FOR TARGETS AMONG DYSREGULATED GENES

TF_NAME	MATRIX_ID	Z_SCORE	P_VALUE
EGR1	MA0162.1	3,91755	4,32E-05
TFAP2A	MA0003.1	3,80988	6,80E-05
KLF4	MA0039.2	3,80339	6,91E-05
MYCN	MA0104.2	3,66669	0,000119284
NFKB	MA0061.1	3,65114	0,000125895
SP1	MA0079.2	3,59976	0,000155546
ZFX	MA0146.1	3,30231	0,000467916
PLAG1	MA0163.1	2,96758	0,00146224
NFKB1	MA0105.1	2,86088	0,00207677
MYC	MA0147.1	2,79364	0,00255516
ETS1	MA0098.1	2,20932	0,0134846
RELA	MA0107.1	2,18276	0,0143475
MAX	MA0058.1	2,0039	0,022257
USF1	MA0093.1	1,94528	0,0255732
REL	MA0101.1	1,84356	0,032259
HIF1A::ARNT	MA0259.1	1,72477	0,0419518
GABPA	MA0062.2	1,71586	0,0427221
REST	MA0138.2	1,69181	0,0448553

Table showing transcription factors with targets enriched in the 107 non-Hsa21 dysregulated genes in the meta-analysis. TF matrices retrieved from Jaspar database. P.value cut-off = 0.05.

4.4. Identification of single Hsa21 genes responsible for specific DS phenotypes in public expression data

4.4.1. Analysis of public expression data suggests that NRIP1 affects NEMG expression.

To identify which Hsa21 gene might down-regulate NEMG expression, we screened the Gene Expression Omnibus repository (http://www.ncbi.nlm.nih.gov/geo) for gene expression data related to the modulation of Hsa21 genes. We selected the GSE19836 experiment [De Cegli et al, 2010], a dataset derived from the analysis of a mouse embryonic stem cell (ESC) bank in which 32 orthologs of human chromosome 21 genes, including transcription factors and protein kinases, were individually overexpressed in an inducible manner. We re-analyzed this series by focusing on the mitochondria-related categories and pathways dysregulated by the overexpression of each gene looking for Hsa21 genes that when overexpressed would induce NEMG downregulation. Among the 20 analyzed Hsa21 genes, only *NRIP1*, one of the 7 genes considered "effective" for the expression perturbation in the

manipulated cells [De Cegli et al, 2010], was able to cause NEMG downregulation when over-expressed. Our analysis showed that *NRIP1* over-expression caused a significant enrichment of NEMGs among 298 downregulated genes. The "Mitochondrion" was the most affected Cell Component Gene Ontology (GO) category ($p < 10^{-3}$) (**Fig. 11**), with a cluster of 37 downregulated genes (**Tab. 9**). Motif enrichment analysis, by clustering downregulated genes based on their promoter regions, revealed a significant enrichment ($p < 0.005$) in genes with the *ERRα* motif. Twenty-five downregulated genes, instead of the expected 10, showed promoter regions around the transcription start site containing the *ERRα* motif.

TABLE 9. GENES DOWNREGULATED AFTER NRIP1 OVEREXPRESSION IN THE GSE19836 BELONGING TO THE CELLULAR COMPONENT "MITOCHONDRION" (GO:0005739).

PROBE_SET	GENE_SYMBOL	DESCRIPTION
1434866_x_at	Cpt1a	carnitine palmitoyltransferase 1a, liver
1417956_at	Cidea	cell death-inducing DNA fragmentation factor, alpha subunit-like effector A
1455106_a_at	Ckb	creatine kinase, brain
1428145_at	Acaa2	acetyl-Coenzyme A acyltransferase 2 (mitochondrial 3-oxoacyl-Coenzyme A thiolase)
1427342_at	Fastkd1	FAST kinase domains 1
1454674_at	Fez1	fasciculation and elongation protein zeta 1 (zygin I)
1428516_a_at	Alkbh7	alkB, alkylation repair homolog 7 (E. coli)
1421010_at	Mobp	myelin-associated oligodendrocytic basic protein
1424562_a_at	Slc25a4	solute carrier family 25 (mitochondrial carrier, adenine nucleotide translocator), member 4
1450048_a_at	Idh2	isocitrate dehydrogenase 2 (NADP+), mitochondrial
1418091_at	Tfcp2l1	transcription factor CP2-like 1
1422703_at	Gyk	glycerol kinase
1434499_a_at	Ldhb	lactate dehydrogenase B
1423108_at	Slc25a20	solute carrier family 25 (mitochondrial carnitine/acylcarnitine translocase), member 20
1416457_at	Ddah2	dimethylarginine dimethylaminohydrolase 2
1429021_at	Epha4	Eph receptor A4
1451504_at	Chchd3	coiled-coil-helix-coiled-coil-helix domain containing 3
1433855_at	Abat	4-aminobutyrate aminotransferase
1451744_a_at	Ptgr2	prostaglandin reductase 2
1439947_at	Cyp11a1	cytochrome P450, family 11, subfamily a, polypeptide 1
1418709_at	Cox7a1	cytochrome c oxidase, subunit VIIa 1
1431980_a_at	As3mt	arsenic (+3 oxidation state) methyltransferase
1425140_at	Lactb2	lactamase, beta 2
1419656_at	Slc25a36	solute carrier family 25, member 36
1427705_a_at	Nfkb1	nuclear factor of kappa light polypeptide gene enhancer in B cells 1, p105

1455991_at	Ccbl2	cysteine conjugate-beta lyase 2
1428140_at	Oxct1	3-oxoacid CoA transferase 1
1453738_at	C330018D20Rik	RIKEN cDNA C330018D20 gene
1451084_at	Etfdh	electron transferring flavoprotein, dehydrogenase
1456711_at	4932425I24Rik	RIKEN cDNA 4932425I24 gene
1417089_a_at	Ckmt1	creatine kinase, mitochondrial 1, ubiquitous
1418288_at	Lpin1	lipin 1
1416023_at	Fabp3	fatty acid binding protein 3, muscle and heart
1418640_at	Sirt1	sirtuin 1 (silent mating type information regulation 2, homolog) 1 (S. cerevisiae)
1434996_at	Slc25a16	solute carrier family 25 (mitochondrial carrier, Graves disease autoantigen), member 16
1424056_at	Usp48	ubiquitin specific peptidase 48
1437974_a_at	Hk1	hexokinase 1

Among the other Hsa21 genes which possibly interfere with mitochondrial pathways, neither *DYRK1A*, nor *RCAN1*, nor *GABPA*, all considered "silent" genes [De Cegli et al, 2010], caused NEMG downregulation when overexpressed.

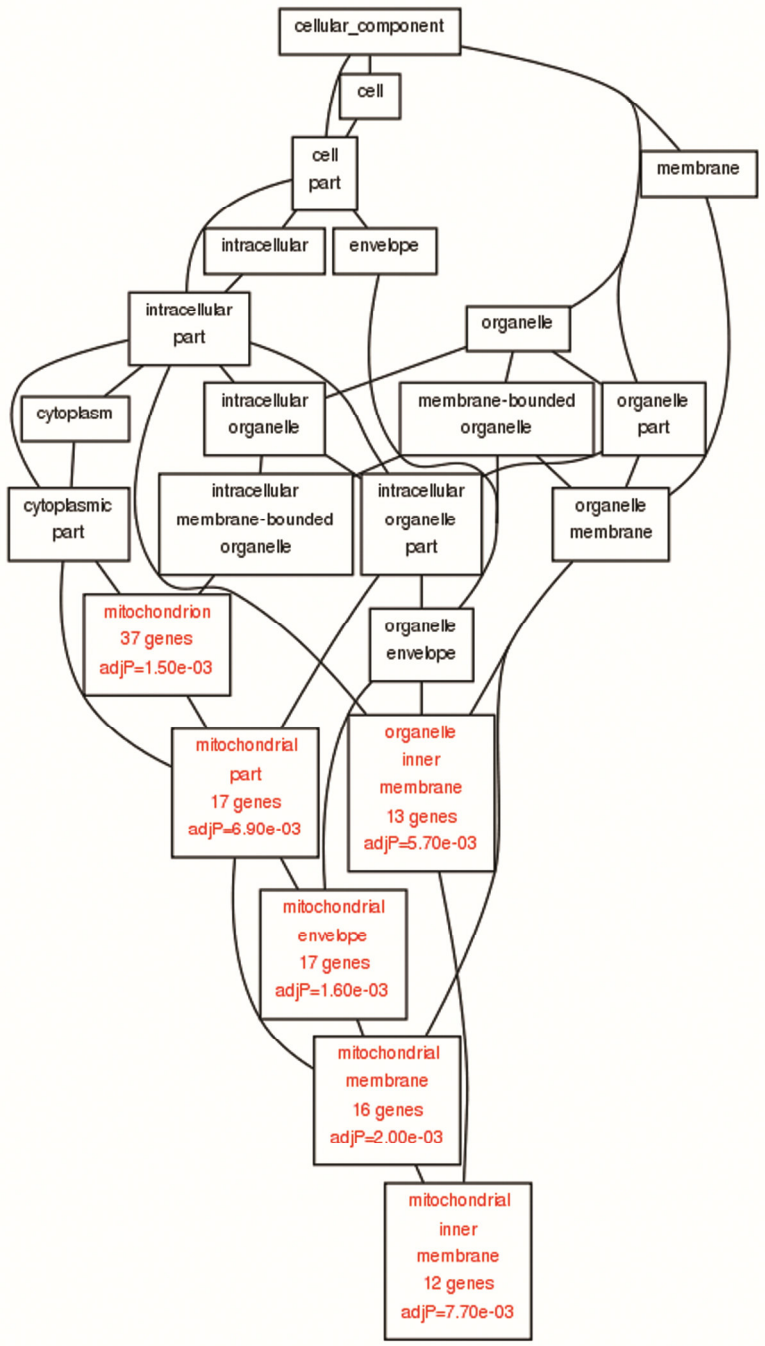

Figure 11. GO terms tree of the cellular component categories enriched in the 298 downregulated genes found in the reanalysis of GEO GSE19836

4.4.2. Modulation of NRIP1 and PGC-1α expression dysregulates the same NEMGs downregulated in DS fetal hearts.

To investigate whether the sets of genes regulated by *NRIP1* and/or *PGC-1α* showed any overlapping to the NEMGs downregulated in DS fetal hearts [Conti et al, 2007], we performed a meta-analysis comparing 3 sets of gene expression data, SET1, SET2 and SET3. SET1 included 123 genes which were both upregulated after *NRIP1* silencing and downregulated after *NRIP1* re-expression in mouse adipocytes [Powelka et al, 2006]. SET2 included 129

genes which were upregulated after *PGC-1α* induction in SAOS2 cells (human osteoblast-like cells) [Schreiber et al, 2004]. SET3 included the 70 genes downregulated in DS fetal heart tissues [Conti et al, 2007] belonging to the "mitochondrion" GO category. The comparison was aimed at identifying genes consistently dysregulated across these studies.

The Venn diagram shows that NEMGs in SET3, which were downregulated in DS fetal hearts, overlap with both SET1 and SET2 (**Fig. 12**). The three sets of genes overlap each other for at least 25 genes. Fifteen genes are consistently dysregulated across all 3 experiments (Fig. 1B). Most of these genes are included in the electron transport chain, mainly in complex I, and in oxidative phosphorylation pathways. It is also interesting to note that 42 genes overlap between the sets of genes inversely regulated by *NRIP1* and *PGC-1α* (SET1 and SET2) in agreement with the antagonistic functions of the two co-regulators [Fritah et al, 2010]. These results support a role of *NRIP1* in downregulating NEMGs in DS fetal hearts.

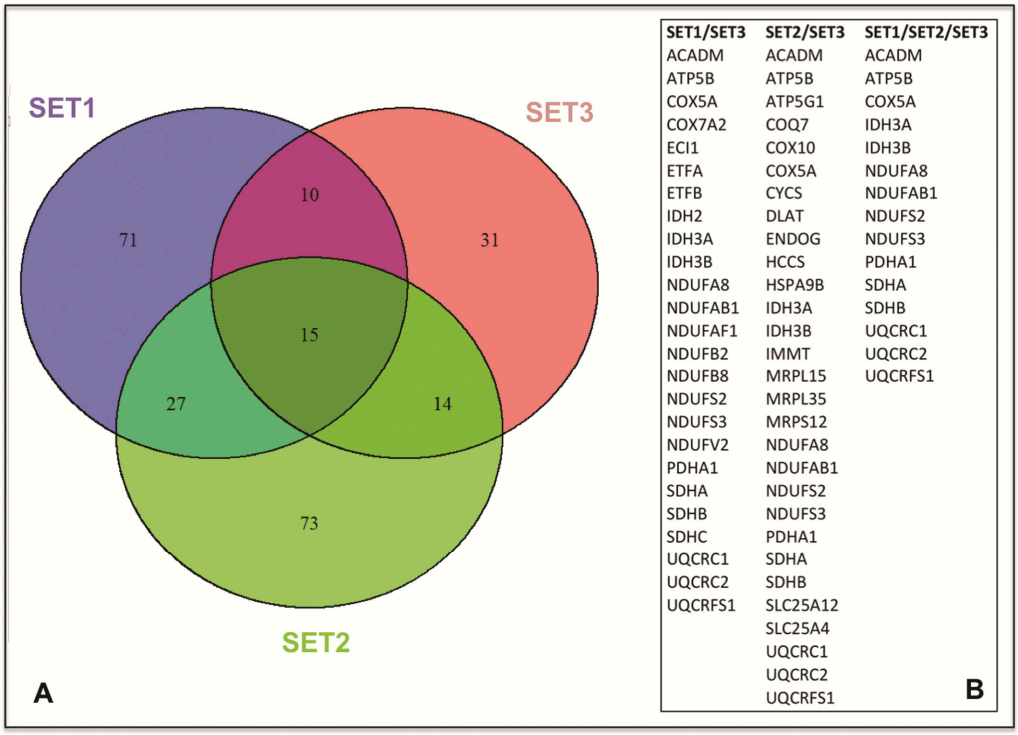

SET1/SET3	SET2/SET3	SET1/SET2/SET3
ACADM	ACADM	ACADM
ATP5B	ATP5B	ATP5B
COX5A	ATP5G1	COX5A
COX7A2	COQ7	IDH3A
ECI1	COX10	IDH3B
ETFA	COX5A	NDUFA8
ETFB	CYCS	NDUFAB1
IDH2	DLAT	NDUFS2
IDH3A	ENDOG	NDUFS3
IDH3B	HCCS	PDHA1
NDUFA8	HSPA9B	SDHA
NDUFAB1	IDH3A	SDHB
NDUFAF1	IDH3B	UQCRC1
NDUFB2	IMMT	UQCRC2
NDUFB8	MRPL15	UQCRFS1
NDUFS2	MRPL35	
NDUFS3	MRPS12	
NDUFV2	NDUFA8	
PDHA1	NDUFAB1	
SDHA	NDUFS2	
SDHB	NDUFS3	
SDHC	PDHA1	
UQCRC1	SDHA	
UQCRC2	SDHB	
UQCRFS1	SLC25A12	
	SLC25A4	
	UQCRC1	
	UQCRC2	
	UQCRFS1	

Figure 12. Comparison of NEMGs downregulated in DS fetal hearts with those dysregulated by NRIP1 and/or PGC-1α. A. Venn Diagram showing overlapping amongst the 3 sets of data. Out of the 70 mitochondrial genes that are downregulated in DS fetal hearts (SET3), 25 overlap the list of NRIP1 regulated genes (SET1), and 29 overlap the list of PGC-1α regulated genes (SET2). B. List of mitochondria-related genes overlapping in the 3 sets of data.

4.4.3. Promoter analysis of genes downregulated in DS fetal hearts shows enrichment for transcription factors repressed by NRIP1.

It has been recently demonstrated that the transcription factors *NRF1* and *ERRα* and their targets are repressed by Hsa21 gene *NRIP1* and induced by *PGC-1α* in a dose dependent manner in neonatal rat cardiomyocytes [Chen et al, 2012]. The promoter regions from -450bp to +50bp of mitochondrial genes downregulated in DS heart tissues were analyzed in order to recognize DNA binding motifs for both *NRF1* and *ERRα* matrices by PSCAN software [Zambelli et al, 2009]. The list of downregulated genes was ranked according to the prediction of binding affinity of their promoter regions to *NRF1* and *ERRα* binding sites with a cut-off of affinity score = 0.80 and p-value < 0.003. Interestingly, among the 65 mitochondrial genes found downregulated in fetal hearts, 40% of these genes have consensus DNA binding sites for the nuclear respiratory factor *NRF1* in their 5' flanking regions (**Tab. 10**), and 20% of them show a high affinity for the estrogen-related receptor *ERRα* (**Tab. 11**).

TABLE 10. MITOCHONDRIAL GENES DOWNREGULATED IN DS HEART TISSUES WITH NRF1 BINDING SITE IN THEIR PROMOTER REGIONS.

GENE NAME	SCORE	PROMOTER REGION	BINDING SITE
ECGF1	1,00	-13	CGCATGCGCA
SCO2	1,00	-14	CGCATGCGCA
PIN4	0,98	-282	CGCGTGCGCA
IDH3A	0,97	-24	CGCTTGCGCA
UQCRC1	0,96	7	CGCTTGCGCG
NDUFB8	0,96	-9	CACATGCGCA
RPL10	0,96	-12	CACATGCGCA
ENDOG	0,91	-161	CGCCTGCGCA
FPGT-TNNI3K	0,91	23	CGCATGCGCC
SDHA	0,91	-88	CGCCTGCGCA
UQCRC2	0,91	-264	CGCATGCGCC
ETFB	0,90	-9	CGCCTGCGCG
GLUD1	0,90	-31	CGCCTGCGCG
NDUFAB1	0,90	-43	CGCCTGCGCG
CYCS	0,90	-208	CGCAAGCGCA
SDHB	0,90	-65	CGCATGCCCA
HSPA9	0,89	-171	CGCATGTGCG
MRPL15	0,88	-52	CGCGCGCGCA
SLC25A12	0,88	-63	CGCGTGCGGA
VDAC1	0,88	-59	TGCGTGCGCA
HCCS	0,88	-25	CGCGTGCCCG
IDH3B	0,87	-166	TGCTTGCGCA

IDH2	0,86	-262	CGCTTGCGAG
COX4NB	0,84	-292	CACGTCCGCA
COQ7	0,81	-363	CGCCCGCGCA
ETFA	0,81	-71	CGCCTGCCCA
GOT1	0,81	-395	CGCCCGCGCA
NDUFA13	0,81	-265	GGCCTGCGCA
NDUFS2	0,81	-78	CGCCTGCGTA
PDHA1	0,81	-165	CGCAGGCGCT
DLAT	0,80	33	AGCCTGCGCG
GCSH	0,80	-18	CGCCTCCGCG
MOSC2	0,80	-6	AGCCTGCGCG
AK2	0,80	-303	CCCACGCGCA

NRF1 target genes are sorted with a cut-off affinity score = 0.80

TABLE 11. MITOCHONDRIAL GENES DOWNREGULATED IN DS HEART TISSUES WITH ERRα BINDING SITE IN THEIR PROMOTER REGIONS.

GENE NAME	SCORE	PROMOTER REGION	BINDING SITE
HSPA9	0,95	-66	GACTCAAGGTCACA
MOSC2	0,94	-174	CGCTGAAGGTCATG
SDHA	0,93	-390	TTGTGGAGGTCACA
TXN2	0,92	-298	ATCACGAGGTCAAA
MRPL35	0,92	-231	ATCACAAGGTCAGG
BDH1	0,91	-193	GGATCAAGGACAGA
NDUFB8	0,90	-208	AGAAAAAGGACACA
COX7A2	0,90	-48	TCGAAAAGGTCAGG
SDHB	0,90	-446	ATCACGAGGTCAGG
DLAT	0,89	-428	AACTGAAGGTGACA
NDUFAB1	0,88	-417	AAAAAAAGGACAAA
COQ7	0,88	-108	TCGAAGAGGTCACG
MRPS12	0,88	23	ACCTAAAGGTGAGG
TIMM23	0,87	-6	CCCGGAAGGTCAGC
ETFA	0,87	-296	ACCCCGAGGTCAGC
ATP5B	0,87	-289	TGATCTAGGTGACA
IDH3B	0,86	-153	GTGGGGAGGTCATG
ECI1	0,86	-292	AGCTCGCGGTCACG
MRPL15	0,85	-112	ACTAAAAGGACAAC
ETFB	0,85	-449	ACATGGAGGTGAAG
COX4NB	0,85	-94	GCACGGAGGTCACC
CYCS	0,84	-367	ACCTAGAGGTCTCC
TNNI3K	0,84	-329	TTTTCAAGATCATT
UQCRFS1	0,84	-236	ATCTCTAGGTCTTC

SLC25A4	0,83	-205	GTTTAAAGGGCACA
GOT1	0,83	-405	TGGTCAAGGTCGCC
PIN4	0,83	-99	TCTTATTGGTCAGA
SCO2	0,81	-258	CCATGGCGGTCAGC
NFS1	0,81	-92	CGAGCGAGGTGAGG
CKMT2	0,81	-437	GGAAGGAGGTCCCT
IMMT	0,80	-41	ATATCCAGCTCATA
DLST	0,80	-191	TCCTGAAGGTGTAT
MIPEP	0,80	-265	GCCTGAAGGAGAAG
COX10	0,80	-14	GCCTGAAGGACTTC

ERRα target genes are sorted with a cut-off affinity score = 0.80

4.5. Validation of NRIP1 role in DS mitochondrial dysfunction

4.5.1. NRIP1 attenuation by siRNA affects NEMG expression in DS-HFFs.

We previously demonstrated that *NRIP1* is upregulated in human fetal fibroblasts from DS fetuses (DS-HFFs) [Piccoli et al, 2013].

To test the hypothesis that *NRIP1* overexpression perturbs mitochondrial function and that this effect is associated with *PGC-1α* downregulation, we performed silencing experiments of *NRIP1* gene in DS-HFFs. Seventy-two hours after transfection of a specific SMART pool of siRNAs in DS-HFFs, an inverse correlation between *NRIP1* and *PGC-1α* expression, in a siRNA dosage-dependent way, was demonstrated by qRT-PCR (**Fig. 13**).

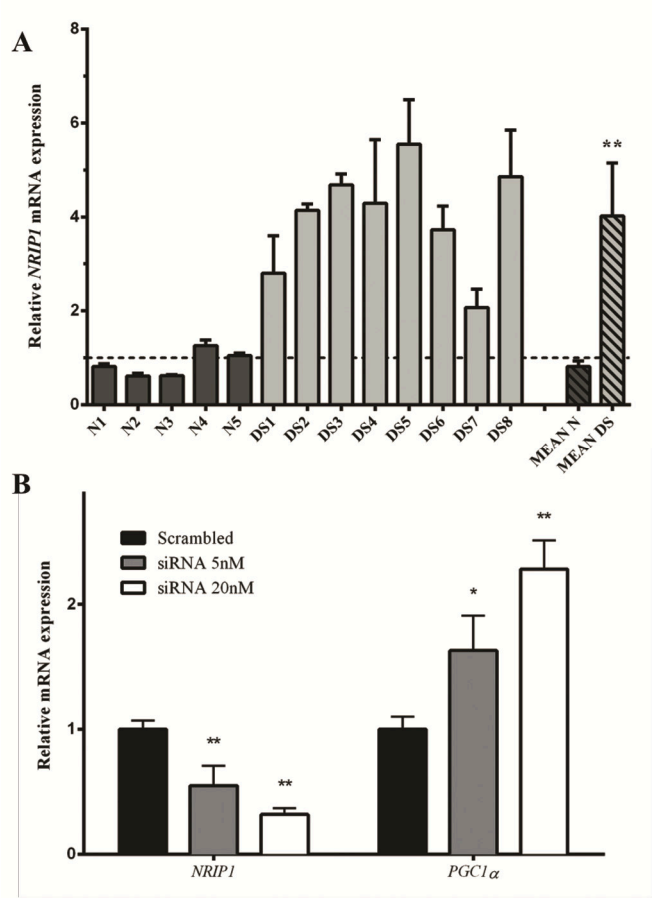

Figure 13. NRIP1 and PGC-1α expression in NRIP1-silenced DS-HFFs. **A**. NRIP1 mRNA expression level in euploid cells (N1-N5), and in trisomic (DS1-DS8) HFF lines used for silencing experiments. For each sample, values represent the average determination ± SEM for 3 qRT-PCR experiments. A pool of euploid cells was used as calibrator. ** = $p<10^{-4}$. P-value expresses significance for euploid vs trisomic comparisons. **B**. NRIP1 and PGC-1α expression levels in trisomic cells transfected with a scrambled siRNA and with a NRIP1-specific SMART pool of siRNAs. A decrease in NRIP1 expression level corresponds to an increase on PGC-1α expression level in a siRNA-dependent way. Values represent the average determination ± SEM for 8 NRIP1-silenced DS-HFFs carried out in triplicate. * = $p<0.05$, ** = $p<0.01$. P-values express significance for NRIP1-silenced vs scrambled comparisons.

By immunofluorescence analysis we demonstrated that the *NRIP1* fluorescent signal was more intense over nuclei of DS-HFFs (**Fig. 14B**) with respect to euploid HFFs (**Fig. 14A**) indicating a higher concentration of the *NRIP1* protein in trisomic cells. In DS-HFFs treated with siRNAs, *NRIP1* fluorescent signal was significantly decreased in a siRNA dosage-dependent way (**Fig. 14D-E**).

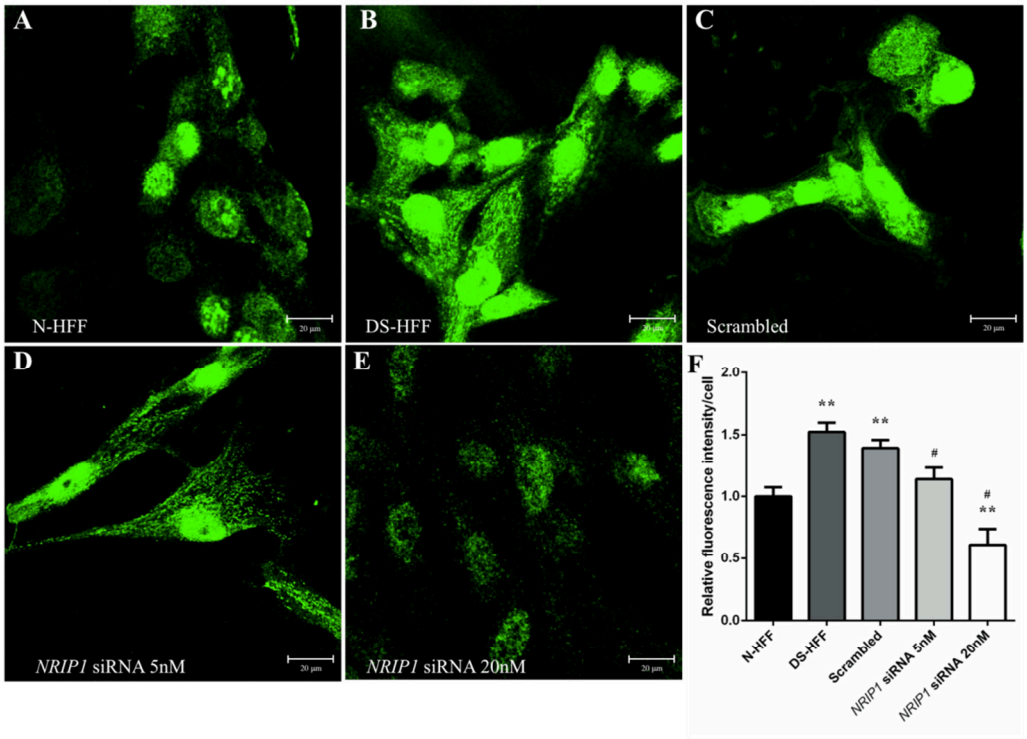

Figure 14. **NRIP1 immunofluorescence in NRIP1-silenced DS-HFFs**. Representative images of NRIP1 immunofluorescence analysis in (**A**) euploid cells, (**B**) trisomic cells, and trisomic cells transfected (**C**) with a scrambled siRNA, (**D**) with 5nM NRIP1 siRNA and (**E**) 20nM NRIP1 siRNA. **F**. Semi quantitative analysis of the immunodetected signals, by ImageJ software (means ± SEM of 3 assayed samples). Fifty randomly selected, different cells for each sample/experimental condition were analyzed. A decrease of the fluorescent signal is observed in silenced vs scrambled DS-HFFs. Signal from 5nM NRIP1 siRNA transfected cells is comparable with euploid HFFs. Statistical significance: ** = $p<0.01$ for trisomic vs euploid comparisons; # = $p<0.05$ for NRIP1-silenced vs scrambled comparisons.

To determine the effects of *NRIP1* attenuation by siRNA on other mitochondria-related genes, we compared the expression of 7 genes in silenced vs scrambled cells using qRT-PCR. Five out of 7 analyzed genes were significantly upregulated after *NRIP1* attenuation by siRNA (**Fig. 15**). Also the average mtDNA content, evaluated by measuring the *D-LOOP/ACTIN* ratio, was increased after *NRIP1* attenuation by siRNA and consequent *PGC-1α* overexpression.

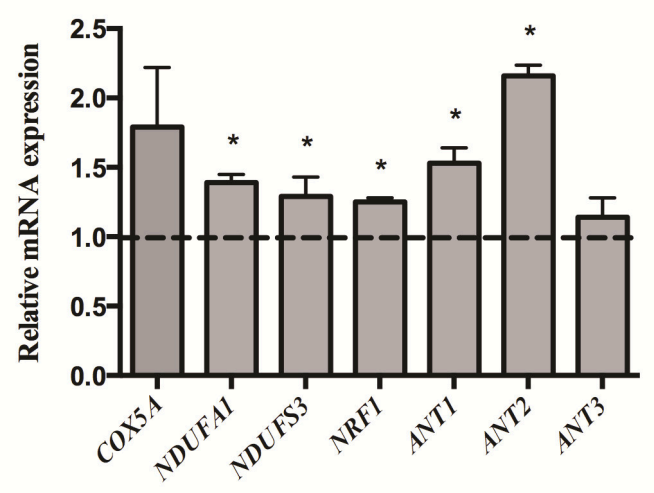

Figure 15. Mitochondria-related gene expression in NRIP1-silenced DS-HFFs. Relative mRNA expression of 7 mitochondria-related genes was measured in NRIP1-silenced DS-HFFs vs scrambled transfected DS-HFFs. Five out of the 7 genes show a significant increase in their expression level. Values represent the average determination ± SEM for 3 DS-HFF samples carried out in triplicate. A pool of scrambled transfected euploid cells was used as calibrator. * = $p<0.05$. P-value express statistical significance for NRIP1-silenced vs scrambled comparisons.

4.5.2. Mitochondrial function is improved in DS-HFFs after NRIP1 attenuation by siRNA.

ROS production was measured by confocal microscopy imaging of cells treated with the redox-sensitive fluorescent probe dichlorofluorescein (DCF). Seventy-two hours after transfection with *NRIP1* siRNA, DCF-related fluorescence was lower with respect to scrambled DS-HFFs. Semi-quantitative analysis of fluorescent signals demonstrated that, on an average basis, the ROS-related DCF fluorescence decreased up to 50% in a siRNA dosage-dependent manner (**Fig. 16**).

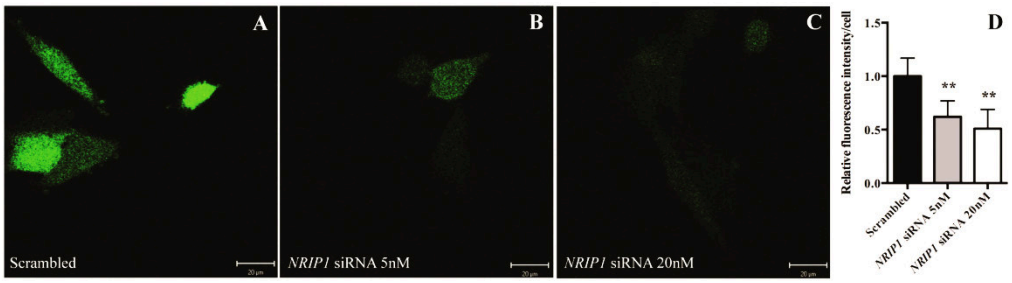

Figure 16. ROS decrease in NRIP1-silenced DS-HFFs. Confocal microscopy live cell imaging of the DCF fluorescence in transfected DS-HFFs: (**A**) scrambled, (**B**) 5nM NRIP1 siRNA and (**C**) 20nM NRIP1 siRNA. **D**. Semi-quantitative analysis of the DCF-related fluorescence, by ImageJ software (means ± SEM of 3 assayed samples). Fifty randomly selected, different cells for each sample/experimental condition were analyzed. A significant decrease of DCF-related fluorescence is observed after NRIP1 attenuation in a siRNA-dependent way. ** = $p<10^{-4}$. P-value express statistical significance for NRIP1-silenced vs scrambled comparisons.

Then, to confirm even further that *NRIP1* attenuation by siRNA improves mitochondrial function, we incubated trisomic silenced cells with the MitoTracker Red dye, a reagent that stains mitochondria in live cells and whose accumulation is dependent upon membrane potential. A significant 50% increase of the MitoTracker Red-related fluorescence was observed in *NRIP1*-silenced cells when compared with scrambled controls, thus indicating an increase in respiratory activity (**Fig. 17**).

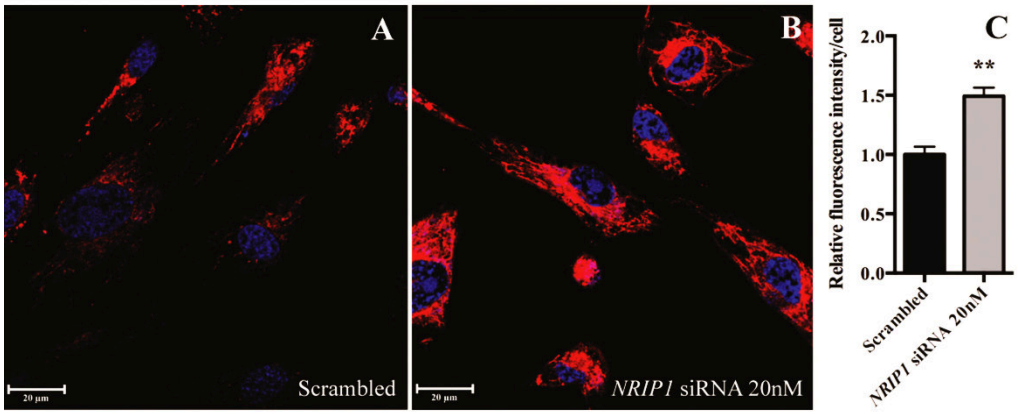

Figure 17. Mitochondrial activity in DS NRIP1-silenced DS-HFFs. Confocal microscopy live cell imaging of the Mitotracker fluorescence in transfected DS-HFFs: (**A**) scrambled and (**B**) with 20nM NRIP1 siRNA. C. Semi quantitative analysis of the Mitotracker-related fluorescence, by ImageJ software (means ± SEM of 5 assayed samples). Fifty randomly selected, different cells for each sample/experimental condition were analyzed. An increase of Mitotracker related fluorescence is observed in NRIP1-silenced DS-HFFs. ** = $p<0.005$. P-value express statistical significance for NRIP1-silenced vs scrambled comparisons.

ATP content was strongly increased in silenced DS-HFFs (**Fig. 18**). We used a chimera of the ATP-sensitive photoprotein luciferase specifically targeted to mitochondria (mtLuc) to obtain a dynamic monitoring of $[ATP]_m$. Since basal ATP content is highly dependent on the abundance of transfected luciferase, we determined the exact amount of the luciferase transduced under our experimental conditions through an immunoblot assay. We found that the levels of luciferase protein transduced in *NRIP1*-silenced DS-HFFs were comparable with those detected in control cells transfected with the non-targeting scrambled siRNA (**Fig. 19**).

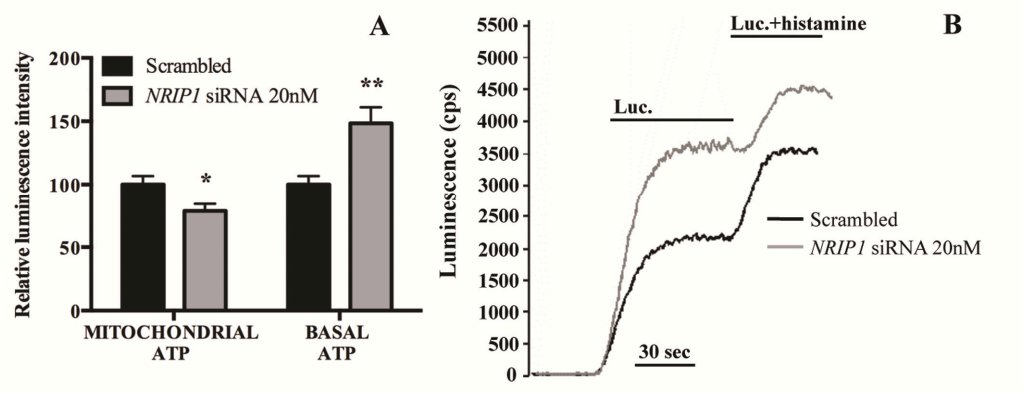

Figure 18. Mitochondrial ATP measurement. **A**. Barplot of the mitochondrial ATP content and of the basal ATP content in scrambled and NRIP1 siRNA-transfected DS-HFFs. **B**. The traces show mitochondrial $[ATP]_m$ changes elicited by mitochondrial $[Ca^{2+}]$ increase in cells perfused with 100µM histamine as agonist. mtLuc luminescence data are expressed as a percentage of the initial value ± SEM (n=4). The traces are representative of four independent experiments. * = p=0.05, ** = $p=10^{-4}$. P-values express statistical significance for NRIP1-silenced vs scrambled comparisons.

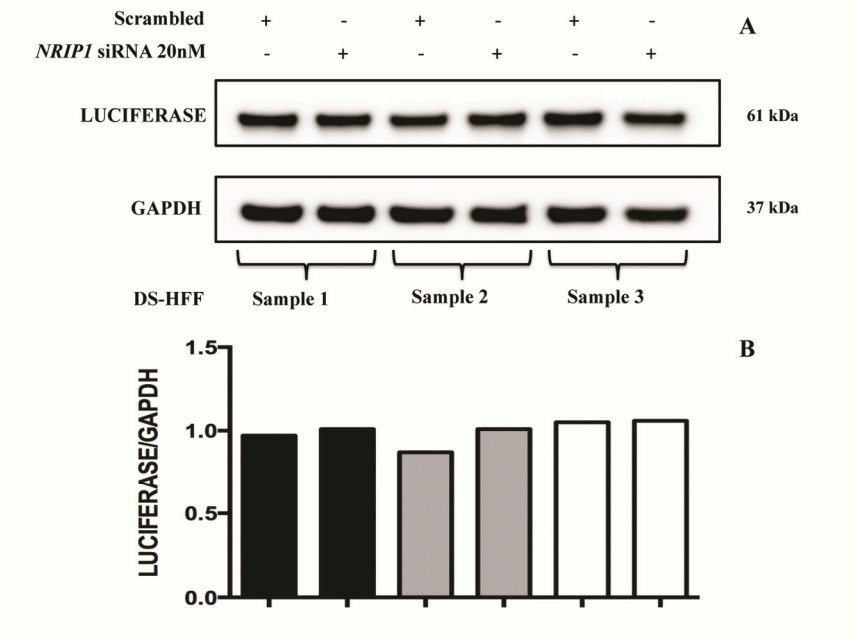

Figure 19. Luciferase expression following NRIP1 attenuation by siRNA. **A**. Representative immunoblot of luciferase protein in 3 NRIP1-silenced or scrambled DS-HFFs transfected with a luciferase–encoding plasmid specifically targeted to mitochondria (mtLuc) and cultured in complete medium for 72h. **B**. Quantification of luciferase accumulation by LUCIFERASE/GAPDH ratio.

4.6. Analysis of public expression data suggest that RUNX1 affects ECM gene expression

To identify which Hsa21 gene might upregulate ECM gene expression, we screened the same GEO series used in the previous part of the study [GSE19836, De Cegli et al, 2010]. We reanalyzed this series by focusing on ECM-related categories and pathways dysregulated by the overexpression of each gene, looking for Hsa21 genes that when expressed would induce ECM upregulation. Among the 20 analyzed Hsa21 genes, only the Runt-related transcription factor 1 (*RUNX1*), was able to cause ECM gene upregulation when overexpressed. Our analysis showed that *RUNX1* overexpression caused a significant enrichment among the 573 upregulated genes (logFC>0.3, Adj.P-val <0.01). The "extracellular matrix" (GO:0031012) was the most affected Cell Component Gene Ontology category (P-val = 3.00e-04) (**Fig. 20**), with a cluster of 32 upregulated genes (**Tab. 12**). No other Hsa21 transcription factor or regulator under analysis showed a similar effect.

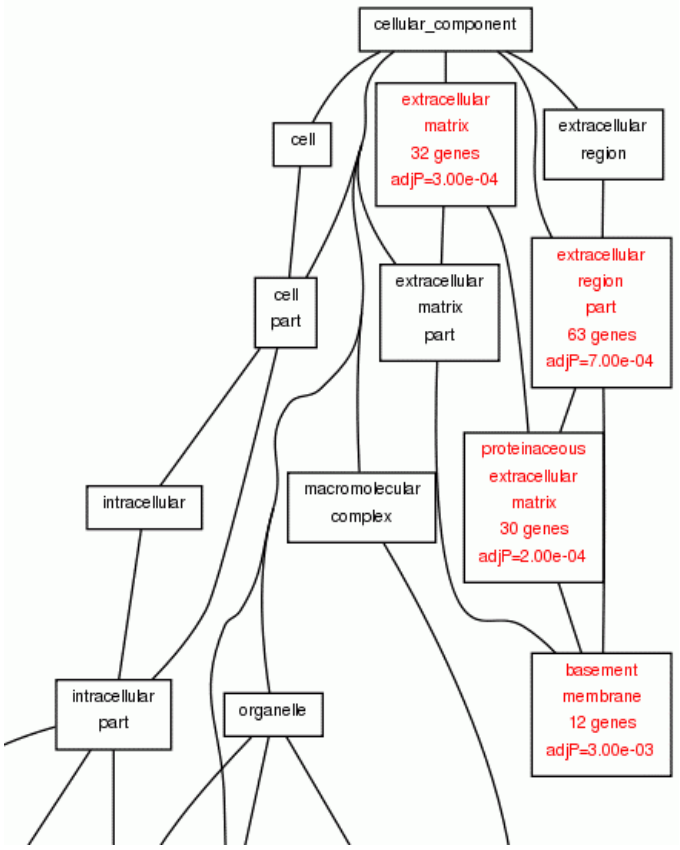

Figure 20. GO terms tree of the cellular component categories enriched among the genes found downregulated in the reanalysis of GEO GSE19836 series

TABLE 12. GENES UPREGULATED AFTER RUNX1 OVEREXPRESSION IN THE GSE19836 BELONGING TO THE CELLULAR COMPONENT "EXTRACELLULAR MATRIX" (GO: 0031012).

PROBE_SET	GENE_SYMBOL	DESCRIPTION
1455965_at	Adamts4	a disintegrin-like and metallopeptidase (reprolysin type) with thrombospondin type 1 motif, 4
1416298_at	Mmp9	matrix metallopeptidase 9
1416531_at	Gsto1	glutathione S-transferase omega 1
1419613_at	Col7a1	collagen, type VII, alpha 1
1450704_at	Ihh	Indian hedgehog
1418910_at	Bmp7	bone morphogenetic protein 7
1418477_at	Matn1	matrilin 1, cartilage matrix protein
1424131_at	Col6a3	collagen, type VI, alpha 3
1437277_x_at	Tgm2	transglutaminase 2, C polypeptide
1419573_a_at	Lgals1	lectin, galactose binding, soluble 1
1426642_at	Fn1	fibronectin 1
1420569_at	Chad	Chondroadherin
1415935_at	Smoc2	SPARC related modular calcium binding 2
1420855_at	Eln	Elastin
1450673_at	Col9a2	collagen, type IX, alpha 2
1416589_at	Sparc	secreted acidic cysteine rich glycoprotein
1460187_at	Sfrp1	secreted frizzled-related protein 1
1426231_at	Vit	Vitrin
1419527_at	Comp	cartilage oligomeric matrix protein
1419091_a_at	Anxa2	annexin A2
1438312_s_at	Ltbp3	latent transforming growth factor beta binding protein
1449335_at	Timp3	tissue inhibitor of metalloproteinase 3
1417389_at	Gpc1	glypican 1
1416740_at	Col5a1	collagen, type V, alpha 1
1421279_at	Lamc2	laminin, gamma 2
1448870_at	Ltbp1	latent transforming growth factor beta binding protein
1452106_at	Npnt	Nephronectin
1460227_at	Timp1	tissue inhibitor of metalloproteinase 1
1448598_at	Mmp17	matrix metallopeptidase 17
1420891_at	Wnt7b	wingless-related MMTV integration site 7B
1422571_at	Thbs2	thrombospondin 2

4.6.1. Promoter analysis of genes upregulated in DS fetal hearts shows enrichment for ECM genes induced by RUNX1.

We, therefore, performed a transcription factor-binding site (TFBS) analysis on the list of ECM genes upregulated in DS fetal hearts with the PSCAN software, in order to scan promoters of these genes for consensus sequences according to JASPAR database. This analysis identified *RUNX1* as transcription factor with high binding specificity with ECM genes upregulated in DS hearts (**Tab. 13**).

About 60% of ECM genes overexpressed in DS hearts shows consensus sequences for *RUNX1*.

Molecular and functional studies are currently in progress in order to evaluate the effects of *RUNX1*-upregulation on ECM gene expression and on cellular phenotype in euploid and trisomic fetal skin fibroblasts.

TABLE 13. ECM GENES UPREGULATED IN DS HEARTS WITH CONSENSUS SEQUENCE FOR RUNX1

GENE_SYMBOL	RUNX1_MATRIX_ SCORE	DESCRIPTION
ECM2	2,498	extracellular matrix protein 2, female organ and adipocyte specific [Source:HGNC Symbol;Acc:3154]
COL6A2	2,107	collagen, type VI, alpha 2 [Source:HGNC Symbol;Acc:2212]
GPC3	1,987	glypican 3 [Source:HGNC Symbol;Acc:4451]
APP	1,823	amyloid beta (A4) precursor protein [Source:HGNC Symbol;Acc:620]
ADAMTS5	1,567	ADAM metallopeptidase with thrombospondin type 1 motif, 5 [Source:HGNC Symbol;Acc:221]
ITGB4	1,481	integrin, beta 4 [Source:HGNC Symbol;Acc:6158]
COL18A1	1,262	collagen, type XVIII, alpha 1 [Source:HGNC Symbol;Acc:2195]
MMP11	1,254	matrix metallopeptidase 11 (stromelysin 3) [Source:HGNC Symbol;Acc:7157]
FLRT2	0,958	fibronectin leucine rich transmembrane protein 2 [Source:HGNC Symbol;Acc:3761]
APP	0,841	amyloid beta (A4) precursor protein [Source:HGNC Symbol;Acc:620]
COL3A1	0,766	collagen, type III, alpha 1 [Source:HGNC Symbol;Acc:2201]
DCN	0,754	decorin [Source:HGNC Symbol;Acc:2705]
ADAMTS7	0,714	ADAM metallopeptidase with thrombospondin type 1 motif, 7 [Source:HGNC Symbol;Acc:223]
COLEC10	0,710	collectin sub-family member 10 (C-type lectin) [Source:HGNC Symbol;Acc:2220]
WNT4	0,687	wingless-type MMTV integration site family, member 4 [Source:HGNC Symbol;Acc:12783]
HAPLN1	0,656	hyaluronan and proteoglycan link protein 1 [Source:HGNC Symbol;Acc:2380]
COL5A1	0,594	collagen, type V, alpha 1 [Source:HGNC Symbol;Acc:2209]
DCN	0,516	decorin [Source:HGNC Symbol;Acc:2705]
C1QTNF3	0,377	C1q and tumor necrosis factor related protein 3 [Source:HGNC Symbol;Acc:14326]
LAMA4	0,346	laminin, alpha 4 [Source:HGNC Symbol;Acc:6484]
FBLN1	0,331	fibulin 1 [Source:HGNC Symbol;Acc:3600]
COL9A3	0,316	collagen, type IX, alpha 3 [Source:HGNC Symbol;Acc:2219]

APP	0,245	amyloid beta (A4) precursor protein [Source:HGNC Symbol;Acc:620]
VCAN	0,215	versican [Source:HGNC Symbol;Acc:2464]
COL13A1	0,164	collagen, type XIII, alpha 1 [Source:HGNC Symbol;Acc:2190]
COL14A1	0,121	collagen, type XIV, alpha 1 [Source:HGNC Symbol;Acc:2191]
DTL	0,111	denticleless E3 ubiquitin protein ligase homolog (Drosophila) [Source:HGNC Symbol;Acc:30288]
ASPN	0,026	asporin [Source:HGNC Symbol;Acc:14872]

Data obtained with PSCAN software

5. DISCUSSION

In this study we have used multiple strategies of meta-analysis of public expression data in order to address possible roles of Hsa21 genes involved in DS phenotypes. We first performed a meta-analysis merging data from microarray experiments and comparing DS samples versus controls. This meta-analysis highlighted genes that are consistently dysregulated in different DS tissue including brain, heart and different DS cell cultures.

We used a data integration approach of DS-related Affymetrix expression arrays starting from feature-level extraction output (FLEO) files (CEL files). Working with FLEO files, indeed, allows for better standardization of information and the incorporation of data from unpublished studies, even if it requires significant effort to acquire and manage the datasets due to increased data complexity [Ramasamasy et al, 2008]. In addition, our approach allowed to eliminate bias due to specific algorithms used in the original studies, and to permit consistent handling of all datasets. FLEO files are likely to be available, especially for newer studies, because the widely supported MIAME requirements [Brazma et al, 2001] now ask authors to make the FLEO data available in public microarray repositories.

A great part of meta-analysis studies, and the only existing DS-related meta-analysis study [Vilardell et al, 2011], were conducted on published gene list (PGL) or on gene expression data matrix (GEDM). PGL represents the genes that are considered as differentially expressed by the authors in a given study and are often presented in the main or supplementary text of microarray-based studies, and are thus easy to obtain. Unfortunately, PGLs are of limited use for meta-analysis since they represent only a subset of the genes actually studied, and information from many genes will be completely absent. Furthermore, PGLs depend heavily on the preprocessing algorithm, the analysis method, the significance threshold, and the annotation builds used in the original study, all of which usually differ between studies [Suárez-Fariñas et al, 2005]. Thus individual patient-level data (IPD), which for microarrays represents the measurement for every probe in every hybridization, are far more useful. The gene expression data matrix (GEDM) represents the gene expression summary for every probe and sample and is thus ideally suited as input for meta-analysis. Published GEDMs, however, are unsuitable for meta-analysis because they depend on the choice of the preprocessing algorithms used, which may produce non-combinable results.

We have chosen a meta-analysis approach suitable to avoid or at least reduce the problem of “publication bias”, which is a consequence of selectively publishing statistically significant and favorable results [Dickersin et al, 1992]. Indeed, within a single-study microarray analysis, the particular choice of down-stream analysis may lead to different results depending on the objective

of the study [Mondry et al, 2007]. We do not expect to find a publication bias at a gene level in a given study because of the discovery-driven and high-density nature of microarrays.

Moreover, we have focused on the Affymetrix platform in order to reduce variance arising from platform inconsistencies. Despite this, non-biological experimental variation or “batch effects" are commonly observed across multiple batches of microarray experiments, often rendering the task of combining data more difficult. Batch effects have been observed from the earliest microarray experiments [Lander, 1999], and can be caused by many factors including the batch of amplification reagent used, the time of day when an assay is done, or even the atmospheric ozone level [Fare et al, 2003]. Batch effects are also inevitable when new samples or replicates are incrementally added to an existing array data set or in a meta-analysis of multiple studies that pools microarray data across different labs, array types, or platforms [Rhodes et al, 2004]. In order to correct or at least reduce the batch effects, we used a newly developed algorithm, called ComBat, which is based on empirical Bayes frameworks. This algorithm ran quite appropriately with our datasets, even though, as adverse effect, we observed a substantial flattening in the Fold change values.

A weak point in our data integration approach, particularly while dealing with different chipsets, is the loss of a certain part of expression data. Specifically, in our case, even if we took into account chipsets with more than 22000 annotated identifiers (i.e., Affymetrix Gene 1.0 ST array), during the merging process we lost all the identifiers not present in the totality of the arrays. We, thereby, covered a total number of 11547 unique Ensembl gene IDs.

5.1. Meta-analysis of DS expression studies

First, we performed a wide integration of gene expression raw data in DS samples and controls obtained from different cells or tissues (brain, heart and others), different stages of development (adult, postnatal, embryonic) and different versions of GeneChips. It is per se interesting that, in spite of such heterogeneity, common dosage effects could be identified at all and it should be highlighted that whole-genome data was fairly robust across experiments. We detected a clear enrichment of Hsa21 upregulated genes (**Fig. 6**). However, not a single region was identified but rather several small regions on Hsa21 that agglomerate a large amount of significant dosage effects. This finding agrees with results obtained analyzing single DS-patients with partial duplications [Korbel et al, 2009; Lyle et al, 2009], and provides a discussion topic about the presence of a single DS critical region (DSCR) hypothesized before.

We studied 135 Hsa21 genes represented in the analyzed chips and matched with the probe sets using the latest Ensembl gene Id annotation (v. 17.1.0, ENSG). Seventy-one of these showed consistent dosage effects, while the other 64 showed logFC and significance values under the threshold, indicating both an influence of the tissue specific expression and/or a strong mechanism of dosage compensation. The limitation of detecting reliable fold-changes of low magnitude with microarray technology is not excluded.

Aside from the 71 Hsa21 genes, further 107 non-Hsa21 genes were found dysregulated after meta-analysis. Functional class scoring of the list of these genes showed that the most enriched categories or pathways were related to morphogenesis, apoptosis, synaptic plasticity and ECM. GSEA analysis also revealed that dysregulation affects many genes involved in cell cycle and cell proliferation.

We have analyzed literature about studies on proliferation, differentiation morphogenesis and cell death in DS human subjects and murine models. Many studies consistently demonstrate altered proliferation and cell cycle regulation in the pre- and post-natal brains of both DS individuals and mouse models of DS [Bartesaghi et al, 2011]. The authors hypothesized that altered neurogenesis is implicated in the hypo-cellularity found in trisomic brains. Not irrelevant to the development of Alzheimer's disease (AD), which is increased in DS subjects, might be Hsa21 dosage effects for APP (beta-amyloid precursor protein) involved in senile plaque formation in DS and AD disease [Rachidi and Lopes, 2007]. Apoptosis or programmed cell death is physiologically involved in development and aging, as well as in numerous pathological processes. Altered apoptosis has been proposed as a putative mechanism underlying many DS phenotypes. Indeed, different studies have demonstrated that apoptosis has a prominent role in other important DS phenotypes, such as neurodegeneration in later life stages, impaired retinal development, heart anomalies, immunological alterations and predisposition to the development of different types of cancers [Rueda et al, 2013]. Intellectual deficiency in DS features abnormalities in learning [Gardiner et al., 2010] and, most notably, in hippocampus-dependent explicit memory [Vicari, 2001]. Synaptic plasticity is believed to be the process central to learning and memory. This belief is strengthened by experiments where drugs that normalize aberrant plasticity in hippocampal slices isolated from mouse models of DS also confer improvements in cognition in intact adult mice [Cramer and Galdzicki, 2012]. Regarding the ECM genes, we previously found that this category of genes is significantly dysregulated in fetal hearts [Conti et al, 2007]. Overexpression of this gene family is likely to affect cell adhesion properties, possibly determining an increase in adhesiveness as extensively discussed in the background section. It is, therefore, reasonable to hypothesize that the overexpression of Hsa21 gene or genes mapping to this region might be responsible for an altered morphogenesis of the heart.

Analysis of the pathways affected by DS with GSEA software highlighted the dysregulation of the *PGC-1α* pathway. *PGC-1α* is the master regulator of mitochondrial biogenesis. It is highly expressed in metabolically active tissues, including heart, and it has been involved in increased mitochondrial respiration. *PGC-1α* is a coactivator for many factors including *CBP*, *Scr-1*, *PPARa*, *GR* (glucocorticoid receptor), *THR* (thyroid hormone receptor), several orphan receptors and *MEF2*. Moreover, Czubryt et al. (2003) identified *PGC-1α* as a key target of the *MEF2/HDAC* regulatory pathway and demonstrated this pathway's importance in maintenance of cardiac mitochondrial function. **Table 14** reports the genes belonging to the gene-set "BIOCARTA_PGC1A_PATHWAY" that were found dysregulated in the meta-analysis. ECM and mitochondrial implications in DS will be further discussed below.

TABLE 14. GENES BELONGING TO THE PGC1A PATHWAY ENRICHED IN THE META-ANALYSIS. Data retrieved from GSEA java application.

GENE SYMBOL	GENE_TITLE	RUNNING ES	CORE ENRICH.
PPP3CA	protein phosphatase 3 (formerly 2B), catalytic subunit, alpha isoform (calcineurin A alpha)	-0.568	Yes
CAMK2B	calcium/calmodulin-dependent protein kinase (CaM kinase) II beta	-0.542	Yes
SLC2A4	solute carrier family 2 (facilitated glucose transporter), member 4	-0.500	Yes
MEF2A	MADS box transcription enhancer factor 2, polypeptide A (myocyte enhancer factor 2A)	-0.456	Yes
CAMK2A	calcium/calmodulin-dependent protein kinase (CaM kinase) II alpha	-0.434	Yes
ESRRA	estrogen-related receptor alpha	-0.377	Yes
PPARGC1A	peroxisome proliferative activated receptor, gamma, coactivator 1, alpha	-0.289	Yes
CAMK4	calcium/calmodulin-dependent protein kinase IV	-0.192	Yes
MEF2D	MADS box transcription enhancer factor 2, polypeptide D (myocyte enhancer factor 2D)	-0.094	Yes
PPP3CC	protein phosphatase 3 (formerly 2B), catalytic subunit, gamma isoform (calcineurin A gamma)	0.014	Yes

Finally, transcription factor binding analysis of the 107 non-Hsa21 genes dysregulated in the meta-analysis with Pscan software, demonstrated a

significant enrichment for the TF motifs showed in **Table 8**. We were particularly intrigued by *EGR1* (also known as *Zif268*, *KROX-24*, and *NGFI-A*), because it has been found dysregulated in gene expression studies of experimental models of other neurodegenerative diseases, including Huntington's [Crocker et al, 2006] and age-related cognitive impairment [Blalock et al, 2003]. It could be also a candidate gene involved in the higher risk of developing acute myeloid leukemia (AML) in DS [Stoddart et al, 2014]. Moreover, this gene may exert a protective role against neuroblastoma in DS subjects, since its expression increases during treatment of this pediatric malignancy with mitochondrial inhibitors [Wang et al, 2014].

Comparison of our meta-analysis with another meta-analysis [Vilardell et al, 2011] integrating 45 DS experiments, showed variable dosage effects with respect to analyzed tissues. The two meta-analyses revealed a fair degree of concordance taking into account that the cell model, platform and, especially, the methodology used were completely different (**Fig. 21**). On these bases, the 67 genes in common between the 2 methodologies (**Tab. 15**) acquire more relevance in the context of the development to the DS phenotypes.

A group of 54 Hsa21 genes showed a common dosage effect in the 2 meta-analyses: this group may represent a quota of genes independent from tissue, species or experimental specificity. These genes are also apparently less subjected to compensation mechanisms. Hsa21 dosage effects included, for example *APP* involved in senile plaque formation in DS and Alzheimer's disease [Rachidi and Lopes, 2007]; *COL6A2*, *COL18A1* and *ADAMTS1*, three ECM genes which are implicated in the heart morphogenesis [Wirring et al, 2007; Camenish et al, 2001]; *SUMO3*, a protein that can modulate the activity of *NRIP1* and *PGC1α* [Rytinki and Palvimo, 2007; Rytinki and Palvimo 2008]; the same *NRIP1* and the transcription factor *RUNX1* that are further discussed below.

Among the non-Hsa21 gene, 13 were in common, included *EGR1*, which has been discussed above and *SFRP1*, a gene classified as tumor suppressor that that could have important implications in the higher risk of DS subjects in developing hematopoietic malignancies [Surana et al, 2014].

Figure 21. Venn diagram showing the intersections between the list of the consistently dysregulated genes in DS found in meta-analysis performed in this study (green circle) and in the meta-analysis performed by Vilardell et al. (red)

TABLE 15. LIST OF THE 67 DYSREGULATED GENES COMMON TO THE META-ANALYSIS PERFORMED IN THIS STUDY AND THE VILARDELL'S META-ANALYSIS

ENSEMBL_ GENE_ID	CHR	GENE_ SYMBOL	DESCRIPTION
ENSG00000154734	21	ADAMTS1	ADAM metallopeptidase with thrombospondin type 1 motif, 1 [Source:HGNC Symbol;Acc:217]
ENSG00000160216	21	AGPAT3	1-acylglycerol-3-phosphate O-acyltransferase 3 [Source:HGNC Symbol;Acc:326]
ENSG00000142192	21	APP	amyloid beta (A4) precursor protein [Source:HGNC Symbol;Acc:620]
ENSG00000182240	21	BACE2	beta-site APP-cleaving enzyme 2 [Source:HGNC Symbol;Acc:934]
ENSG00000156273	21	BACH1	BTB and CNC homology 1, basic leucine zipper transcription factor 1 [Source:HGNC Symbol;Acc:935]
ENSG00000154640	21	BTG3	BTG family, member 3 [Source:HGNC Symbol;Acc:1132]
ENSG00000157617	21	C2CD2	C2 calcium-dependent domain containing 2 [Source:HGNC Symbol;Acc:1266]
ENSG00000159228	21	CBR1	carbonyl reductase 1 [Source:HGNC Symbol;Acc:1548]
ENSG00000159231	21	CBR3	carbonyl reductase 3 [Source:HGNC Symbol;Acc:1549]
ENSG00000160200	21	CBS	cystathionine-beta-synthase [Source:HGNC Symbol;Acc:1550]
ENSG00000156261	21	CCT8	chaperonin containing TCP1, subunit 8 (theta) [Source:HGNC Symbol;Acc:1623]
ENSG00000182871	21	COL18A1	collagen, type XVIII, alpha 1 [Source:HGNC Symbol;Acc:2195]
ENSG00000142173	21	COL6A2	collagen, type VI, alpha 2 [Source:HGNC Symbol;Acc:2212]
ENSG00000160213	21	CSTB	cystatin B (stefin B) [Source:HGNC Symbol;Acc:2482]

ENSG00000159147	21	DONSON	downstream neighbor of SON [Source:HGNC Symbol;Acc:2993]
ENSG00000157538	21	DSCR3	Down syndrome critical region gene 3 [Source:HGNC Symbol;Acc:3044]
ENSG00000157557	21	ETS2	v-ets avian erythroblastosis virus E26 oncogene homolog 2 [Source:HGNC Symbol;Acc:3489]
ENSG00000154727	21	GABPA	GA binding protein transcription factor, alpha subunit 60kDa [Source:HGNC Symbol;Acc:4071]
ENSG00000159131	21	GART	phosphoribosylglycinamide formyltransferase, phosphoribosylglycinamide synthetase [Source:HGNC Symbol;Acc:4163]
ENSG00000155304	21	HSPA13	heat shock protein 70kDa family, member 13 [Source:HGNC Symbol;Acc:11375]
ENSG00000142166	21	IFNAR1	interferon (alpha, beta and omega) receptor 1 [Source:HGNC Symbol;Acc:5432]
ENSG00000159128	21	IFNGR2	interferon gamma receptor 2 (interferon gamma transducer 1) [Source:HGNC Symbol;Acc:5440]
ENSG00000205726	21	ITSN1	intersectin 1 (SH3 domain protein) [Source:HGNC Symbol;Acc:6183]
ENSG00000154721	21	JAM2	junctional adhesion molecule 2 [Source:HGNC Symbol;Acc:14686]
ENSG00000160285	21	LSS	lanosterol synthase (2,3-oxidosqualene-lanosterol cyclase) [Source:HGNC Symbol;Acc:6708]
ENSG00000198862	21	LTN1	listerin E3 ubiquitin protein ligase 1 [Source:HGNC Symbol;Acc:13082]
ENSG00000160294	21	MCM3AP	minichromosome maintenance complex component 3 associated protein [Source:HGNC Symbol;Acc:6946]
ENSG00000159256	21	MORC3	MORC family CW-type zinc finger 3 [Source:HGNC Symbol;Acc:23572]
ENSG00000154719	21	MRPL39	mitochondrial ribosomal protein L39 [Source:HGNC Symbol;Acc:14027]
ENSG00000157601	21	MX1	myxovirus (influenza virus) resistance 1, interferon-inducible protein p78 (mouse) [Source:HGNC Symbol;Acc:7532]
ENSG00000180530	21	NRIP1	nuclear receptor interacting protein 1 [Source:HGNC Symbol;Acc:8001]
ENSG00000159086	21	PAXBP1	PAX3 and PAX7 binding protein 1 [Source:HGNC Symbol;Acc:13579]
ENSG00000160209	21	PDXK	pyridoxal (pyridoxine, vitamin B6) kinase [Source:HGNC Symbol;Acc:8819]
ENSG00000141959	21	PFKL	phosphofructokinase, liver [Source:HGNC Symbol;Acc:8876]
ENSG00000185808	21	PIGP	phosphatidylinositol glycan anchor biosynthesis, class P [Source:HGNC Symbol;Acc:3046]
ENSG00000160310	21	PRMT2	protein arginine methyltransferase 2 [Source:HGNC Symbol;Acc:5186]
ENSG00000183527	21	PSMG1	proteasome (prosome, macropain) assembly chaperone 1 [Source:HGNC Symbol;Acc:3043]
ENSG00000183255	21	PTTG1IP	pituitary tumor-transforming 1 interacting protein [Source:HGNC Symbol;Acc:13524]
ENSG00000159216	21	RUNX1	runt-related transcription factor 1 [Source:HGNC Symbol;Acc:10471]
ENSG00000160307	21	S100B	S100 calcium binding protein B [Source:HGNC Symbol;Acc:10500]

ENSG00000156304	21	SCAF4	SR-related CTD-associated factor 4 [Source:HGNC Symbol;Acc:19304]
ENSG00000185437	21	SH3BGR	SH3 domain binding glutamic acid-rich protein [Source:HGNC Symbol;Acc:10822]
ENSG00000142168	21	SOD1	superoxide dismutase 1, soluble [Source:HGNC Symbol;Acc:11179]
ENSG00000159140	21	SON	SON DNA binding protein [Source:HGNC Symbol;Acc:11183]
ENSG00000184900	21	SUMO3	small ubiquitin-like modifier 3 [Source:HGNC Symbol;Acc:11124]
ENSG00000159082	21	SYNJ1	synaptojanin 1 [Source:HGNC Symbol;Acc:11503]
ENSG00000156299	21	TIAM1	T-cell lymphoma invasion and metastasis 1 [Source:HGNC Symbol;Acc:11805]
ENSG00000142188	21	TMEM50B	transmembrane protein 50B [Source:HGNC Symbol;Acc:1280]
ENSG00000182670	21	TTC3	tetratricopeptide repeat domain 3 [Source:HGNC Symbol;Acc:12393]
ENSG00000160201	21	U2AF1	U2 small nuclear RNA auxiliary factor 1 [Source:HGNC Symbol;Acc:12453]
ENSG00000184787	21	UBE2G2	ubiquitin-conjugating enzyme E2G 2 [Source:HGNC Symbol;Acc:12483]
ENSG00000156256	21	USP16	ubiquitin specific peptidase 16 [Source:HGNC Symbol;Acc:12614]
ENSG00000155313	21	USP25	ubiquitin specific peptidase 25 [Source:HGNC Symbol;Acc:12624]
ENSG00000182093	21	WRB	tryptophan rich basic protein [Source:HGNC Symbol;Acc:12790]
ENSG00000105655	19	ISYNA1	inositol-3-phosphate synthase 1 [Source:HGNC Symbol;Acc:29821]
ENSG00000104067	15	TJP1	tight junction protein 1 [Source:HGNC Symbol;Acc:11827]
ENSG00000133110	13	POSTN	periostin, osteoblast specific factor [Source:HGNC Symbol;Acc:16953]
ENSG00000119471	9	HSDL2	hydroxysteroid dehydrogenase like 2 [Source:HGNC Symbol;Acc:18572]
ENSG00000107104	9	KANK1	KN motif and ankyrin repeat domains 1 [Source:HGNC Symbol;Acc:19309]
ENSG00000164985	9	PSIP1	PC4 and SFRS1 interacting protein 1 [Source:HGNC Symbol;Acc:9527]
ENSG00000104332	8	SFRP1	secreted frizzled-related protein 1 [Source:HGNC Symbol;Acc:10776]
ENSG00000075624	7	ACTB	actin, beta [Source:HGNC Symbol;Acc:132]
ENSG00000113657	5	DPYSL3	dihydropyrimidinase-like 3 [Source:HGNC Symbol;Acc:3015]
ENSG00000120738	5	EGR1	early growth response 1 [Source:HGNC Symbol;Acc:3238]
ENSG00000182551	2	ADI1	acireductone dioxygenase 1 [Source:HGNC Symbol;Acc:30576]
ENSG00000159176	1	CSRP1	cysteine and glycine-rich protein 1 [Source:HGNC Symbol;Acc:2469]
ENSG00000049245	1	VAMP3	vesicle-associated membrane protein 3 [Source:HGNC Symbol;Acc:12644]

In order to address possible role of Hsa21 genes in two aspects of the DS phenotype, namely mitochondrial dysfunction and increased cell adhesiveness that are widely described in literature and that came out from our previous investigations [Conti et al, 2007], we applied a second strategic approach. We analyzed public expression data to identify genes affecting the regulation of the two main gene categories dysregulated in trisomic fetal hearts: NEMGs and ECM genes.

5.2. Mitochondrial dysfunction in DS and validation of an Hsa21 candidate gene for NEMGs downregulation

Previous analyses, demonstrated a global mitochondrial dysfunction in several DS models [Kim et al, 2001; Busciglio et al, 2002; Helguera et al, 2013; Shukkur et al, 2006] and a significant dysregulation of NEMGs in the heart [Conti et al, 2007], brain [Mao et al, 2005], and fibroblasts [Piccoli et al, 2013] from human fetuses with DS. From these studies it emerged that genes and transcription factors responsible for the activity of respiratory complexes and mitochondrial biogenesis are globally repressed. Thus, we speculated that most of the underexpressed NEMGs might be under the same regulatory control and that this control might be affected by the trisomy of Hsa21.

We then, looked for a regulator of NEMGs that maps to Hsa21 and that is upregulated in DS samples, by virtue of a gene dosage effect. To this aim, we re-analyzed the expression data from the GEO repository (http://www.ncbi.nlm.nih.gov/geo) by focusing on an experiment in which regulatory genes mapping to Hsa21 were individually overexpressed in mouse ESCs [De Cegli et al, 2010]. Our analysis demonstrated that only one gene is able to cause NEMG downregulation and that no other Hsa21 tested gene exerts such an effect. This gene is *NRIP1* which encodes for a corepressor protein. Although the mean dysregulation of each NEMG elicited by *NRIP1* overexpression was not very strong, the number of affected genes was significantly enriched ($p < 0.001$). The role of *NRIP1* in mitochondrial dysfunction is supported by previous findings demonstrating that, both in cellular and in animal models, *NRIP1* silencing upregulates the expression of genes responsible for mitochondrial biogenesis and oxidative phosphorylation whereas, *NRIP1* re-expression downregulates them [Powelka et al, 2006; Seth et al, 2007]. Experiments of *NRIP1* manipulation, performed in transgenic mice and human cells, have actually demonstrated that even mild variations in *NRIP1* expression can significantly affect oxidative metabolism and mitochondrial biogenesis [Powelka et al, 2006; Seth et al, 2007; Fritah et al, 2010; Chen et al, 2012].

NRIP1 is supposed to exert a repression of mitochondrial biogenesis by either interacting with nuclear receptors [Fritah et al, 2010; Nautiyal et al, 2013] or

regulating *PGC-1α* activity [Scarpulla et al, 2011; Hallberg et al, 2008; Rytinki et al, 2009]. Intriguingly, the pathway related to this gene has been found enriched among the downregulated genes in the meta-analysis. *PGC-1α* knockout mice show not only a decreased number of mitochondria but also a decreased respiratory capacity in skeletal muscle [Leone et al, 2005]. In particular, under physiological conditions, *PGC-1α*, by coactivating several transcription factors, including nuclear receptors such as *PPARγ*, *PPARα* and *ERRα*, promotes mitochondrial biogenesis and regulates mitochondrial respiratory efficiency [Leone et al, 2005; Scarpulla et al, 2011; Scarpulla et al, 2012]. Interestingly among the 37 NEMGs downregulated after *NRIP1* induction in the GEO GSE 19836 experiment [De Cegli et al, 2010], we observed an enrichment both of genes involved in *PPAR*s pathways (8 genes) and of genes containing the *ERRα* motif in their promoter regions (25 genes) ($p<0.0005$). Notably, the known targets of *PGC-1α*, namely, *CIDEA* [Hallberg et al, 2008] and *ANT1/SLC25A4* [Schreiber et al, 2004], are included in the list of genes that are downregulated following *NRIP1* overexpression [De Cegli et al, 2010].The alteration of the *PGC-1α* pathway also results of our meta-analysis.

To investigate whether the NEMGs repressed by *NRIP1* and induced by *PGC-1α* corresponded to the NEMGs downregulated genes in DS fetal hearts [Conti et al, 2007], we compared our microarray data with the results of 2 experiments in which the gene expression of *NRIP1* or *PGC-1α* was modulated. We found that the correspondence between the three sets of genes was remarkably high, considering that they all derived from different species, tissues, and experimental approaches. The high number of overlappings among the three sets is in agreement with previous research indicating an interrelationship between *PGC-1α* and *NRIP1* activity on mitochondrial pathways [Chen et al, 2012].

To biologically validate the important results coming from a bioinformatic strategy, we have verified the potential role of *NRIP1* in mitochondrial dysfunction in DS demonstrating an inverse correlation between *NRIP1* and *PGC-1α* expression. Moreover *NRIP1* siRNA-mediated attenuation in DS-HFFs, and the consequent *PGC-1α* and *NRF1* upregulation, elicited a significant increase in mtDNA. This result fully corroborates similar experiments performed in cardiomyocytes [Chen et al, 2012]. In the same trisomic fibroblasts, ROS production was decreased and mitochondrial activity was increased, demonstrating that the induction of NEMG expression in silenced DS-HFFs counteracts mitochondrial impairment and partially rescues mitochondrial function. Interestingly, in *NRIP1*-silenced trisomic cells, we found a significant 50% increase in basal ATP content. These results, together with the finding that *NRIP1* attenuation by siRNA leads to an increase in the adenine nucleotide translocators *ANT1/SLC25A4* and *ANT2/SLC25A5*, suggest

that a more efficient exchange of adenosine 5′-triphosphate is induced, thus, benefitting the mitochondrial activity and function of these cells, as demonstrated by the reduction in ROS production at the mitochondrial level (**Fig. 16**).

Furthermore, the *NRIP1*-dependent repression of genes involved in mitochondrial function is closely linked with post-natal impaired cardiac function because of reduced mitochondrial electron-transport chain activity and oxygen consumption. *NRIP1* hyperexpressing mice, indeed, are affected by cardiac hypertrophy [Fritah et al, 2010].

Mitochondrial dysfunction might also contribute to determining DS mental retardation and other DS associated post-natal pathologies, like Alzheimer's disease (AD) and obesity. It is known that mitochondria also play a central role in many neurodegenerative diseases such as AD, Parkinson's disease, Huntington's disease, and amyotrophic lateral sclerosis. Impaired energy metabolism, defective mitochondrial enzymatic activity, abnormal mitochondrial respiration, mutated mtDNAs, and oxidative stress are all common features of these neurodegenerative conditions [Petrozzi et al, 2007].

It is interesting to note that the bioinformatic functional analysis of the 25 genes overlapping SET1 (genes regulated by *NRIP1*) and SET3 (genes downregulated in DS fetal hearts) showed that 16 out of 25 genes are involved in the mitochondrial dysfunction pathways described in AD and Parkinson's disease (KEGG Pathways http://www.genome.jp/kegg/, [Kanehisa et al, 2000]). However, given that there is a high prevalence of AD in DS patients, we cannot neglect the possibility that the overexpression of the Hsa21 gene *APP* might have a main role in the development of AD in DS patients.

Taken all together, the bioinformatic analysis corroborated by the biological approaches, suggest that *NRIP1* is a key gene in the regulation of the mitochondrial pathways, even though possibly it is not the only protagonist responsible for mitochondrial dysfunction in DS.

5.3. *ECM genes dysregulation in DS and identification of a Hsa21 candidate gene*

In the last part of the study, we looked for a regulator of ECM genes that maps to Hsa21 and that is upregulated in DS samples, by virtue of a gene dosage effect. To this aim, we re-analyzed the same GEO series discussed above [De Cegli et al, 2010]. Our analysis demonstrated that only one gene is able to cause the overexpression of 32 ECM genes, when overexpressed, and that no other Hsa21 tested gene exerts such an effect. This gene is *RUNX1*.

The protein encoded by this gene represents the alpha subunit of *CBF*, a transcription factor thought to be involved in the development of normal hematopoiesis. The association of *RUNX1* with the ECM genes is supported by experiments that demonstrated that ectopic expression of *RUNX1* in 3T3 fibroblasts induced deep alterations in the distribution of *N-cadherin* in favor of the plasma membrane, an increased expression of *Integrin β5*, and increased survival at confluence [Wotton et al, 2008].

Furthermore, transcription factor-binding site (TFBS) analysis on the list of ECM genes upregulated in DS fetal hearts identified *RUNX1* as transcription factor with high binding specificity with ECM genes upregulated in DS hearts (**Tab. 13**). About 60% of ECM genes overexpressed in DS hearts showed consensus sequences for *RUNX1*.

Our interest in ECM proteins is justified by the role they play in cushion development. Since DS is a major cause of congenital heart defects, their dysregulation may represent a key pathogenetic mechanism. Intriguingly, among the genes with consensus sequence for *RUNX1* we found in our study, there are crucial genes implicated in the embryonic development and in particular in the heart morphogenesis, such as *VCAN*, *HAPLN1*/*CRTL1* and *ADAMTS*. *RUNX1* is included in the 3.7 Mb minimal region for DS-CHD [Liu et al, 2013]

Indeed, the development of the AV valves begins with the swelling of the endocardial lining of the AV junction and the formation of the AV cushions. The cushions then become populated by endocardially derived cells resulting from endocardial-to-mesenchymal transition (EMT). At this point in time, the endocardial cushion mesenchyme contains a variety of ECM components, including *Crtl1*, hyaluronan, and versican [Wirring et al, 2007; Camenish et al, 2001].

Versican is a chondroitin sulfate proteoglycan abundantly expressed within the extracellular matrix compartment of the developing and mature cardiovascular system. Alterations in its expression have been associated with vascular disease [Wight and Merrilees, 2004] and its expression is required for normal early heart development [Mjaatvedt et al, 1998]. Analysis of *Vcan* transgenic mice has established the requirement for versican in cardiac development and its role in skeletogenesis. The *ADAMTS* family includes several versican-degrading proteases that are active during remodeling of the embryonic provisional matrix, especially during sculpting of versican-rich tissues. Versican is cleaved at specific peptide bonds by *ADAMTS* proteases, and the cleavage products are detectable by neo-epitope antibodies. Myocardial compaction, closure of the secondary palate (in which neural crest derived cells participate), endocardial cushion remodeling, myogenesis and interdigital web regression are developmental contexts in which *ADAMTS*-mediated versican proteolysis has been identified as a crucial requirement [Nandadasa et al, 2014].

Vcan dysregulation can induce changes in the distribution of periostin, another important molecule of the heart cushion extracellular matrix, and then may affect the developing valves by altering the structural integrity of the ECM through altered interaction with other molecules such as fibronectin, collagen and other proteoglycans [Norris et al, 2007], found dysregulated in our data as well. Additionally, because it interacts directly with integrin, attachment-dependent signaling may be altered affecting cell migration and epithelial mesenchymal transition in the cushion primordia of the septa and valves [Yan and Shao, 2006].

Cartilage Link Protein 1 (*Crtl1*; also known as Hyaluronan and Proteoglycan Binding Protein 1- *Hapln1*) is a glycoprotein found in the extracellular matrix (ECM) and is expressed in endocardial and endocardially-derived cells in the developing heart, including cells in the AV and outflow tract (OFT) cushions [Binette et al, 1994; Matsumoto et al, 2006]. *Crtl1* is involved in the formation and stabilization of proteoglycan and hyaluronan aggregates [Matsumoko et a, 2006] and is important for preventing aggregate degradation by proteases such as members of the *ADAMTS* and *MMP* families [Miwa et al, 2006]. Alteration in the expression of *Crtl1* results in impairment of growth and development of several tissues, including the cartilage, heart, and central nervous system [Wirring et al, 2007]. *Crtl1* null mice are characterized by craniofacial abnormalities and shortened long bones, abnormalities attributed to a reduction in aggrecan within the cartilage resulting in an inability of chondrocytes towards differentiation and hypertrophy [Watanabe et al, 1999]. Cardiac malformations seen in *Crtl1* knockout mice include muscular ventricular septal defects, AV septal defects, and thin myocardium [Wirring et al, 2007]. *Crtl1* knockout mice die perinatally; this has has been attributed to compromised lung development [Watanabe et al, 1999].

6. CONCLUSIONS

Combination of different meta-analysis strategies led us to identify genes and pathways consistently dysregulated in nine independent studies on DS. In particular, two Hsa21 genes were identified, namely *NRIP1* and *RUNX1*, which could play important roles in the development of DS phenotypes, as they affect mitochondrial function and ECM gene expression.

These results provide the basis for clinical trials aimed at restoring altered functions in DS subjects to prevent specific phenotypic features such as neurodegeneration, cardiac hypertrophy, diabetes and obesity.

For instance, a possible therapeutic approach to counteract mitochondrial dysfunction in DS could be based either on *PGC-1α* activators, already tested in other disease mouse models [Rodgers et al, 2005; Dong et al, 2007; Lagouge et al, 2006; Jager et al, 2007], or on *PPARγ* agonists, which attenuate mitochondrial dysfunction in AD mouse models [Bastin et al, 2008; Nicolakakis et al, 2008; Escribano et al, 2009; Johri et al, 2012; Yamaguchi et al, 2012]. Such drugs are routinely used in clinical practice for the treatment of metabolic syndromes, type 2 diabetes, and neurodegenerative diseases such as AD [Watson et al, 2005; Sato et al, 2011; Marciano et al, 2014] and could, therefore, be immediately introduced in clinical trials.

ECM protein expression affects heart development [Combs et al, 2009]. Our analysis demonstrates that ECM genes are upregulated in DS tissues, suggesting that this altered expression might be a prelude to heart defects. Other factors, such as differences in the genetic background, different Hsa21 haplotypes, stochastic and/or environmental factors, could play a critical role in determining the final pathogenetic result. The analysis identified in *RUNX1* a candidate transcription factor mapping to chromosome 21 that could be responsible for the upregulation of ECM genes. Studies to biologically validate its role in DS are currently in progress.

ACKNOWLEDGEMENTS

Everyone who knows me is also aware of the fact that I am person of few words but, at the end of this study, there are some people who I especially want to thank. Without their help I would not have been able to learn all the things that I have learned in the past years, and complete my Ph.D. degree.

I would like to thank my supervisor, Prof. Lucio Nitsch, being one of the most brilliant minds I have encountered in my life, for the guidance and advice he has provided throughout my time as his student.

I would like to thank Dr. Anna Conti for her maternal patience. I have been extremely lucky to work with a person who cared so much about my work, and who responded to my questions and queries so promptly. She generously paved the way for my development as a research scientist.

I would like to thank Dr. Antonella Izzo for supporting and helping me during this journey. She was one of the first friendly faces to greet me when I entered the lab and she has always been a tremendous help no matter the task or circumstance.

I am also indebted to the many people who in some way contributed to the progress and publication of the work contained herein, in particular Prof. Paolo Pinton and Prof. Dario Greco, for offering me the opportunity to visit their groups in Ferrara and Helsinki and leading me working on diverse exciting experiments.

Thank you also to the other people who are not mentioned here but have helped in making the Citogenetics lab a very special place to stay over all these years.

Finally, thank you to my family for the unconditional love and encouragement provided that served as a secure anchor during the hard and easy times.

7. REFERENCES

Alizadeh, A.A., Eisen, M.B., Davis, R.E., Ma, C., Lossos, I.S., Rosenwald, A., Boldrick, J.C., Sabet, H., Tran, T., Yu, X. *et al.* (2000) Distinct types of diffuse large B-cell lymphoma identified by gene expression profiling. *Nature*, **403**, 503-511.

Amano, K., Sago, H., Uchikawa, C., Suzuki, T., Kotliarova, S.E., Nukina, N., Epstein, C.J. and Yamakawa, K. (2004) Dosage-dependent over-expression of genes in the trisomic region of Ts1Cje mouse model for Down syndrome. *Hum Mol Genet*, **13**, 1333-1340.

Antonarakis, S.E. and Epstein, C.J. (2006) The challenge of Down syndrome. *Trends Mol Med*, **12**, 473-479.

Ashburner, M., Ball, C.A., Blake, J.A., Botstein, D., Butler, H., Cherry, J.M., Davis, A.P., Dolinski, K., Dwight, S.S., Eppig, J.T. *et al.* (2000) Gene ontology: tool for the unification of biology. The Gene Ontology Consortium. *Nat Genet*, **25**, 25-29.

Askanas, V., McFerrin, J., Baque, S., Alvarez, R.B., Sarkozi, E. and Engel, W.K. (1996) Transfer of beta-amyloid precursor protein gene using adenovirus vector causes mitochondrial abnormalities in cultured normal human muscle. *Proc Natl Acad Sci U S A*, **93**, 1314-1319.

Barlow, G.M., Chen, X.N., Shi, Z.Y., Lyons, G.E., Kurnit, D.M., Celle, L., Spinner, N.B., Zackai, E., Pettenati, M.J., Van Riper, A.J. *et al.* (2001) Down syndrome congenital heart disease: a narrowed region and a candidate gene. *Genet Med*, **3**, 91-101.

Bartesaghi, R., Guidi, S. and Ciani, E. (2011) Is it possible to improve neurodevelopmental abnormalities in Down syndrome? *Rev Neurosci*, **22**, 419-455.

Bastin, J., Aubey, F., Rotig, A., Munnich, A. and Djouadi, F. (2008) Activation of peroxisome proliferator-activated receptor pathway stimulates the mitochondrial respiratory chain and can correct deficiencies in patients' cells lacking its components. *J Clin Endocrinol Metab*, **93**, 1433-1441.

Belichenko, P.V., Kleschevnikov, A.M., Salehi, A., Epstein, C.J. and Mobley, W.C. (2007) Synaptic and cognitive abnormalities in mouse models of Down syndrome: exploring genotype-phenotype relationships. *J Comp Neurol*, **504**, 329-345.

Benjamini, Y., Hochberg, Y. (1995) Controlling the false discovery rate: A practical and powerful approach to multiple testing. *Journal of the Royal Statistical Society* **57**: 289–300.

Bianchi, F., Nuciforo, P., Vecchi, M., Bernard, L., Tizzoni, L., Marchetti, A., Buttitta, F., Felicioni, L., Nicassio, F. and Di Fiore, P.P. (2007) Survival prediction of stage I lung adenocarcinomas by expression of 10 genes. *J Clin Invest*, **117**, 3436-3444.

Blalock, E.M., Chen, K.C., Sharrow, K., Herman, J.P., Porter, N.M., Foster, T.C. and Landfield, P.W. (2003) Gene microarrays in hippocampal aging: statistical profiling identifies novel processes correlated with cognitive impairment. *J Neurosci*, **23**, 3807-3819.

Bonora, M., Giorgi, C., Bononi, A., Marchi, S., Patergnani, S., Rimessi, A., Rizzuto, R. and Pinton, P. (2013) Subcellular calcium measurements in mammalian cells using jellyfish photoprotein aequorin-based probes. *Nat Protoc*, **8**, 2105-2118.

Bonora, M., Patergnani, S., Rimessi, A., De Marchi, E., Suski, J.M., Bononi, A., Giorgi, C., Marchi, S., Missiroli, S., Poletti, F. *et al.* (2012) ATP synthesis and storage. *Purinergic Signal*, **8**, 343-357.

Bozon, B., Davis, S. and Laroche, S. (2002) Regulated transcription of the immediate-early gene Zif268: mechanisms and gene dosage-dependent function in synaptic plasticity and memory formation. *Hippocampus*, **12**, 570-577.

Brazma, A. (2009) Minimum Information About a Microarray Experiment (MIAME)--successes, failures, challenges. *ScientificWorldJournal*, **9**, 420-423.

Brettschneider, J., Collin, F., Bolstad, B.M., and Speed, T.P. (2008) Quality Assessment for Short Oligonucleotide Microarray Data. *Technometrics* **50**, 241-264

Busciglio, J., Pelsman, A., Wong, C., Pigino, G., Yuan, M., Mori, H. and Yankner, B.A. (2002) Altered metabolism of the amyloid beta precursor protein is associated with mitochondrial dysfunction in Down's syndrome. *Neuron*, **33**, 677-688.

Busciglio, J. and Yankner, B.A. (1995) Apoptosis and increased generation of reactive oxygen species in Down's syndrome neurons in vitro. *Nature*, **378**, 776-779.

Bushdid, P.B., Osinska, H., Waclaw, R.R., Molkentin, J.D. and Yutzey, K.E. (2003) NFATc3 and NFATc4 are required for cardiac development and mitochondrial function. *Circ Res*, **92**, 1305-1313.

Carter, S.L., Eklund, A.C., Mecham, B.H., Kohane, I.S. and Szallasi, Z. (2005) Redefinition of Affymetrix probe sets by sequence overlap with cDNA

microarray probes reduces cross-platform inconsistencies in cancer-associated gene expression measurements. *BMC bioinformatics*, **6**, 107.

Chan, C.K., Rolle, M.W., Potter-Perigo, S., Braun, K.R., Van Biber, B.P., Laflamme, M.A., Murry, C.E. and Wight, T.N. (2010) Differentiation of cardiomyocytes from human embryonic stem cells is accompanied by changes in the extracellular matrix production of versican and hyaluronan. *J Cell Biochem*, **111**, 585-596.

Chen, Y., Wang, Y., Chen, J., Chen, X., Cao, W., Chen, S., Xu, S., Huang, H. and Liu, P. (2012) Roles of transcriptional corepressor RIP140 and coactivator PGC-1alpha in energy state of chronically infarcted rat hearts and mitochondrial function of cardiomyocytes. *Molecular and cellular endocrinology*, **362**, 11-18.

Choi, J.K., Choi, J.Y., Kim, D.G., Choi, D.W., Kim, B.Y., Lee, K.H., Yeom, Y.I., Yoo, H.S., Yoo, O.J. and Kim, S. (2004) Integrative analysis of multiple gene expression profiles applied to liver cancer study. *FEBS Lett*, **565**, 93-100.

Choi, J.K., Yu, U., Kim, S. and Yoo, O.J. (2003) Combining multiple microarray studies and modeling interstudy variation. *Bioinformatics*, **19 Suppl 1**, i84-90.

Chou, C.Y., Liu, L.Y., Chen, C.Y., Tsai, C.H., Hwa, H.L., Chang, L.Y., Lin, Y.S. and Hsieh, F.J. (2008) Gene expression variation increase in trisomy 21 tissues. *Mamm Genome*, **19**, 398-405.

Chrast, R., Scott, H.S., Papasavvas, M.P., Rossier, C., Antonarakis, E.S., Barras, C., Davisson, M.T., Schmidt, C., Estivill, X., Dierssen, M. *et al.* (2000) The mouse brain transcriptome by SAGE: differences in gene expression between P30 brains of the partial trisomy 16 mouse model of Down syndrome (Ts65Dn) and normals. *Genome Res*, **10**, 2006-2021.

Christian, M., White, R. and Parker, M.G. (2006) Metabolic regulation by the nuclear receptor corepressor RIP140. *Trends Endocrinol Metab*, **17**, 243-250.

Combs, M.D. and Yutzey, K.E. (2009) Heart valve development: regulatory networks in development and disease. *Circ Res*, **105**, 408-421.

Conesa, A., Nueda, M.J., Ferrer, A. and Talon, M. (2006) maSigPro: a method to identify significantly differential expression profiles in time-course microarray experiments. *Bioinformatics*, **22**, 1096-1102.

Conti, A., Fabbrini, F., D'Agostino, P., Negri, R., Greco, D., Genesio, R., D'Armiento, M., Olla, C., Paladini, D., Zannini, M. *et al.* (2007) Altered

expression of mitochondrial and extracellular matrix genes in the heart of human fetuses with chromosome 21 trisomy. *BMC Genomics*, **8**, 268.

Costa, A.C. and Scott-McKean, J.J. (2013) Prospects for improving brain function in individuals with Down syndrome. *CNS Drugs*, **27**, 679-702.

Cramer, N. and Galdzicki, Z. (2012) From abnormal hippocampal synaptic plasticity in down syndrome mouse models to cognitive disability in down syndrome. *Neural Plast*, **2012**, 101542.

Crocker, S.F., Costain, W.J. and Robertson, H.A. (2006) DNA microarray analysis of striatal gene expression in symptomatic transgenic Huntington's mice (R6/2) reveals neuroinflammation and insulin associations. *Brain Res*, **1088**, 176-186.

Czubryt, M.P., McAnally, J., Fishman, G.I. and Olson, E.N. (2003) Regulation of peroxisome proliferator-activated receptor gamma coactivator 1 alpha (PGC-1 alpha) and mitochondrial function by MEF2 and HDAC5. *Proc Natl Acad Sci U S A*, **100**, 1711-1716.

Dai, M., Wang, P., Boyd, A.D., Kostov, G., Athey, B., Jones, E.G., Bunney, W.E., Myers, R.M., Speed, T.P., Akil, H. *et al.* (2005) Evolving gene/transcript definitions significantly alter the interpretation of GeneChip data. *Nucleic Acids Res*, **33**, e175.

Dan, S., Tsunoda, T., Kitahara, O., Yanagawa, R., Zembutsu, H., Katagiri, T., Yamazaki, K., Nakamura, Y. and Yamori, T. (2002) An integrated database of chemosensitivity to 55 anticancer drugs and gene expression profiles of 39 human cancer cell lines. *Cancer Res*, **62**, 1139-1147.

Dauphinot, L., Lyle, R., Rivals, I., Dang, M.T., Moldrich, R.X., Golfier, G., Ettwiller, L., Toyama, K., Rossier, J., Personnaz, L. *et al.* (2005) The cerebellar transcriptome during postnatal development of the Ts1Cje mouse, a segmental trisomy model for Down syndrome. *Hum Mol Genet*, **14**, 373-384.

De Cegli, R., Romito, A., Iacobacci, S., Mao, L., Lauria, M., Fedele, A.O., Klose, J., Borel, C., Descombes, P., Antonarakis, S.E. *et al.* (2010) A mouse embryonic stem cell bank for inducible overexpression of human chromosome 21 genes. *Genome biology*, **11**, R64.

de la Torre, R. and Dierssen, M. (2012) Therapeutic approaches in the improvement of cognitive performance in Down syndrome: past, present, and future. *Prog Brain Res*, **197**, 1-14.

DeRisi, J., Penland, L., Brown, P.O., Bittner, M.L., Meltzer, P.S., Ray, M., Chen, Y., Su, Y.A. and Trent, J.M. (1996) Use of a cDNA microarray to analyse gene expression patterns in human cancer. *Nat Genet*, **14**, 457-460.

Dickersin, K., Min, Y.I. and Meinert, C.L. (1992) Factors influencing publication of research results. Follow-up of applications submitted to two institutional review boards. *Jama*, **267**, 374-378.

Dong, F., Li, Q., Sreejayan, N., Nunn, J.M. and Ren, J. (2007) Metallothionein prevents high-fat diet induced cardiac contractile dysfunction: role of peroxisome proliferator activated receptor gamma coactivator 1alpha and mitochondrial biogenesis. *Diabetes*, **56**, 2201-2212.

Dupuy, A. and Simon, R.M. (2007) Critical review of published microarray studies for cancer outcome and guidelines on statistical analysis and reporting. *J Natl Cancer Inst*, **99**, 147-157.

Edwards, H., Xie, C., LaFiura, K.M., Dombkowski, A.A., Buck, S.A., Boerner, J.L., Taub, J.W., Matherly, L.H. and Ge, Y. (2009) RUNX1 regulates phosphoinositide 3-kinase/AKT pathway: role in chemotherapy sensitivity in acute megakaryocytic leukemia. *Blood*, **114**, 2744-2752.

Ein-Dor, L., Kela, I., Getz, G., Givol, D. and Domany, E. (2005) Outcome signature genes in breast cancer: is there a unique set? *Bioinformatics*, **21**, 171-178.

El Khoudary, S.R., Wildman, R.P., Matthews, K., Thurston, R.C., Bromberger, J.T. and Sutton-Tyrrell, K. (2012) Endogenous sex hormones impact the progression of subclinical atherosclerosis in women during the menopausal transition. *Atherosclerosis*, **225**, 180-186.

Epstein, C.J., Korenberg, J.R., Anneren, G., Antonarakis, S.E., Ayme, S., Courchesne, E., Epstein, L.B., Fowler, A., Groner, Y., Huret, J.L. *et al.* (1991) Protocols to establish genotype-phenotype correlations in Down syndrome. *Am J Hum Genet*, **49**, 207-235.

Escribano, L., Simon, A.M., Perez-Mediavilla, A., Salazar-Colocho, P., Del Rio, J. and Frechilla, D. (2009) Rosiglitazone reverses memory decline and hippocampal glucocorticoid receptor down-regulation in an Alzheimer's disease mouse model. *Biochem Biophys Res Commun*, **379**, 406-410.

Fare, T.L., Coffey, E.M., Dai, H., He, Y.D., Kessler, D.A., Kilian, K.A., Koch, J.E., LeProust, E., Marton, M.J., Meyer, M.R. *et al.* (2003) Effects of atmospheric ozone on microarray data quality. *Analytical chemistry*, **75**, 4672-4675.

Ferencz, C., Neill, C.A., Boughman, J.A., Rubin, J.D., Brenner, J.I. and Perry, L.W. (1989) Congenital cardiovascular malformations associated with chromosome abnormalities: an epidemiologic study. *The Journal of pediatrics*, **114**, 79-86.

FitzPatrick, D.R., Ramsay, J., McGill, N.I., Shade, M., Carothers, A.D. and Hastie, N.D. (2002) Transcriptome analysis of human autosomal trisomy. *Hum Mol Genet*, **11**, 3249-3256.

Flicek, P., Amode, M.R., Barrell, D., Beal, K., Billis, K., Brent, S., Carvalho-Silva, D., Clapham, P., Coates, G., Fitzgerald, S. *et al.* (2014) Ensembl 2014. *Nucleic Acids Res*, **42**, D749-755.

Franceschini, A., Szklarczyk, D., Frankild, S., Kuhn, M., Simonovic, M., Roth, A., Lin, J., Minguez, P., Bork, P., von Mering, C. *et al.* (2013) STRING v9.1: protein-protein interaction networks, with increased coverage and integration. *Nucleic Acids Res*, **41**, D808-815.

Fritah, A., Christian, M. and Parker, M.G. (2010) The metabolic coregulator RIP140: an update. *American journal of physiology. Endocrinology and metabolism*, **299**, E335-340.

Gardiner, K. (2003) Predicting pathway perturbations in Down syndrome. *J Neural Transm Suppl*, 21-37.

Gardiner, K. (2006) Transcriptional dysregulation in Down syndrome: predictions for altered protein complex stoichiometries and post-translational modifications, and consequences for learning/behavior genes ELK, CREB, and the estrogen and glucocorticoid receptors. *Behavior genetics*, **36**, 439-453.

Gautier, L., Cope, L., Bolstad, B.M. and Irizarry, R.A. (2004) affy--analysis of Affymetrix GeneChip data at the probe level. *Bioinformatics*, **20**, 307-315.

Gittenberger-de Groot, A.C., Bartram, U., Oosthoek, P.W., Bartelings, M.M., Hogers, B., Poelmann, R.E., Jongewaard, I.N. and Klewer, S.E. (2003) Collagen type VI expression during cardiac development and in human fetuses with trisomy 21. *Anat Rec A Discov Mol Cell Evol Biol*, **275**, 1109-1116.

Golub, T.R., Slonim, D.K., Tamayo, P., Huard, C., Gaasenbeek, M., Mesirov, J.P., Coller, H., Loh, M.L., Downing, J.R., Caligiuri, M.A. *et al.* (1999) Molecular classification of cancer: class discovery and class prediction by gene expression monitoring. *Science*, **286**, 531-537.

Gotea, V. and Ovcharenko, I. (2008) DiRE: identifying distant regulatory elements of co-expressed genes. *Nucleic Acids Res*, **36**, W133-139.

Grutzmann, R., Boriss, H., Ammerpohl, O., Luttges, J., Kalthoff, H., Schackert, H.K., Kloppel, G., Saeger, H.D. and Pilarsky, C. (2005) Meta-analysis of microarray data on pancreatic cancer defines a set of commonly dysregulated genes. *Oncogene*, **24**, 5079-5088.

Hallberg, M., Morganstein, D.L., Kiskinis, E., Shah, K., Kralli, A., Dilworth, S.M., White, R., Parker, M.G. and Christian, M. (2008) A functional interaction between RIP140 and PGC-1alpha regulates the expression of the lipid droplet protein CIDEA. *Molecular and cellular biology*, **28**, 6785-6795.

Handschin, C., Rhee, J., Lin, J., Tarr, P.T. and Spiegelman, B.M. (2003) An autoregulatory loop controls peroxisome proliferator-activated receptor gamma coactivator 1alpha expression in muscle. *Proc Natl Acad Sci U S A*, **100**, 7111-7116.

Hatano, S., Kimata, K., Hiraiwa, N., Kusakabe, M., Isogai, Z., Adachi, E., Shinomura, T. and Watanabe, H. (2012) Versican/PG-M is essential for ventricular septal formation subsequent to cardiac atrioventricular cushion development. *Glycobiology*, **22**, 1268-1277.

Helguera, P., Seiglie, J., Rodriguez, J., Hanna, M., Helguera, G. and Busciglio, J. (2013) Adaptive downregulation of mitochondrial function in down syndrome. *Cell Metab*, **17**, 132-140.

Hermjakob, H., Montecchi-Palazzi, L., Lewington, C., Mudali, S., Kerrien, S., Orchard, S., Vingron, M., Roechert, B., Roepstorff, P., Valencia, A. *et al.* (2004) IntAct: an open source molecular interaction database. *Nucleic Acids Res*, **32**, D452-455.

Hinton, R.B. and Yutzey, K.E. (2011) Heart valve structure and function in development and disease. *Annu Rev Physiol*, **73**, 29-46.

Huang, D.W., Sherman, B.T., Lempicki, R.A. (2009) Systematic and integrative analysis of large gene lists using DAVID bioinformatics resources. *Nature Protocols* **4**, 44–57.

Irizarry, R.A., Hobbs, B., Collin, F., Beazer-Barclay, Y.D., Antonellis, K.J., Scherf, U. and Speed, T.P. (2003) Exploration, normalization, and summaries of high density oligonucleotide array probe level data. *Biostatistics*, **4**, 249-264.

Jager, S., Handschin, C., St-Pierre, J. and Spiegelman, B.M. (2007) AMP-activated protein kinase (AMPK) action in skeletal muscle via direct phosphorylation of PGC-1alpha. *Proc Natl Acad Sci U S A*, **104**, 12017-12022.

Johnson, W.E., Li, C. and Rabinovic, A. (2007) Adjusting batch effects in microarray expression data using empirical Bayes methods. *Biostatistics*, **8**, 118-127.

Johri, A. and Beal, M.F. (2012) Mitochondrial dysfunction in neurodegenerative diseases. *J Pharmacol Exp Ther*, **342**, 619-630.

Jones, M.W., Errington, M.L., French, P.J., Fine, A., Bliss, T.V., Garel, S., Charnay, P., Bozon, B., Laroche, S. and Davis, S. (2001) A requirement for the immediate early gene Zif268 in the expression of late LTP and long-term memories. *Nat Neurosci*, **4**, 289-296.

Joshi-Tope, G., Gillespie, M., Vastrik, I., D'Eustachio, P., Schmidt, E., de Bono, B., Jassal, B., Gopinath, G.R., Wu, G.R., Matthews, L. *et al.* (2005) Reactome: a knowledgebase of biological pathways. *Nucleic Acids Res*, **33**, D428-432.

Kahlem, P., Sultan, M., Herwig, R., Steinfath, M., Balzereit, D., Eppens, B., Saran, N.G., Pletcher, M.T., South, S.T., Stetten, G. *et al.* (2004) Transcript level alterations reflect gene dosage effects across multiple tissues in a mouse model of down syndrome. *Genome Res*, **14**, 1258-1267.

Kanehisa, M. and Goto, S. (2000) KEGG: kyoto encyclopedia of genes and genomes. *Nucleic Acids Res*, **28**, 27-30.

Kauffmann, A., Gentleman, R. and Huber, W. (2009) arrayQualityMetrics--a bioconductor package for quality assessment of microarray data. *Bioinformatics*, **25**, 415-416.

Kim, S.H., Fountoulakis, M., Dierssen, M. and Lubec, G. (2001) Decreased protein levels of complex I 30-kDa subunit in fetal Down syndrome brains. *J Neural Transm Suppl*, 109-116.

Kiskinis, E., Hallberg, M., Christian, M., Olofsson, M., Dilworth, S.M., White, R. and Parker, M.G. (2007) RIP140 directs histone and DNA methylation to silence Ucp1 expression in white adipocytes. *The EMBO journal*, **26**, 4831-4840.

Knapska, E. and Kaczmarek, L. (2004) A gene for neuronal plasticity in the mammalian brain: Zif268/Egr-1/NGFI-A/Krox-24/TIS8/ZENK? *Prog Neurobiol*, **74**, 183-211.

Korbel, J.O., Tirosh-Wagner, T., Urban, A.E., Chen, X.N., Kasowski, M., Dai, L., Grubert, F., Erdman, C., Gao, M.C., Lange, K. *et al.* (2009) The genetic architecture of Down syndrome phenotypes revealed by high-resolution analysis of human segmental trisomies. *Proc Natl Acad Sci U S A*, **106**, 12031-12036.

Korenberg, J.R., Kawashima, H., Pulst, S.M., Ikeuchi, T., Ogasawara, N., Yamamoto, K., Schonberg, S.A., West, R., Allen, L., Magenis, E. *et al.* (1990) Molecular definition of a region of chromosome 21 that causes features of the Down syndrome phenotype. *Am J Hum Genet*, **47**, 236-246.

Kurnit, D.M., Aldridge, J.F., Neve, R.L. and Matthysse, S. (1985) Genetics of congenital heart malformations: a stochastic model. *Ann N Y Acad Sci*, **450**, 191-204.

Lagouge, M., Argmann, C., Gerhart-Hines, Z., Meziane, H., Lerin, C., Daussin, F., Messadeq, N., Milne, J., Lambert, P., Elliott, P. *et al.* (2006) Resveratrol improves mitochondrial function and protects against metabolic disease by activating SIRT1 and PGC-1alpha. *Cell*, **127**, 1109-1122.

Lander, E.S. (1999) Array of hope. *Nat Genet*, **21**, 3-4.

Leone, T.C., Lehman, J.J., Finck, B.N., Schaeffer, P.J., Wende, A.R., Boudina, S., Courtois, M., Wozniak, D.F., Sambandam, N., Bernal-Mizrachi, C. *et al.* (2005) PGC-1alpha deficiency causes multi-system energy metabolic derangements: muscle dysfunction, abnormal weight control and hepatic steatosis. *PLoS biology*, **3**, e101.

Li, C.M., Guo, M., Salas, M., Schupf, N., Silverman, W., Zigman, W.B., Husain, S., Warburton, D., Thaker, H. and Tycko, B. (2006) Cell type-specific over-expression of chromosome 21 genes in fibroblasts and fetal hearts with trisomy 21. *BMC medical genetics*, **7**, 24.

Lincoln, J., Lange, A.W. and Yutzey, K.E. (2006) Hearts and bones: shared regulatory mechanisms in heart valve, cartilage, tendon, and bone development. *Dev Biol*, **294**, 292-302.

Liu, C., Belichenko, P.V., Zhang, L., Fu, D., Kleschevnikov, A.M., Baldini, A., Antonarakis, S.E., Mobley, W.C. and Yu, Y.E. (2011) Mouse models for Down syndrome-associated developmental cognitive disabilities. *Dev Neurosci*, **33**, 404-413.

Liu, C., Morishima, M., Jiang, X., Yu, T., Meng, K., Ray, D., Pao, A., Ye, P., Parmacek, M.S. and Yu, Y.E. (2013) Engineered chromosome-based genetic mapping establishes a 3.7 Mb critical genomic region for Down syndrome-associated heart defects in mice. *Hum Genet*.

Lyle, R., Bena, F., Gagos, S., Gehrig, C., Lopez, G., Schinzel, A., Lespinasse, J., Bottani, A., Dahoun, S., Taine, L. *et al.* (2009) Genotype-phenotype correlations in Down syndrome identified by array CGH in 30 cases of partial trisomy and partial monosomy chromosome 21. *Eur J Hum Genet*, **17**, 454-466.

Lyle, R., Gehrig, C., Neergaard-Henrichsen, C., Deutsch, S. and Antonarakis, S.E. (2004) Gene expression from the aneuploid chromosome in a trisomy mouse model of down syndrome. *Genome Res*, **14**, 1268-1274.

Maglott, D., Ostell, J., Pruitt, K.D. and Tatusova, T. (2007) Entrez Gene: gene-centered information at NCBI. *Nucleic Acids Res*, **35**, D26-31.

Mao, R., Wang, X., Spitznagel, E.L., Jr., Frelin, L.P., Ting, J.C., Ding, H., Kim, J.W., Ruczinski, I., Downey, T.J. and Pevsner, J. (2005) Primary and secondary transcriptional effects in the developing human Down syndrome brain and heart. *Genome biology*, **6**, R107.

Matsumoto, K., Kamiya, N., Suwan, K., Atsumi, F., Shimizu, K., Shinomura, T., Yamada, Y., Kimata, K. and Watanabe, H. (2006) Identification and characterization of versican/PG-M aggregates in cartilage. *J Biol Chem*, **281**, 18257-18263.

Matys, V., Kel-Margoulis, O.V., Fricke, E., Liebich, I., Land, S., Barre-Dirrie, A., Reuter, I., Chekmenev, D., Krull, M., Hornischer, K. *et al.* (2006) TRANSFAC and its module TRANSCompel: transcriptional gene regulation in eukaryotes. *Nucleic Acids Res*, **34**, D108-110.

McCall, M.N., Murakami, P.N., Lukk, M., Huber, W. and Irizarry, R.A. (2011) Assessing affymetrix GeneChip microarray quality. *BMC bioinformatics*, **12**, 137.

Meyer, P.E., Lafitte, F. and Bontempi, G. (2008) minet: A R/Bioconductor package for inferring large transcriptional networks using mutual information. *BMC bioinformatics*, **9**, 461.

Mitra, R., Nogee, D.P., Zechner, J.F., Yea, K., Gierasch, C.M., Kovacs, A., Medeiros, D.M., Kelly, D.P. and Duncan, J.G. (2012) The transcriptional coactivators, PGC-1alpha and beta, cooperate to maintain cardiac mitochondrial function during the early stages of insulin resistance. *Journal of molecular and cellular cardiology*, **52**, 701-710.

Miwa, H.E., Gerken, T.A., Huynh, T.D., Flory, D.M. and Hering, T.M. (2006) Mammalian expression of full-length bovine aggrecan and link protein: formation of recombinant proteoglycan aggregates and analysis of proteolytic cleavage by ADAMTS-4 and MMP-13. *Biochim Biophys Acta*, **1760**, 472-486.

Mootha, V.K., Lindgren, C.M., Eriksson, K.F., Subramanian, A., Sihag, S., Lehar, J., Puigserver, P., Carlsson, E., Ridderstrale, M., Laurila, E. *et al.* (2003) PGC-1alpha-responsive genes involved in oxidative phosphorylation are coordinately downregulated in human diabetes. *Nat Genet*, **34**, 267-273.

Nautiyal, J., Christian, M. and Parker, M.G. (2013) Distinct functions for RIP140 in development, inflammation, and metabolism. *Trends Endocrinol Metab*, **24**, 451-459.

Nicolakakis, N., Aboulkassim, T., Ongali, B., Lecrux, C., Fernandes, P., Rosa-Neto, P., Tong, X.K. and Hamel, E. (2008) Complete rescue of cerebrovascular function in aged Alzheimer's disease transgenic mice by antioxidants and pioglitazone, a peroxisome proliferator-activated receptor gamma agonist. *J Neurosci*, **28**, 9287-9296.

Normand, S.L. (1999) Meta-analysis: formulating, evaluating, combining, and reporting. *Stat Med*, **18**, 321-359.

Ntzani, E.E. and Ioannidis, J.P. (2003) Predictive ability of DNA microarrays for cancer outcomes and correlates: an empirical assessment. *Lancet*, **362**, 1439-1444.

O'Leary, D.A., Pritchard, M.A., Xu, D., Kola, I., Hertzog, P.J. and Ristevski, S. (2004) Tissue-specific overexpression of the HSA21 gene GABPalpha: implications for DS. *Biochim Biophys Acta*, **1739**, 81-87.

Paik, S. (2007) Development and clinical utility of a 21-gene recurrence score prognostic assay in patients with early breast cancer treated with tamoxifen. *Oncologist*, **12**, 631-635.

Park, S.C., Mathews, R.A., Zuberbuhler, J.R., Rowe, R.D., Neches, W.H. and Lenox, C.C. (1977) Down syndrome with congenital heart malformation. *American journal of diseases of children*, **131**, 29-33.

Parman, C., Halling, C. (2008) affyQCReport: A Package to Generate QC Reports for Affymetrix Array Data.

Patergnani, S., Suski, J.M., Agnoletto, C., Bononi, A., Bonora, M., De Marchi, E., Giorgi, C., Marchi, S., Missiroli, S., Poletti, F. *et al.* (2011) Calcium signaling around Mitochondria Associated Membranes (MAMs). *Cell Commun Signal*, **9**, 19.

Perou, C.M., Jeffrey, S.S., van de Rijn, M., Rees, C.A., Eisen, M.B., Ross, D.T., Pergamenschikov, A., Williams, C.F., Zhu, S.X., Lee, J.C. *et al.* (1999) Distinctive gene expression patterns in human mammary epithelial cells and breast cancers. *Proc Natl Acad Sci U S A*, **96**, 9212-9217.

Person, A.D., Klewer, S.E. and Runyan, R.B. (2005) Cell biology of cardiac cushion development. *Int Rev Cytol*, **243**, 287-335.

Petrozzi, L., Ricci, G., Giglioli, N.J., Siciliano, G. and Mancuso, M. (2007) Mitochondria and neurodegeneration. *Biosci Rep*, **27**, 87-104.

Piccoli, C., Izzo, A., Scrima, R., Bonfiglio, F., Manco, R., Negri, R., Quarato, G., Cela, O., Ripoli, M., Prisco, M. *et al.* (2013) Chronic pro-oxidative state and mitochondrial dysfunctions are more pronounced in fibroblasts from Down syndrome foeti with congenital heart defects. *Hum Mol Genet*, **22**, 1218-1232.

Piwowar, H.A., Day, R.S. and Fridsma, D.B. (2007) Sharing detailed research data is associated with increased citation rate. *PLoS One*, **2**, e308.

Powelka, A.M., Seth, A., Virbasius, J.V., Kiskinis, E., Nicoloro, S.M., Guilherme, A., Tang, X., Straubhaar, J., Cherniack, A.D., Parker, M.G. *et al.*

(2006) Suppression of oxidative metabolism and mitochondrial biogenesis by the transcriptional corepressor RIP140 in mouse adipocytes. *J Clin Invest*, **116**, 125-136.

Rachidi, M. and Lopes, C. (2007) Mental retardation in Down syndrome: from gene dosage imbalance to molecular and cellular mechanisms. *Neurosci Res*, **59**, 349-369.

Ramasamy, A., Mondry, A., Holmes, C.C. and Altman, D.G. (2008) Key issues in conducting a meta-analysis of gene expression microarray datasets. *PLoS Med*, **5**, e184.

Rhodes, D.R., Yu, J., Shanker, K., Deshpande, N., Varambally, R., Ghosh, D., Barrette, T., Pandey, A. and Chinnaiyan, A.M. (2004) Large-scale meta-analysis of cancer microarray data identifies common transcriptional profiles of neoplastic transformation and progression. *Proc Natl Acad Sci U S A*, **101**, 9309-9314.

Roat, E., Prada, N., Ferraresi, R., Giovenzana, C., Nasi, M., Troiano, L., Pinti, M., Nemes, E., Lugli, E., Biagioni, O. *et al.* (2007) Mitochondrial alterations and tendency to apoptosis in peripheral blood cells from children with Down syndrome. *FEBS Lett*, **581**, 521-525.

Rodgers, J.T., Lerin, C., Haas, W., Gygi, S.P., Spiegelman, B.M. and Puigserver, P. (2005) Nutrient control of glucose homeostasis through a complex of PGC-1alpha and SIRT1. *Nature*, **434**, 113-118.

Romero, P., Wagg, J., Green, M.L., Kaiser, D., Krummenacker, M. and Karp, P.D. (2005) Computational prediction of human metabolic pathways from the complete human genome. *Genome biology*, **6**, R2.

Ronan, A., Fagan, K., Christie, L., Conroy, J., Nowak, N.J. and Turner, G. (2007) Familial 4.3 Mb duplication of 21q22 sheds new light on the Down syndrome critical region. *J Med Genet*, **44**, 448-451.

Rueda, N., Florez, J. and Martinez-Cue, C. (2013) Apoptosis in Down's syndrome: lessons from studies of human and mouse models. *Apoptosis*, **18**, 121-134.

Rytinki, M.M. and Palvimo, J.J. (2008) SUMOylation modulates the transcription repressor function of RIP140. *J Biol Chem*, **283**, 11586-11595.

Rytinki, M.M. and Palvimo, J.J. (2009) SUMOylation attenuates the function of PGC-1alpha. *J Biol Chem*, **284**, 26184-26193.

Saran, N.G., Pletcher, M.T., Natale, J.E., Cheng, Y. and Reeves, R.H. (2003) Global disruption of the cerebellar transcriptome in a Down syndrome mouse model. *Hum Mol Genet*, **12**, 2013-2019.

Scarpulla, R.C. (2011) Metabolic control of mitochondrial biogenesis through the PGC-1 family regulatory network. *Biochim Biophys Acta*, **1813**, 1269-1278.

Scarpulla, R.C., Vega, R.B. and Kelly, D.P. (2012) Transcriptional integration of mitochondrial biogenesis. *Trends Endocrinol Metab*, **23**, 459-466.

Schreiber, S.N., Emter, R., Hock, M.B., Knutti, D., Cardenas, J., Podvinec, M., Oakeley, E.J. and Kralli, A. (2004) The estrogen-related receptor alpha (ERRalpha) functions in PPARgamma coactivator 1alpha (PGC-1alpha)-induced mitochondrial biogenesis. *Proc Natl Acad Sci U S A*, **101**, 6472-6477.

Schuchmann, S. and Heinemann, U. (2000) Increased mitochondrial superoxide generation in neurons from trisomy 16 mice: a model of Down's syndrome. *Free radical biology & medicine*, **28**, 235-250.

Seidah, N.G., Poirier, S., Denis, M., Parker, R., Miao, B., Mapelli, C., Prat, A., Wassef, H., Davignon, J., Hajjar, K.A. *et al.* (2012) Annexin A2 is a natural extrahepatic inhibitor of the PCSK9-induced LDL receptor degradation. *PLoS One*, **7**, e41865.

Seth, A., Steel, J.H., Nichol, D., Pocock, V., Kumaran, M.K., Fritah, A., Mobberley, M., Ryder, T.A., Rowlerson, A., Scott, J. *et al.* (2007) The transcriptional corepressor RIP140 regulates oxidative metabolism in skeletal muscle. *Cell Metab*, **6**, 236-245.

Sharma, H.S., Peters, T.H., Moorhouse, M.J., van der Spek, P.J. and Bogers, A.J. (2006) DNA microarray analysis for human congenital heart disease. *Cell Biochem Biophys*, **44**, 1-9.

Shin, J.H., London, J., Le Pecheur, M., Hoger, H., Pollak, D. and Lubec, G. (2004) Aberrant neuronal and mitochondrial proteins in hippocampus of transgenic mice overexpressing human Cu/Zn superoxide dismutase 1. *Free radical biology & medicine*, **37**, 643-653.

Shukkur, E.A., Shimohata, A., Akagi, T., Yu, W., Yamaguchi, M., Murayama, M., Chui, D., Takeuchi, T., Amano, K., Subramhanya, K.H. *et al.* (2006) Mitochondrial dysfunction and tau hyperphosphorylation in Ts1Cje, a mouse model for Down syndrome. *Hum Mol Genet*, **15**, 2752-2762.

Smyth, G.K., Michaud, J. and Scott, H.S. (2005) Use of within-array replicate spots for assessing differential expression in microarray experiments. *Bioinformatics*, **21**, 2067-2075.

Sommer, C.A., Pavarino-Bertelli, E.C., Goloni-Bertollo, E.M. and Henrique-Silva, F. (2008) Identification of dysregulated genes in lymphocytes

from children with Down syndrome. *Genome / National Research Council Canada = Genome / Conseil national de recherches Canada*, **51**, 19-29.

Staunton, J.E., Slonim, D.K., Coller, H.A., Tamayo, P., Angelo, M.J., Park, J., Scherf, U., Lee, J.K., Reinhold, W.O., Weinstein, J.N. *et al.* (2001) Chemosensitivity prediction by transcriptional profiling. *Proc Natl Acad Sci U S A*, **98**, 10787-10792.

Stoddart, A., Fernald, A.A., Wang, J., Davis, E.M., Karrison, T., Anastasi, J. and Le Beau, M.M. (2014) Haploinsufficiency of del(5q) genes, Egr1 and Apc, cooperate with Tp53 loss to induce acute myeloid leukemia in mice. *Blood*, **123**, 1069-1078.

Suarez-Farinas, M., Noggle, S., Heke, M., Hemmati-Brivanlou, A. and Magnasco, M.O. (2005) Comparing independent microarray studies: the case of human embryonic stem cells. *BMC Genomics*, **6**, 99.

Subramanian, A., Tamayo, P., Mootha, V.K., Mukherjee, S., Ebert, B.L., Gillette, M.A., Paulovich, A., Pomeroy, S.L., Golub, T.R., Lander, E.S. *et al.* (2005) Gene set enrichment analysis: a knowledge-based approach for interpreting genome-wide expression profiles. *Proc Natl Acad Sci U S A*, **102**, 15545-15550.

Supek, F., Bosnjak, M., Skunca, N. and Smuc, T. (2011) REVIGO summarizes and visualizes long lists of gene ontology terms. *PLoS One*, **6**, e21800.

Surana, R., Sikka, S., Cai, W., Shin, E.M., Warrier, S.R., Tan, H.J., Arfuso, F., Fox, S.A., Dharmarajan, A.M. and Kumar, A.P. (2014) Secreted frizzled related proteins: Implications in cancers. *Biochim Biophys Acta*, **1845**, 53-65.

van 't Veer, L.J., Dai, H., van de Vijver, M.J., He, Y.D., Hart, A.A., Mao, M., Peterse, H.L., van der Kooy, K., Marton, M.J., Witteveen, A.T. *et al.* (2002) Gene expression profiling predicts clinical outcome of breast cancer. *Nature*, **415**, 530-536.

Ventura, B. (2005) Mandatory submission of microarray data to public repositories: how is it working? *Physiol Genomics*, **20**, 153-156.

Vicari S. (2001) Implicit versus explicit memory function in children with Down and Williams syndrome. *Downs Syndr Res Pract*, **7**, 35-40.

Vilardell, M., Civit, S. and Herwig, R. (2013) An integrative computational analysis provides evidence for FBN1-associated network deregulation in trisomy 21. *Biol Open*, **2**, 771-778.

Vilardell, M., Rasche, A., Thormann, A., Maschke-Dutz, E., Perez-Jurado, L.A., Lehrach, H. and Herwig, R. (2011) Meta-analysis of heterogeneous Down Syndrome data reveals consistent genome-wide dosage effects related to neurological processes. *BMC Genomics*, **12**, 229.

Vo, N., Fjeld, C. and Goodman, R.H. (2001) Acetylation of nuclear hormone receptor-interacting protein RIP140 regulates binding of the transcriptional corepressor CtBP. *Molecular and cellular biology*, **21**, 6181-6188.

Walker, E., Hernandez, A.V. and Kattan, M.W. (2008) Meta-analysis: Its strengths and limitations. *Cleve Clin J Med*, **75**, 431-439.

Wang, J., Duncan, D., Shi, Z. and Zhang, B. (2013) WEB-based GEne SeT AnaLysis Toolkit (WebGestalt): update 2013. *Nucleic Acids Res*, **41**, W77-83.

Wang, S.S., Hsiao, R., Limpar, M.M., Lomahan, S., Tran, T.A., Maloney, N.J., Ikegaki, N. and Tang, X.X. (2014) Destabilization of MYC/MYCN by the mitochondrial inhibitors, metaiodobenzylguanidine, metformin and phenformin. *Int J Mol Med*, **33**, 35-42.

Watanabe, H. and Yamada, Y. (1999) Mice lacking link protein develop dwarfism and craniofacial abnormalities. *Nat Genet*, **21**, 225-229.

Wei, L.N., Hu, X., Chandra, D., Seto, E. and Farooqui, M. (2000) Receptor-interacting protein 140 directly recruits histone deacetylases for gene silencing. *J Biol Chem*, **275**, 40782-40787.

Wilson, C.L. and Miller, C.J. (2005) Simpleaffy: a BioConductor package for Affymetrix Quality Control and data analysis. *Bioinformatics*, **21**, 3683-3685.

Wirrig, E.E., Snarr, B.S., Chintalapudi, M.R., O'Neal J, L., Phelps, A.L., Barth, J.L., Fresco, V.M., Kern, C.B., Mjaatvedt, C.H., Toole, B.P. *et al.* (2007) Cartilage link protein 1 (Crtl1), an extracellular matrix component playing an important role in heart development. *Dev Biol*, **310**, 291-303.

Wotton, S., Terry, A., Kilbey, A., Jenkins, A., Herzyk, P., Cameron, E. and Neil, J.C. (2008) Gene array analysis reveals a common Runx transcriptional programme controlling cell adhesion and survival. *Oncogene*, **27**, 5856-5866.

Wright, T.C., Orkin, R.W., Destrempes, M. and Kurnit, D.M. (1984) Increased adhesiveness of Down syndrome fetal fibroblasts in vitro. *Proc Natl Acad Sci U S A*, **81**, 2426-2430.

Yamaguchi, Y., Saito, K., Matsuno, T., Takeda, K. and Hino, M. (2012) Effects of ZSET1446/ST101 on cognitive deficits and amyloid beta deposition in the senescence accelerated prone mouse brain. *J Pharmacol Sci*, **119**, 160-166.

Yla-Herttuala, S., Luoma, J., Nikkari, T. and Kivimaki, T. (1989) Down's syndrome and atherosclerosis. *Atherosclerosis*, **76**, 269-272.

Zambelli, F., Pesole, G. and Pavesi, G. (2009) Pscan: finding over-represented transcription factor binding site motifs in sequences from co-regulated or co-expressed genes. *Nucleic Acids Res*, **37**, W247-252.

Human Molecular Genetics, 2013, Vol. 22, No. 6 **1218–1232**
doi:10.1093/hmg/dds529
Advance Access published on December 20, 2012

Chronic pro-oxidative state and mitochondrial dysfunctions are more pronounced in fibroblasts from Down syndrome foeti with congenital heart defects

Claudia Piccoli[1,†], Antonella Izzo[2,†], Rosella Scrima[1], Ferdinando Bonfiglio[2], Rosanna Manco[2], Rosa Negri[2], Giovanni Quarato[1], Olga Cela[1], Maria Ripoli[1], Marina Prisco[3], Flaviana Gentile[4], Gaetano Calì[4], Paolo Pinton[5], Anna Conti[2], Lucio Nitsch[2,†] and Nazzareno Capitanio[1,*,†]

[1]Department of Clinical and Experimental Medicine, University of Foggia, Foggia 71100, Italy, [2]Department of Cellular and Molecular Biology and Pathology and [3]Department of Biological Sciences, University of Naples Federico II, Naples 80131, Italy, [4]Institute of Experimental Endocrinology and Oncology, National Research Council, Naples 80131, Italy and [5]Department of Experimental and Diagnostic Medicine, University of Ferrara, Ferrara 44100, Italy

Received October 27, 2012; Revised and Accepted December 12, 2012

Trisomy of chromosome 21 is associated to congenital heart defects in ∼50% of affected newborns. Transcriptome analysis of hearts from trisomic human foeti demonstrated that genes involved in mitochondrial function are globally downregulated with respect to controls, suggesting an impairment of mitochondrial function. We investigated here the properties of mitochondria in fibroblasts from trisomic foeti with and without cardiac defects. Together with the upregulation of Hsa21 genes and the downregulation of nuclear encoded mitochondrial genes, an abnormal mitochondrial cristae morphology was observed in trisomic samples. Furthermore, impairment of mitochondrial respiratory activity, specific inhibition of complex I, enhanced reactive oxygen species production and increased levels of intra-mitochondrial calcium were demonstrated. Seemingly, mitochondrial dysfunction was more severe in fibroblasts from cardiopathic trisomic foeti that presented a more pronounced pro-oxidative state. The data suggest that an altered bioenergetic background in trisomy 21 foeti might be among the factors responsible for a more severe phenotype. Since the mitochondrial functional alterations might be rescued following pharmacological treatments, these results are of interest in the light of potential therapeutic interventions.

INTRODUCTION

Down syndrome (DS) is characterized by a complex phenotype in which over 80 features occur with various degrees of expression and frequency (1). DS is a major cause of congenital heart defects (CHD) mainly endocardial cushion defects, the most frequent being atrioventricular canal defects followed by ventricular septal defects and tetralogy of Fallot (2). By comparing the gene expression profiles of 10 human hearts from trisomic foeti to five foetal hearts of non-trisomic controls, we previously demonstrated a global upregulation of chromosome 21 (Hsa21) genes and a dysregulation of ∼400 genes localized on other chromosomes (3). Microarray analysis clearly showed the downregulation of genes encoding all five mitochondrial complex subunits and of genes implicated in mitochondrial biogenesis. This suggested that the corresponding proteins and enzymatic activities might be reduced in DS subjects and that mitochondrial function could be consequently impaired.

*To whom correspondence should be addressed at: Department of Clinical and Experimental Medicine, Via Pinto 1 c/o OO.RR., 71100 Foggia, Italy. Tel: +39 881711148; Fax: +39 881714745; Email: n.cap@unifg.it
†The authors wish it to be known that, in their opinion, the first two authors (C.P., A.I.) should be regarded as joint First Authors and that the last two authors (L.N., N.C.) contributed equally to the work.

Trisomy of chromosome 21 has been associated with mitochondrial dysfunction in cells and tissues from DS subjects (4–6) and in mouse models (7,8). These results led to the hypothesis that mitochondrial dysfunction contributes to the DS phenotype. Protein levels of mitochondrial complexes I, III and V were decreased in cerebellar and brain regions of DS subjects (9). Complex I was also deficient in mouse models of trisomy of chromosome 16. The results were similar to those obtained from models of Parkinson's disease, suggesting that different neurodegenerative diseases may be associated with the same mitochondrial dysfunction (10).

Recently, it has been also reported that the mitochondrial energy production apparatus was less efficient in foetal DS fibroblasts, due to the dysregulation of adenine nucleotide translocator, ATP synthase and adenylate kinase, and a selective deficit of complex I, which contributes to reactive oxygen species (ROS) overproduction in DS mitochondria. These events were attributed to changes in the cAMP/PKA signalling pathway (11,12), which is known to affect the abundance of the transcriptional coactivator *PGC-1α* (peroxisome proliferator-activated receptor gamma coactivator 1-alpha). This protein, that plays a central role in regulating mitochondrial biogenesis and respiratory function through the interaction with transcriptional partners, like *NRF1*, *ERRα*, *PPARs* and *YY1*, is negatively controlled by the co-repressor *RIP140*, a gene mapping to Hsa21 (13).

Even though these results are indicative of widespread mitochondrial dysfunction in DS, molecular studies have not yet been performed to investigate the basis of mitochondrial dysfunction at the transcriptional level. Furthermore, no hypotheses have been formulated about the mechanisms by which trisomy of Hsa21 genes might induce such a dysfunction.

The original contribution of the present study consists of a contemporary analysis of mitochondrial features at the molecular, morphological and functional level in 13 human primary lines of foetal fibroblasts (HFF) derived from Hsa21 trisomic foeti, with or without CHD, and from euploid controls. The mitochondrial defects associated with DS were analysed taking into account the regulation of the Hsa21 and mitochondrial-related genes and the cardiac phenotype, in order to identify pathways involved in mitochondrial function and dysrupted by the Hsa21 trisomy. A striking and more severe ROS- and Ca^{2+}-related mitochondrial dysfunction emerged in cardiopathic-derived Hsa21 trisomic fibroblasts, unveiling a more pronounced pro-oxidative state.

RESULTS

The present study combines the molecular, morphological and functional analyses of mitochondria in 13 human primary cultures of HFF. Five were from euploid foeti (N-HFF, N standing for normal), and eight (DS-HFF) were derived from Hsa21 trisomic foeti [four samples from DS foeti with heart defects, named CDS-HFF (CDS standing for Cardiopathic Down Syndrome), and four samples from DS foeti without heart defects, named NCDS-HFF (NCDS standing for Non Cardiopathic Down Syndrome)].

Gene expression is dysregulated in DS-HFF samples

The analysis of HFF karyotypes demonstrated that all trisomic fibroblasts showed three copies of Hsa21 as the only cytogenetic alteration (data not shown). The expression of some Hsa21 genes was determined by quantitative real-time PCR (qRT-PCR) experiments comparing DS-HFF versus N-HFF. In particular, the Hsa21 genes *BTG3*, *SOD1*, *ITSN1*, *DYRK1A*, *NRF2* and *RIP140* were upregulated in trisomic fibroblasts when compared with controls (Fig. 1A), thus confirming the gene dosage effects that was previously demonstrated in human foetal tissues (3,14). We then focused on genes that mapped to chromosomes different from Hsa21 and were involved in multiple mitochondrial functions, such as the respiratory chain, mitochondrial biogenesis and morphology, and genes involved in related pathways, such as the *Calcineurin/NFAT* (Nuclear factor of activated T-cells) axe. Most of the analysed genes were significantly downregulated in trisomic versus euploid fibroblasts (Fig. 1B), demonstrating that trisomy of chromosome 21 perturbs the expression of genes involved in mitochondrial pathways. Moreover, *NFATc3* and *NFATc4* were significantly downregulated while *DYRK1A* and *RCAN1*, two Hsa21 genes involved in regulating the levels of *NFATc* phosphorylation, were upregulated in trisomic versus euploid fibroblasts (Fig. 1C).

Mitochondria of DS-HFF show morphological abnormalities

Electron microscopy (EM) of trisomic fibroblasts revealed that a significant number of mitochondria had an abnormal morphology, showing an increased size, irregular shape, evident breaks, mainly of inner membranes. In addition, the mitochondria showed alterations in the pattern of cristae where some were broadened and arranged concentrically or oriented parallel to the long axis of the organelle (longitudinal cristae) (Fig. 2A). Broken mitochondria and mitochondria with concentric and longitudinal cristae were significantly more abundant in trisomic samples than in the euploid ones ($P < 0.05$) (Fig. 2B). Stereological analysis demonstrated that the mitochondrial volume density, expressed as a percentage of cellular volume, was similar in euploid and trisomic samples while the cristae volume density, expressed as a percentage of mitochondrial volume, was significantly lower in all DS-HFF samples when compared with N-HFF ($P < 0.05$) (Fig. 2C and D).

The functional mitochondrial phenotype is altered in CDS-HFF

Endogenous oxygen consumption rate in intact HFF

The respiratory activity of N-HFF and DS-HFF samples was compared by high-resolution oxymetry. The oxygen consumption rate (OCR) was assessed in intact cells relying on endogenous respiratory substrates and corrected for the residual KCN-sensitive OCR and, therefore, attributable to mitochondrial respiratory chain-dependent activity. Figure 3A shows the results of a systematic analysis whereby the activity of each cellular sample was measured. Although a relatively large inter-individual variability was observed within each of

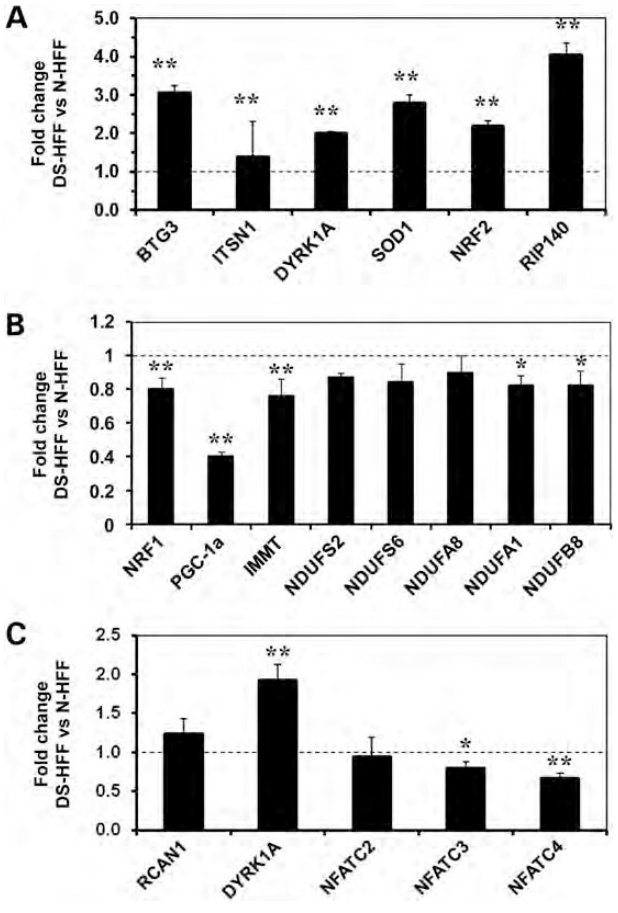

Figure 1. Gene expression is dysregulated in DS fibroblasts. Gene expression fold change in DS-HFF samples versus N-HFF samples for Hsa21 genes (**A**), nuclear-encoded mitochondrial genes (**B**) and calcineurin/NFAT-related genes (**C**) as obtained by qRT-PCR. Values represent the mean of three replicates ± SEM. $^{*}P < 0.05$, $^{**}P < 0.01$, N-HFF, Euploid fibroblasts; DS-HFF, Hsa21 trisomic fibroblasts.

the three groups, on an average basis, the resting respiration of DS-HFF showed a significant decrease that was more evident in CDS-HFF (≈43% inhibition) when compared with N-HFF. Conversely, a slight increase in the OCR in the presence of the FoF1-ATP synthase inhibitor oligomycin was observed in DS-HFF, whereas in the presence of the protonophoric uncoupler FCCP a slight, albeit significant, decrease (≈27% inhibition) in the OCR was observed in CDS-HFF when compared with N-HFF. The respiratory control ratio (RCR), attained by dividing the uncoupled OCR by that in the presence of oligomycin, was as high as 14–16 irrespective of the cell group analysed (Fig. 3B). The ATP-synthase independent OCR (leak) was unchanged between N- and DS-HFF, whereas the oxidative phosphorylation-dependent OCR (OXPHOS) was significantly reduced in DS-HFF, and more specifically in CDS-HFF, by 36% when compared with N-HFF (Fig. 3B). The decrease in OCR_{RR}, observed in DS-HFF, individually correlated to the altered mitochondrial morphology and cristae volume density assessed by EM (Fig. 3C). Next, we measured the mitochondrial membrane potential ($\Delta\Psi_m$) by confocal microscopic imaging using the specific mitotropic probe TMRE. A significant difference was not observed in the TMRE-related fluorescence among N-HFF, NCDS-HFF and CDS-HFF (Fig. 4A), even though a finer analysis of the fluorescent signal revealed a less interdigitated mitochondrial network morphology in DS-HFF (Fig. 4B).

Complex I activity

To assess if the observed respiratory deficit in DS-HFF resulted from a specific defect in one or the other of the respiratory chain complexes, the activity of the protonmotive complexes I, III and IV was measured in cell lysates. The activity of citrate synthase, which is an index of mitochondrial mass, was also measured. Figure 5A shows that the activity of complex I was significantly depressed (by about 50%) in both NCDS-HFF and CDS-HFF when compared with N-HFF. The decreased activity of complex I correlated with the altered mitochondrial cristae morphology. Conversely, significant differences in activities of complexes III and IV were not observed among the three cell groups (Fig. 5B and C). Likewise, the citrate synthase activity was practically unaffected (Fig. 5D); therefore, following normalization to the mitochondrial mass, the selective inhibition of complex I in trisomic cells was confirmed (data not shown). Total protein levels per cell were slightly less in trisomic samples but not to a statistically significance degree compared with N-HFF (Fig. 5E).

Mitochondria-related ROS production

Intracellular ROS level was assessed by confocal microscopy imaging of cells treated with the redox-sensitive fluorescent probe DCF. Every trisomic sample displayed an enhanced ROS production when compared with N-HFF, with a larger redox imbalance in CDS-HFF (Fig. 6A). Enlargement of the confocal images showed a compartmentalized, brighter signal of the DCF-related fluorescence with a very low variability within each group. On an average basis, the ROS-related DCF fluorescence was much larger in CDS-HFF when compared with NCDS-HFF (Fig. 6B). Plotting the DCF fluorescence versus the normalized complex I activity for each individual HFF sample suggested the presence of a threshold value of complex I activity below which extra-ROS production was generated (Fig. 6C). To further ascertain the source of the ROS release in DS-HFF, cells were treated with DPI, which is a pan-inhibitor of flavin-containing oxidases (including complex I). DPI treatment was associated with a marked decrease in the ROS over-production in representative samples of both NCDS- and CDS-HFF, whereas it was ineffective in N-HFF (Fig. 7). Production of ROS by the respiratory chain complex I is fostered by the presence of a $\Delta\Psi_m$ (15). Short-time incubation of cells with the uncoupler FCCP significantly inhibited ROS release both in NCDS- and CDS-HFF with a larger effect in the latter (Fig. 7). It has been recently reported that alteration of PKA-dependent signalling affects functioning of the oxidative phosphorylation (OXPHOS) system (11,16,17). Treatment of cells with the cAMP analogue db-cAMP significantly reduced ROS production in both NCDS- and CDS-HFF although the redox state, especially in CDS-HFF, was not fully renormalized to the level of N-HFF (cf. Fig. 7 with 6B).

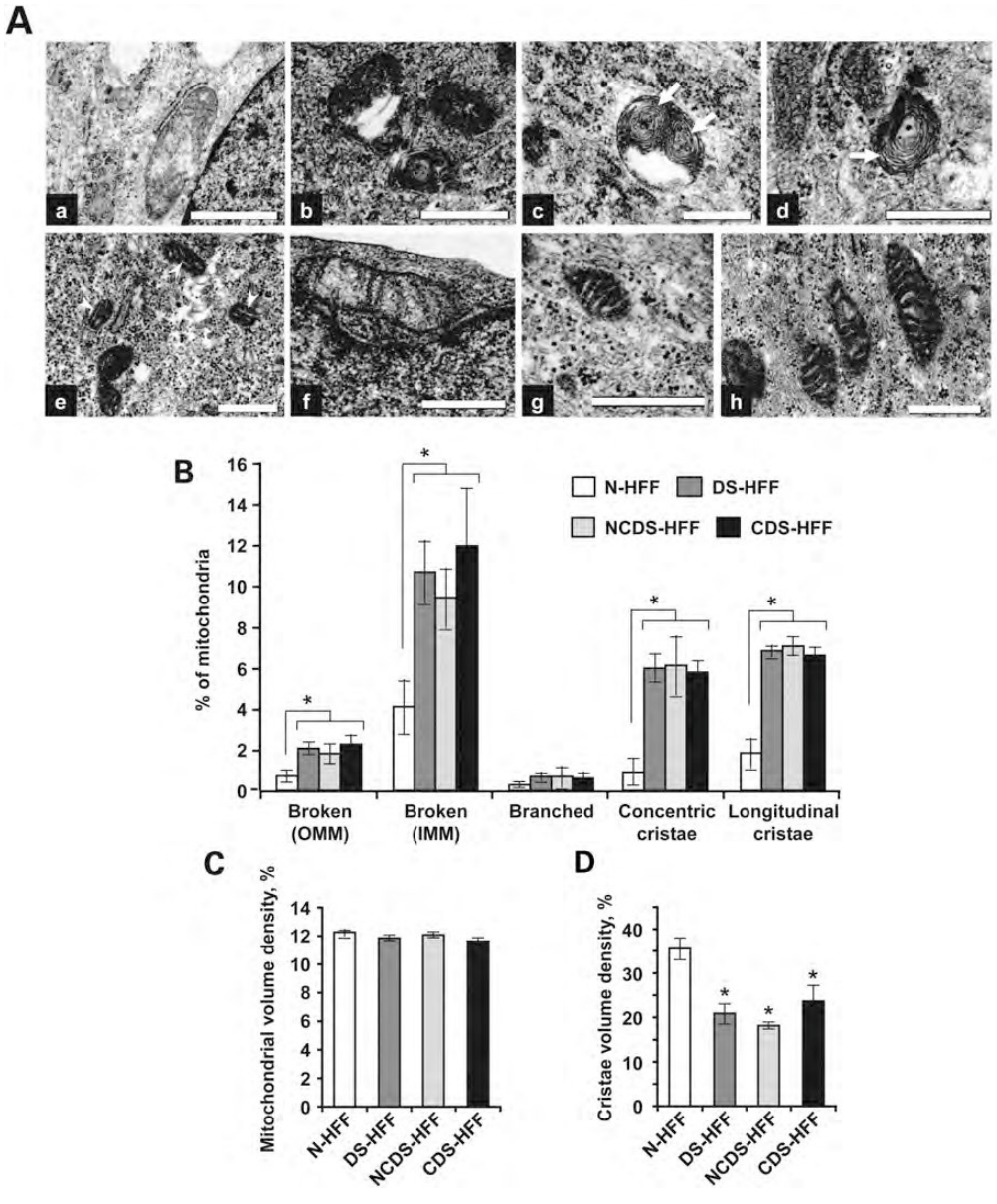

Figure 2. Mitochondria of DS fibroblasts show morphological abnormalities. (**A**) Electron micrographs of morphologically abnormal mitochondria in DS-HFF (a–f) and normal mitochondria in N-HFF (g and h); (a and b) broken mitochondria; (c and d) mitochondria with concentric cristae (arrow); (e) mitochondria with longitudinal cristae (arrow head); (f) mitochondria with significantly reduced cristae; (g and h) mitochondria with unchanged morphology in N-HFF. Scale bars: 500 nm. (**B**) Percentages of mitochondria with abnormal morphology in fibroblasts. (**C**) Mitochondrial volume density relative to cell volume. (**D**) Mitochondrial cristae volume density relative to mitochondrial volume. In (**B**)–(**D**), the mean values ± SEM are shown along with statistical analysis; $^{*}P$ significant cut off < 0.05 Kolmogorov–Smirnov and Kruskall–Wallis tests. N-HFF, euploid fibroblasts; DS-HFF, Hsa21 trisomic fibroblasts; NCDS-HFF, Hsa21 trisomic fibroblasts from DS foeti without heart defects; CDS-HFF, Hsa21 trisomic fibroblasts from DS foeti with heart defects.

Steady-state intra-mitochondrial calcium level

Deregulation of Ca^{2+} homeostasis and Ca^{2+}-mediated signalling has been described in cells derived from trisomic patients or in murine models of DS (18–20). Mitochondria are known to function as a Ca^{2+} buffer by taking up Ca^{2+} mainly via a specific ruthenium red (RR)-inhibitable uniporter (21,22). To verify this point, we evaluated the intramitochondrial level of calcium ($mtCa^{2+}$) using the specific probe Rhod-1. Figure 8A and B shows representative confocal microscopic images of the analysis along with statistical evaluation of the results. It is shown that DS-HFF displayed a statistically significant more intense Rhod-1-related fluorescence signal when compared with N-HFF. However, this was mainly contributed by the CDS-HFF samples. Closer examination of the intracellular fluorescence unveiled a compartmentalization of the brighter signal confirming that it was largely displaying the steady-state $mtCa^{2+}$ level. The enhanced $mtCa^{2+}$ load in DS-HFF correlated positively with the increase in ROS production (Fig. 8C) consistent with the notion that calcium entry in mitochondria induces redox state alterations (23).

To verify the interplay between calcium and ROS, representative trisomic samples were treated with RR and the redox

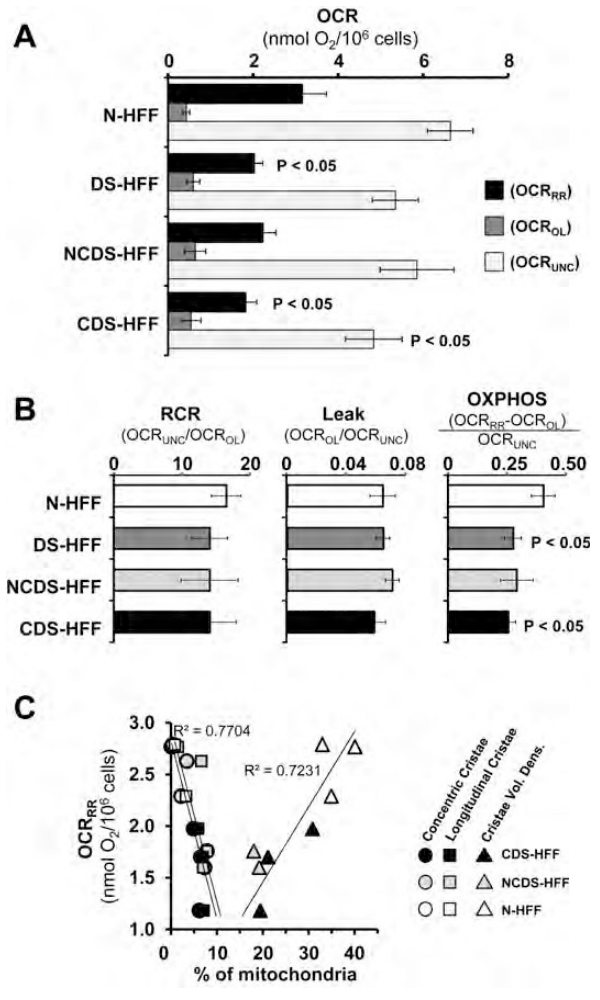

Figure 3. Respirometric analysis in DS fibroblasts. (**A**) OCRs normalized to cell number were assessed by high-resolution oxymetry in intact cells as described in the Materials and Methods. A comparative analysis between five different euploid (N-HFF) and eight different trisomic (DS-HFF) samples is shown; a distinction of the DS-HFF between non-cardiopathic (NCDS-HFF, $n = 4$) and cardiopathic (CDS-HFF, $n = 4$) foetus-derived fibroblasts is also reported. The endogenous OCR were measured under resting conditions (OCR_{RR}), in the presence of oligomycin (OCR_{OL}) and in the uncoupled state in the presence of FCCP (OCR_{UNC}). (**B**) Respiration-linked bioenergetic parameters computed by the OCR measurements shown in (A). RCR, respiratory control ratio; Leak, non-ATP-synthase-controlled respiratory activity; OXPHOS, ATP-synthase-controlled respiratory activity. The bars in (A) and (B) are means ± SEM of the average determinations for each sample carried out at least in triplicate; when statistically significant, the difference when compared with the euploid samples is shown. (**C**) Correlation plots between respiratory activity under resting conditions (OCR_{RR}) and percentage of concentric or longitudinal cristae or of cristae volume density for individual fibroblast samples (see the symbol legend).

state assessed by DCF. As shown in Figure 9A and B, inhibition of the mitochondrial Ca^{2+} porter by RR caused a substantial inhibition of ROS production, suggesting that the entry of Ca^{2+} in the mitochondrial compartment was at least partially responsible for the redox imbalance in trisomic cell samples. Moreover, treatment with RR resulted in enhancement of the respiratory activity in DS-HFF to the level of N-HFF (Fig. 9C). Similar results were obtained evaluating mitochondrial calcium levels by a different method based on a calcium-sensible photoprotein, the aequorin (see Supplementary Material, Text S1 and Fig. S1).

Mitochondrial biogenesis is affected by Hsa21 trisomy

Lastly, to verify if the observed mitochondrial dysfunction was associated to a decreased mitochondrial biogenesis, we quantified the copy number of mitochondrial DNA by absolute qRT-PCR. There was an average value of ∼600 copies per nuclear genome (i.e. per cell) in N-HFF, 500 in NCDS-HFF and 400 in CDS-HFF (Fig. 10A). A statistical significance was attained only for CDS-HFF.

As the mtDNA replication is controlled by *PGC-1α*, which is a master regulator of mitochondrial biogenesis (13), we analysed the correlation between *PGC-1α* expression and the amount of mtDNA. The amount of *PGC-1α* gene transcripts was reduced by ∼40–50% in trisomic samples versus N-HFF (Fig. 10B). Western blotting of *PGC-1α* confirmed at the protein level a significant decrease in NCDS-HFF and an even more marked decrease in CDS-HFF when compared with N-HFF (Fig. 10C). A direct correlation between *PGC-1α* expression and amount of mtDNA was observed in our samples (Fig. 10D).

DISCUSSION

We previously demonstrated that more than 80 genes, encoding mitochondrial enzymes and respiratory chain subunits, are downregulated in foetal trisomic heart tissues (3). Of these genes, 40 % have consensus DNA binding sites for the nuclear respiratory factor *NRF1* in their 5' flanking regions, and 20 % of them show a high affinity for the oestrogen-related receptor *ERRα* (see Supplementary Material, Text S2 and Tables S3 and S4). It has been recently demonstrated that the transcription factors *NRF1* and *ERRα* and their targets are repressed by Hsa21 gene *RIP140* and induced by *PGC-1α* in a dose dependent manner in neonatal rat cardiomyocytes (24). Our results indicate that *NRF1* and *PGC-1α* are significantly downregulated in DS HFF. Western blotting of *PGC-1α* confirmed the downregulation also at the protein level in trisomic fibroblasts. This downregulation correlated well with the downregulation of complex I activity and with the mtDNA copy number decrease (more evidently in CDS-HFF). *PGC-1α* function has been investigated in several specialized cell types and transgenic mouse models, demonstrating its role in the regulation of mitochondrial oxidative metabolism. *PGC-1α* null mice show reduced expression of mitochondrial genes in multiple tissues (25,26). *PGC-1α* controls the expression of nuclear-encoded mitochondrial genes through interactions with its transcriptional partners *NRF1* and *ERRα*, which are also downregulated in DS samples.

Morphological analysis of mitochondria in trisomic versus euploid samples demonstrated ultrastructural changes in DS-HFF mitochondria. These results provide additional evidence of altered mitochondrial morphology observed in DS brain tissues and mouse models (8,27). Silencing experiments demonstrated that the downregulation of *IMMT* causes a drastic change in the organization of the inner membrane

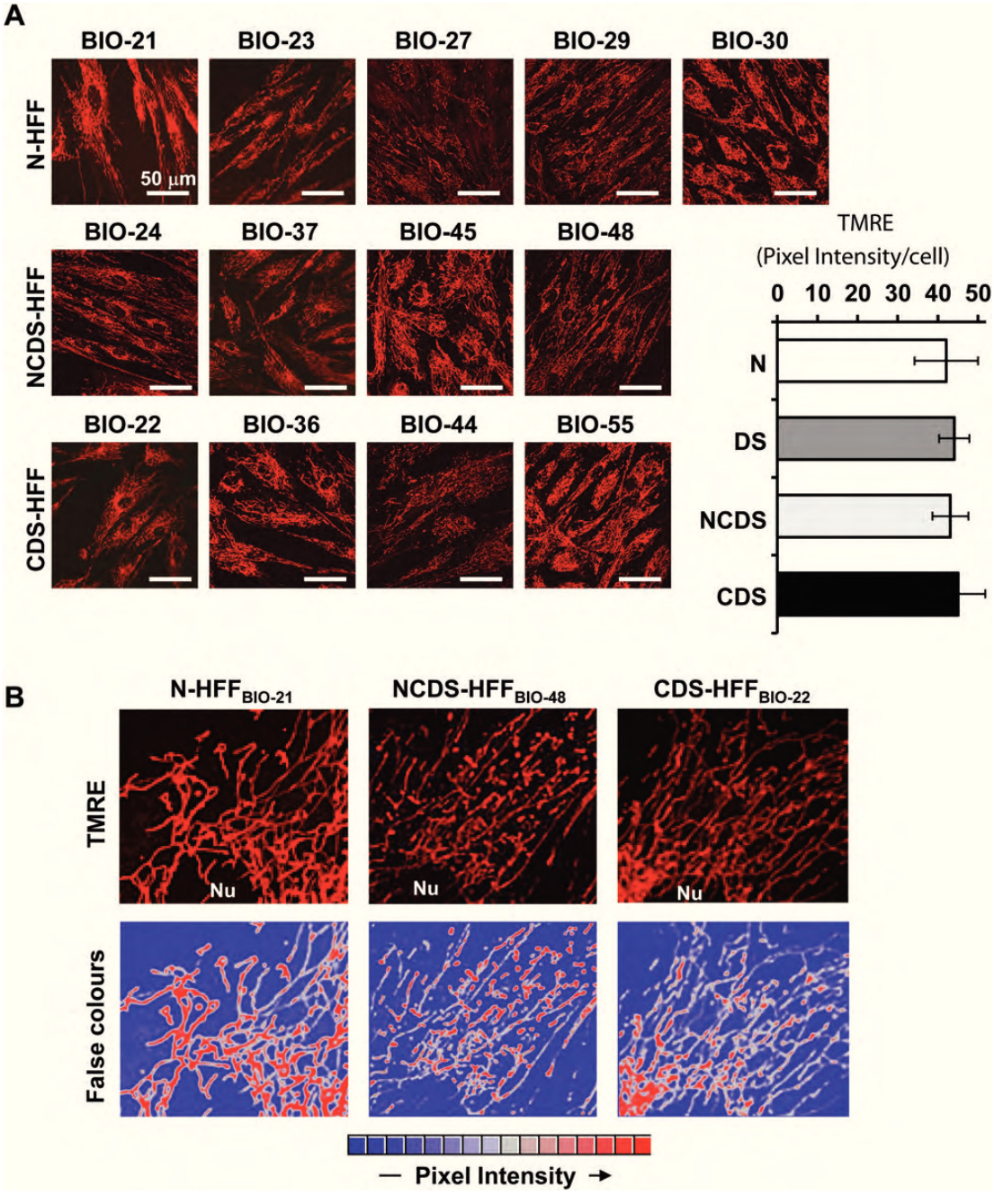

Figure 4. Confocal microscopy analysis of mtΔΨ in DS live fibroblasts. (**A**) Representative LSCM imaging of the TMRE-related fluorescence of euploid (N-HFF) and DS (NCDS-HFF and CDS-HFF) fibroblasts. The horizontal histograms on the right show the statistical analysis of the fluorescence intensity per cell as resulting from the averaged values ± SEM of about 100 randomly selected different cells for each sample from at least in-duplicate experiments. (**B**) Magnifications of intracellular selected details showing the mitochondrial functional network in representative samples of N-, NCDS- and CDS-HFF. A false-colours rendering of the TMRE-related fluorescence imaging is also shown.

that formed concentric layers instead of organizing into tubular cristae (28,29), leading to cristae patterns similar to those observed in DS samples. It is interesting to note that IMMT is significantly downregulated in DS fibroblasts.

Mitochondria have a key role in oxygen metabolism and subsequently they are the major source of ROS formation. Respirometry experiments conducted in this study demonstrated that in DS fibroblasts the OCR was significantly reduced in basal, uncoupled and ATP-synthase-dependent respiratory conditions, thus suggesting an impairment in oxidative phosphorylation competence, especially pronounced in DS fibroblasts from cardiopathic foeti. A correlation between the reduced respiratory activity and the morphological alterations in DS-HFF mitochondria indicates that the occurrence of de-structured cristae might partly account for the dysfunctioning oxidative phosphorylation in trisomic

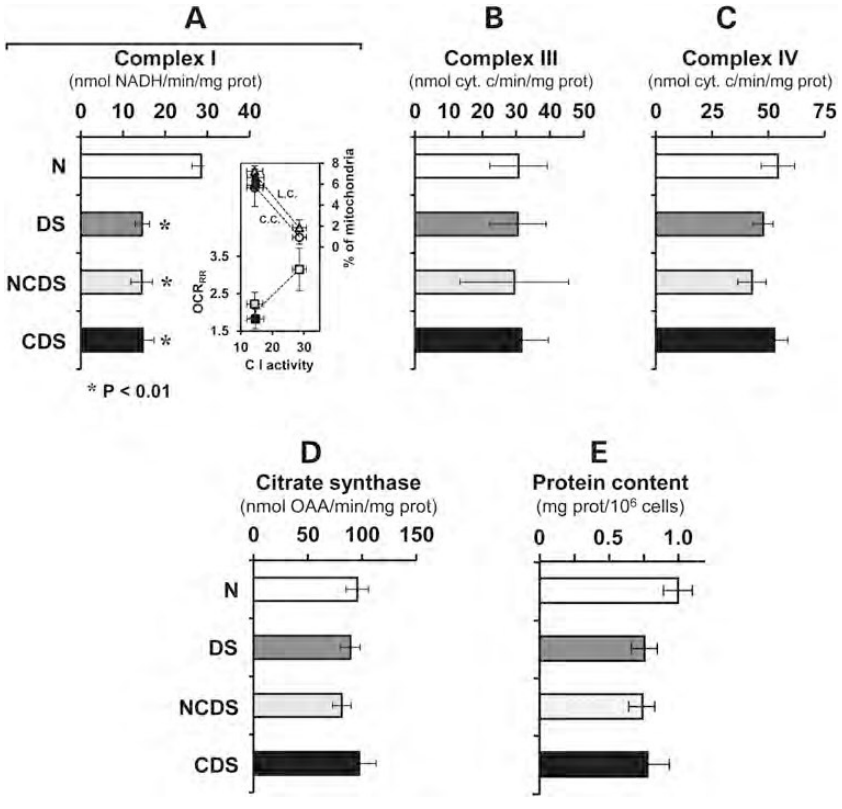

Figure 5. Enzymatic activities of the mitochondrial respiratory chain complexes of DS fibroblasts. The specific activities of (**A**) complex I (NADH-dehydrogenase), (**B**) complex III (cytochrome c reductase), (**C**) complex IV (cytochrome c reductase) were measured in cell lysates under conditions of saturating substrate as described in the Materials and Methods. The inset in (A) shows the correlation plot of the complex I activity versus either the OCR_{RR} (left Y axe) and the cristae morphological features (right Y axe; L.C., longitudinal cristae; C.C., concentric cristae); the values are means ± SEM of the clustered N-, NCDS- and CDS-HFF (same colour as the horizontal bars of the histogram). The citrate synthase activity, a marker of the mitochondrial content and the amount of protein per cell number are also shown in (**D**) and (**E**), respectively. N, DS, NCDS and CDS refer to the fibroblast sampling described in the legend of Figure 3; the bars are means ± SEM of the average determinations for each sample carried out in triplicate; when statistically significant, the difference when compared with the euploid samples is shown.

samples as also suggested by other authors (30,31). The analysis of individual complexes in the mitochondrial respiratory chain showed a strong reduction in the activity of complex I in DS fibroblasts irrespective of whether they were derived from cardiopathic trisomic foeti. Similar results have been recently reported (11). The authors attributed the reduced activity of complex I to defective cAMP/PKA-dependent phosphorylation. The impact of the OXPHOS decrease observed in DS fibroblasts did not result, however, in a severe bioenergetic failure compromising cell growth. This could be explained by an adaptive compensatory increase in the glycolytic flux, as shown in ref. (12), and by the gene-dosage effect of the Hsa21-harbored regulatory glycolytic enzyme phosphofructokinase PFKL (32).

In the present study, we observed a remarkable alteration in the redox homeostasis in DS-HFF highlighted by an increased production of ROS, which localized to an intracellular compartment resembling the mitochondrial network and was sensitive to the FCCP uncoupler and to the complex I inhibitor DPI. These two features would point to complex I as a major ROS generator in DS-HFF sustained by a 'forward electron transfer' mechanism (33,34). ROS production in DS-HFF was substantially suppressed by db-cAMP treatment, supporting the hypothesis that deregulation of post-translational modification of complex I is involved in the redox imbalance observed in DS-HFF.

A feature emerging from the present study is that the redox imbalance observed in DS-HFF was much larger in fibroblasts from cardiopathic foeti irrespective of the similar degree of inhibition of complex I in NCDS- and CDS-HFF. Release of ROS has been repetitively reported to be associated with an overload of Ca^{2+} into the mitochondria, although the mechanism remains to be satisfactorily explained (35,36). Consistent with this notion, we observed that DS-HFF displayed a higher steady level of intramitochondrial Ca^{2+} when compared with N-HFF, with the CDS-HFF exhibiting the highest $mtCa^{2+}$. A linear positive correlation was found between $mtCa^{2+}$ and ROS generation in the three cytotype samples. Most notably, blockage of the major mitochondrial Ca^{2+}-transporting system resulted in substantial depression of ROS overproduction in DS-HFF, whereas it was ineffective in N-HFF. Moreover, ruthenium red treatment resulted in full recovery of the respiratory activity in DS-HFF. All together, these observations would argue for a linkage between chronic intramitochondrial Ca^{2+} levels, inhibition of complex I and mitochondrial ROS production. Although

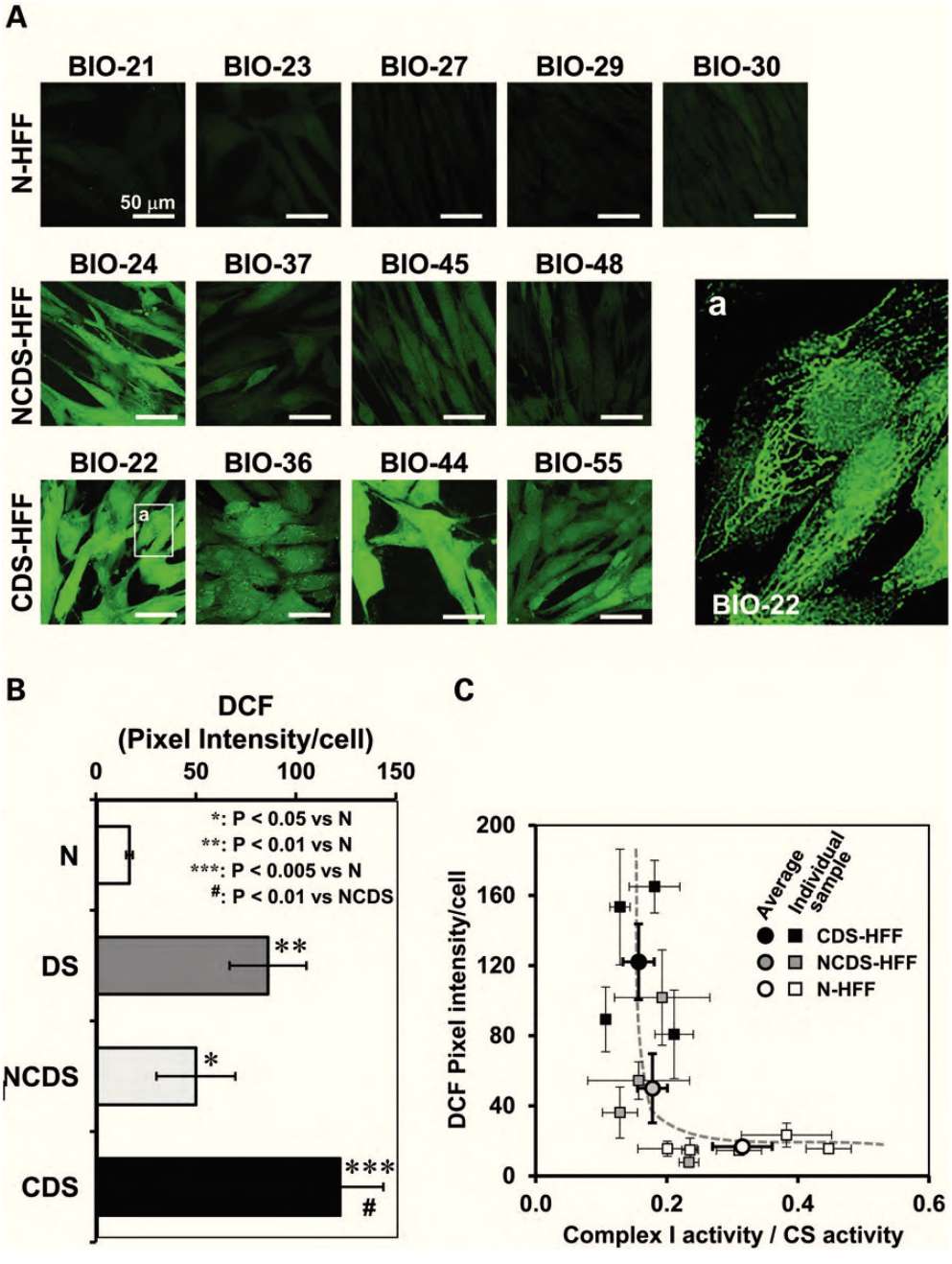

Figure 6. Confocal microscopy analysis of ROS production in DS live fibroblasts. (**A**) Representative LSCM imaging of the DCF-related fluorescence of euploid (N-HFF) and DS (NCDS-HFF and CDS-HFF) fibroblasts. A representative magnification of an intracellular selected detail (white rectangle) of the indicated CDS sample is shown displaying compartmentalization of the brighter DCF fluorescence signal. (**B**) Statistical analysis of the fluorescence intensity per cell as resulting from the averaged values ± SEM of about 100 randomly selected different cells for each sample from at least in-duplicate experiments; statistical analysis of the differences is also shown. (**C**) Correlation plot between the complex I activity normalized to the CS activity and the DCF-related fluorescence signal/cell for individual and averaged fibroblast samples (see symbol legend, means ± SEM).

we have not specifically addressed the cause of the Ca^{2+} homeostasis deregulation in trisomic cells, a survey of the literature suggests that cross-talk between PPARγ and Ca^{2+} mobilization/signalling (37) may be likely in this case. *PGC-1α* is an important coactivator of the *PPARs* transcription factor family, mainly *PPARγ* (38,39). Depression of *PGC-1α* activity, observed in DS-HFF samples, would consequently affect the transcriptional efficiency of *PPARs*-controlled genes.

PGC-1α function is both antagonized and regulated by a gene mapping to Hsa21, the nuclear receptor interacting protein *RIP140*. This highly conserved gene shows a 1.5- to 4-fold upregulation both in the heart and fibroblasts from DS subjects. The upregulation of *RIP140* protein was also demonstrated in the DS hippocampus (40). In the same experiment, the authors demonstrated that *SUMO3* (another gene mapping to Hsa21) is also upregulated in these cells. It was

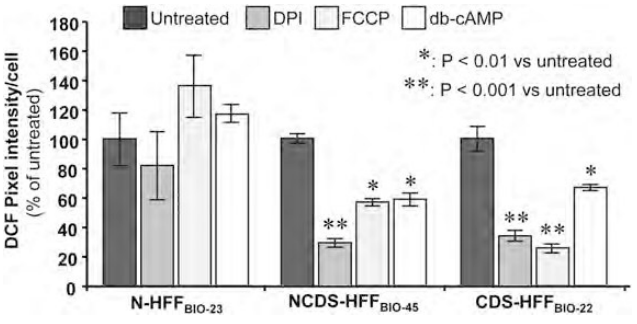

Figure 7. Effect of FCCP, DPI and db-cAMP on ROS production in DS fibroblasts. Cultured foetus-derived fibroblasts representative of euploid (BIO23) and DS non-cardiopathic (BIO45) or cardiopathic (BIO22) samples were treated for 2 h with either of 0.5 μM FCCP, 100 μM DPI or 100 μM db-cAMP and then assessed by LSCM for ROS production by DCF. The values shown are means ± SEM ($n = 3$ under each condition) of the DCF-related fluorescence intensity/cell normalized for each fibroblast sample to untreated cells. When statistically significant, the difference between untreated and compound-treated cells is reported.

demonstrated that the sumoylation of *RIP140* modulates its repressive activity (41). The simultaneous upregulation of both the Hsa21 genes, due to the primary dosage effect, might exert a synergistic effect. Silencing and re-expression experiments showed that *RIP140* expression significantly affects oxidative metabolism and mitochondrial biogenesis (42). Even mild *RIP140* overexpression repressed nuclear mitochondrial genes involved in all the respiratory chain complexes (43). We previously demonstrated that the same genes were repressed in DS foetal hearts (3).

Two other genes mapping to Hsa21, the kinase *DYRK1A* and the regulator of calcineurin 1 (*DSCR1/RCAN1*), were demonstrated to control *PGC-1α* via the *Calcineurin/NFAT* pathway, largely through the binding of *NFATc* to the *PGC-1α* promoter (44). The concurrent overexpression of the Hsa21 genes RIP140, SUMO3, *RCAN1* and *DYRK1A* and the downregulation of NFATc genes (45), observed in DS samples, is expected to result in the depression of *PGC-1α* expression.

In this study, we have demonstrated that some mitochondrial alterations are more pronounced in fibroblasts derived from DS foeti with heart defects. It must be pointed out that not all the subjects with trisomy 21 develop congenital cardiopathies, even though a heart developmental delay has been demonstrated in all DS human embryos at 8–10 gestational weeks (46). This suggests that a different inter-individual genetic background may affect the severity of the cardiopathic outcome in DS patients by impairing the oxidative metabolism. Assuming that altered cardiovascular development in DS likely originates from the trisomy of a critical Hsa21 region between *Tiam1* and *Kcnj6* (47), a more severe cardiac phenotype might be associated with different bioenergetic phenotypes characterized, at the cellular level, by a larger mitochondrial Ca^{2+} load and related ROS generation, as observed in CDS-HFF. Interesting is the evidence that the induction of oxidative stress in pregnant mice on day 7.5 disrupts cardiac neural crest migration and causes outflow tract defects like that observed in DS, and that antioxidant administration before the induction prevents the heart defects (48). Implications of our findings have a potential therapeutic value, as a number of drugs are becoming available to specifically inhibit the observed mitochondrial alterations. Some protocols are being developed to improve oxidative imbalance in DS using antioxidants such as the coenzyme Q10 (49,50). On the basis of our results, we also plan to investigate the effects of PPARγ agonists and/or of PGC-1α activators. The combination of these pharmacologically active compounds might correct mitochondria-related dysfunctions in trisomic foeti/patients.

MATERIALS AND METHODS

Ethics Statement

Human primary lines of HFF used in this study were obtained from the 'Telethon Bank of Fetal Biological Samples' at the University of Naples according to protocols approved by the local Institutional Ethics Committee.

Samples

Skin biopsies were explanted from 13 human foeti after therapeutic abortion at 18–22 gestational weeks and were classified as follows: five euploid human foeti (N-HFF) and eight foeti with trisomy of Hsa21 (DS-HFF) including four foeti with CHD, named CDS-HFF and four foeti without heart defects, named NCDS-HFF (Supplementary Material, Table S1). Fibroblasts from biopsies were cultured in T25 flasks (BD Falcon) with Chang medium B+C (Irvine Scientific) supplemented with 1% penicillin/streptomycin (Gibco) at 37°C in 5% CO_2 atmosphere; all the analyses described throughout this study were carried out at passages 4–5. Karyotype analysis was performed by standard G-banding technique.

The presence of CHD was established by colour Doppler foetal echocardiography followed by direct examination at the time of tissue explantation and dissection.

RNA extraction and quantitative real-time PCR

Total RNA from each sample was extracted using TRIzol reagent (Gibco/BRL Life Technologies, Inc., Gaithersburg, MD, USA) and was reverse-transcribed using the iScript cDNA Synthesis kit (Bio-Rad Laboratories Inc., Hercules, CA, USA). Real-time PCR was performed using iQ Supermix SYBR Green 2X on a Bio-Rad iCycler according to the manufacturer's protocols. PCR reactions were performed in triplicate. Primer pairs (MWG Biotech, Ebersberg, Germany) were designed using the Primer 3 software (http://frodo.wi.mit.edu/primer3) to obtain amplicons ranging from 100 to 150 bp (Supplementary Material, Table S2). *GAPDH* and *RPL13A* housekeeping genes were chosen as reference genes.

Morphological analysis

Fibroblasts from trisomic and euploid foeti were fixed and embedded for the electron microscope, using agarose as an intermediate embedding medium (51). Cells were fixed in petri dishes with 4% paraformaldehyde and 5% glutaraldehyde in PBS buffer (0.1 M, pH 7.3) for 30 min at room temperature,

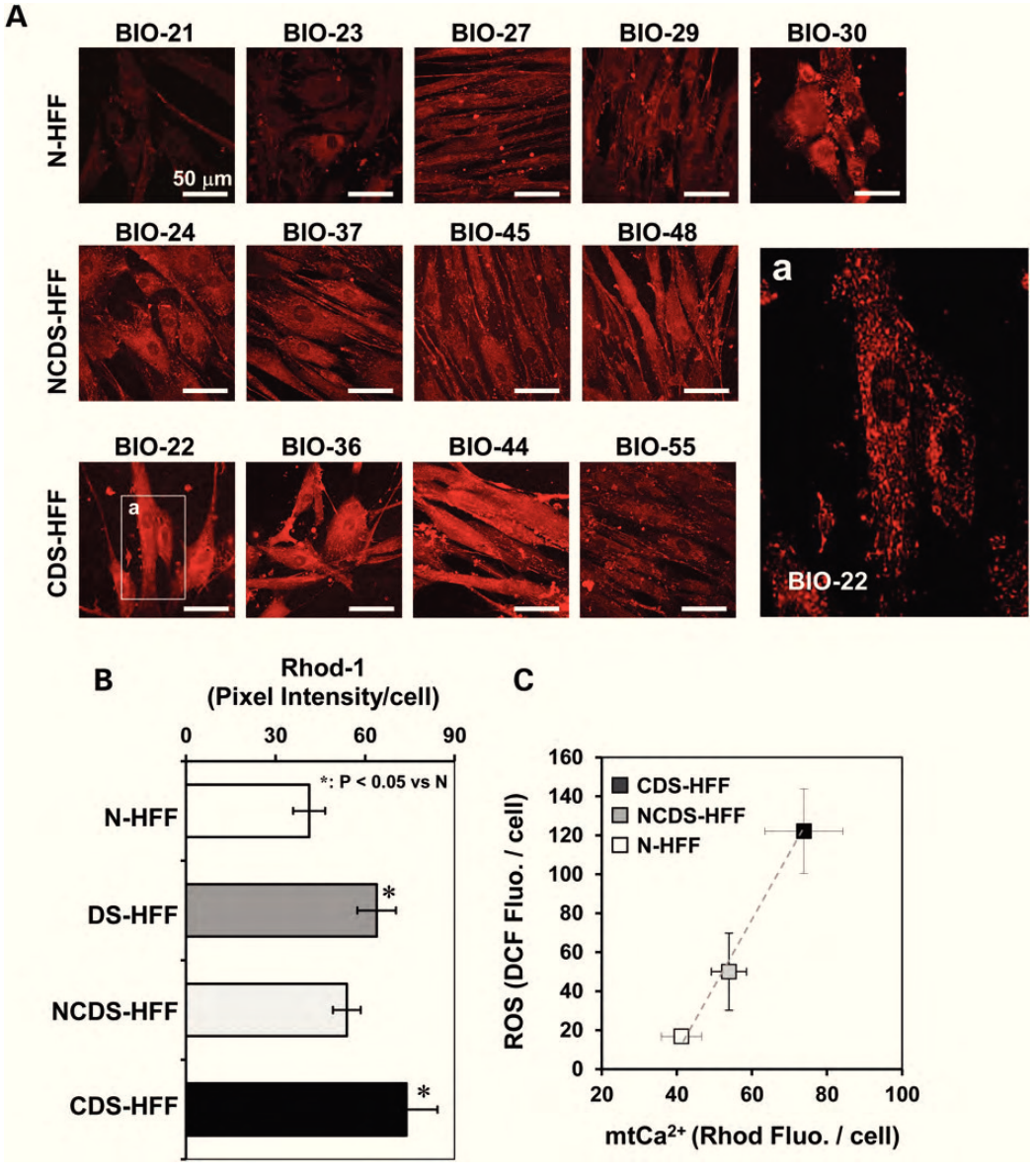

Figure 8. Confocal microscopy analysis of mitochondrial Ca^{2+} in DS live fibroblasts. (**A**) Representative LSCM imaging of the Rhod-1-related fluorescence of euploid (N-HFF) and DS (NCDS-HFF and CDS-HFF) fibroblasts. A representative magnification (white rectangle) of the indicated CDS sample is shown displaying the punctuate compartmentalization of the Rhod-1-fluorescence signal. (**B**) Statistical analysis of the fluorescence intensity per cell as resulting from the averaged values ± SEM of about 100 randomly selected different cells for each sample from at least in-duplicate experiments; when statistically significant, the difference when compared with the euploid samples is shown. (**C**) Correlation plot between the Rhod-1- and DCF-related fluorescence signal/cell for averaged fibroblast samples (see symbol legend, means ± SEM).

then washed in buffer, scraped from culture plates and pelleted by centrifugation for 10 min at 2000*g*; the supernatant was discarded and the cells were resuspended in 1 ml of 2% liquid agarose at 65°C. Again, the reaction tube was centrifuged for 5 min at 1000*g* to concentrate the cells in agarose. The agarose-cell pellet was solidified in ice for 30 min, and then the agarose cone was carefully taken out of the reaction tube and divided into small pieces (1 mm^3). The agarose-cell blocks were post-fixed in osmium tetroxide (1% in PBS buffer) for 1 h at 4°C, dehydrated and transferred first to propylene oxide, then to a mixture of propylene oxide-Epon (1:1) and finally embedded in Epon resin. The Epon blocks were polymerized for 2 days at 60°C and then sectioned with a diamond knife to give thin sections, 70–80 nm each; the sections were picked up on 200 mesh copper grids, stained with uranyl acetate (5% in 50% methanol) and Reynolds lead citrate (52) and observed on a Philips 208S transmission electron microscope. Micrographs were acquired with a Mega View II Soft Imaging System camera. Three N-HFF (BIO-21, BIO-23, BIO-27) and six DS-HFF samples (BIO24, BIO-36, BIO-37, BIO-44, BIO-48 and BIO55) were analysed using the 'fractionator' method to obtain a systematic and uniformly random sampling, which ensures that even for relatively small samples, the error is so small that it may safely be ignored (53). Fifty cells per sample were analysed and for each cell the percentages of inner and outer membrane

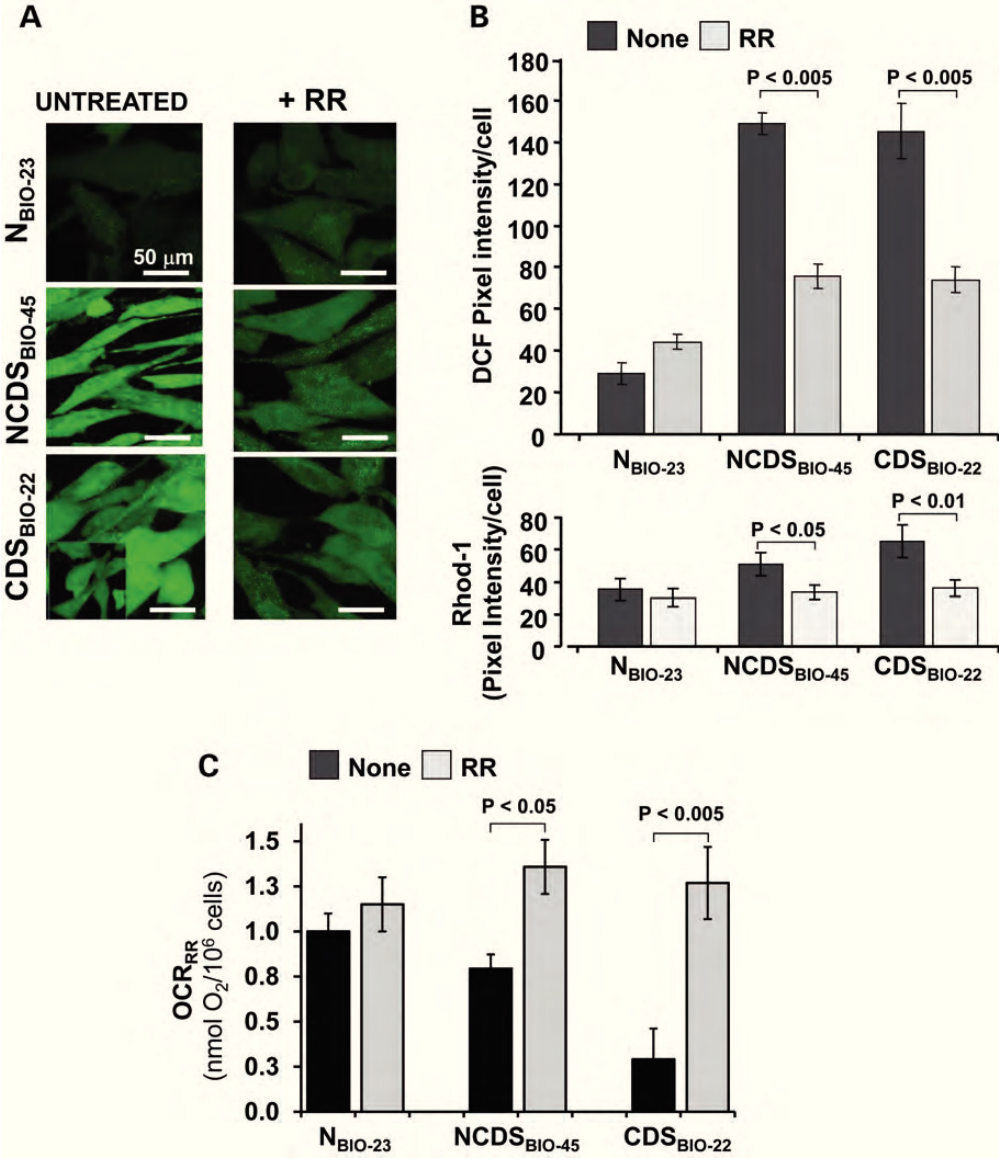

Figure 9. Effect of ruthenium red on ROS production and respiratory activity in DS live fibroblasts. Cultured foetus-derived fibroblasts representative of euploid (BIO23) and DS non-cardiopathic (BIO45) or cardiopathic (BIO22) samples were treated with 10 μM ruthenium red (RR) for 4 h and then assessed by LSCM for ROS production and $mtCa^{2+}$ by DCF and Rhod-1, respectively. (**A**) DCF-related fluorescence imaging of untreated and RR-treated fibroblasts (representative of three different experiments). (**B**) Statistical analysis of the DCF-related (upper histogram) and Rhod-1-related (lower histogram) fluorescence intensity per cell. The average values ± SEM of about 100 randomly selected different cells for each sample from three different experiments are shown. (**C**) Effect of RR on the respiratory activity of the same representative samples of N-, NCDS- and CDS-HFF as in (A). The OCR_{RR} was measured as described in the legend of Figure 3 and treatment with RR as in (A); the bars are means ± SEM of the average determinations for each sample (untreated and RR-treated) carried out in triplicate. When statistically significant, the difference between untreated and RR-treated cells is reported in (B) and (C).

breakages, branched mitochondria and mitochondria with concentric or longitudinal cristae were determined. Furthermore, for each sample, 25 micrographs were collected to evaluate the mitochondrial volume density (Vmt, relative volume of mitochondria on cell volume) and mitochondrial cristae volume density (Vmc, relative volume of mitochondrial cristae on mitochondria volume) (54). The volume density (also named relative volume or volume fraction) is a ratio between volumes. This is an intuitive parameter, unbiasedly estimated by overlaying a test system of points on images and then counting those falling over the objects of interest and those over the reference space. The ratio of points gives the estimation of volume. According to Delesse's principle, the volume fraction of an object varies proportionally to their area fraction as measured in random 2D sections; this means that each point controls an area in a 2D section and is related to a defined volume in the 3D organ (55).

Western blot analysis

Cells were washed twice with ice-cold PBS and lysed in RIPA buffer (NaCl 154 mM; Deoxicolic Acid 12 mM; NaF 0.95 mM;

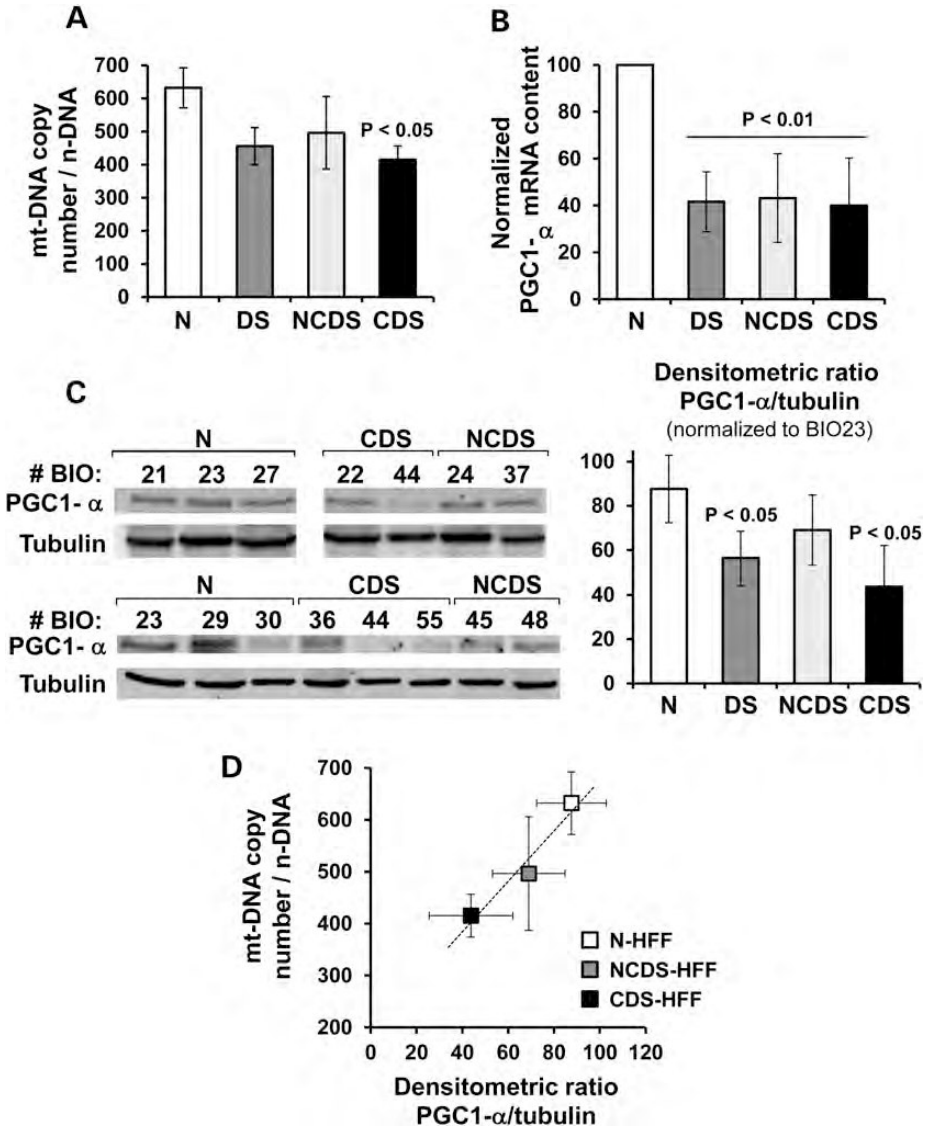

Figure 10. Analysis of the mitochondrial DNA content and expression of PGC-1α in DS fibroblasts. (**A**) Absolute qRT-PCR analysis of mtDNA (see Materials and Methods for details). The bars are means ± SEM from five euploid and eight DS fibroblast samples; a distinction between non-cardiopathic (NCDS, $n = 4$) and cardiopathic (CDS, $n = 4$) foetus-derived fibroblasts is also reported. (**B**) Expression analysis of the PGC-1α by qRT-PCR. The values, means ± SEM, of the DS samples are normalized to that of the euploid fibroblasts. (**C**) Analysis of the PGC-1α protein. (Panel on the left) Western blotting of PGC-1α on total cellular protein extracts from euploid and DS samples (representative of two to three different analyses carried out for each sample). (Panel on the right) Densitometric analysis of the PGC-1α-related immunodetected bands (means ± SEM of two to three assays). To compare different electrophoretic runs, the densitometric value (normalized to tubulin) of the euploid sample BIO-23 was taken as an internal reference. When statistically significant, the *P*-value, when compared with the euploid samples, is shown in (A and B) and (C and **D**) Correlation plot between the normalized PGC-1α protein expression and the mt-DNA copy number for averaged fibroblast samples (see symbol legend, means ± SEM).

Triton X-100 1%; SDS 2%; PMSF 2 mM) in phosphate buffer in the presence of protease inhibitors. The protein concentration was determined using the Bio-Rad protein assay (Bio-Rad Laboratories Inc.). For western blot analysis, total lysates were boiled for 5 min in Laemmli sample buffer and analysed on 7.5% SDS–PAGE. Gels were then blotted onto nitrocellulose transfer membranes (Schleicher and Shuell GmbH, Dassel, Germany) using a Bio-Rad apparatus. After transfer, the filters were blocked at room temperature for 1 h with 5% BSA in TTBS (150 mM NaCl, 20 mM Tris-HCl pH 7.5). After washing twice with TTBS (150 mM NaCl, 20 mM Tris-HCl pH 7.5, 0.1% Tween 20), filters were incubated overnight at 4°C with rabbit polyclonal primary antibody to *PGC-1α* (1:1000, Abcam, Cambridge Science Park, Cambridge, UK). The filters were washed extensively with TTBS and incubated for 1 h at room temperature with anti-rabbit peroxidase-conjugated secondary antibody (Amersham, Little Chalfont, Buckinghamshire, UK) diluted 1:1000 in TTBS. The filters were then washed six times with TTBS and once with TBS and developed using an ECL western blotting substrate detection method (Pierce, Rockford, IL, USA). For reprobing, the nitrocellulose filters were re-hydrated and

stripped for 30 min at 37°C in restore western blotting stripping buffer (Pierce) and washed extensively with TTBS. Results were standardized to alpha tubulin and analysed using NIH Image J (Rasband, W.S., ImageJ, U. S. National Institutes of Health, Bethesda, Maryland, USA, http://imagej.nih.gov/ij/, 1997–2012).

Measurement of the respiratory activity in intact cells

Cultured cells were gently detached from the dish by tripsinization, washed in PBS, harvested by centrifugation at 500*g* for 5 min and immediately assessed for O_2 consumption with a high-resolution oxymeter (Oxygraph-2k, Oroboros Instruments). About 1×10^6 viable cells per ml were assayed in 50 mM KPi, 10 mM Hepes, 1 mM EDTA, pH 7.4 at 37°C; after attainment of a stationary endogenous substrate-sustained resting oxygen consumption rate (OCR_{RR}), 2 μg/ml of the ATP-synthase inhibitor oligomycin was added (OCR_{OL}) followed by addition of 0.5 mM of the uncoupler carbonilcyanide p-triflouromethoxyphenylhydrazone (FCCP) (OCR_{UNC}). The rates of oxygen consumption were corrected for 2 mM KCN-insensitive respiration. The RCR was obtained by the ratio OCR_{UNC}/OCR_{OL}, the leak by the ratio OCR_{OL}/OCR_{UNC} and the ATP-synthesis-linked respiration (OXPHOS) by the ratio $(OCR_{RR}\text{-}OCR_{OL})/OCR_{UNC}$ (56).

Measurement of the activity of mitochondrial respiratory chain complexes

The specific activities of NADH:ubiquinone oxidoreductase (complex I), ubiquinone:cytochrome c oxidoreductase (complex III) and cytochrome c oxidase (complex IV) were assayed spectrophotometrically on frozen-thawn and ultrasound-treated cells in 10 mM Tris, 1 mg/ml serum albumin, pH 8.0. Complex I was assayed (in the presence of 1 μg/ml of antymicin A *plus* 2 mM KCN) by following the initial 2 μg/ml rotenone-sensitive rate of 50 μM NADH oxidation ($\varepsilon_{340nm} = 6.22\ mM^{-1}\ cm^{-1}$) in the presence of 200 μM decylubiquinone (dUQ) as electron acceptor; complex III was assayed (in the presence of rotenone *plus* KCN) by following the initial 1 μg/ml antymicin A-sensitive rate of 50 μM ferri-cytochrome *c* reduction ($\varepsilon_{550nm} = 21.1\ mM^{-1}\ cm^{-1}$) in the presence of 200 μM $dUQH_2$ as electron donor. Complex IV was assayed by following (in the presence of antymicin A) the initial 2 mM KCN-sensitive rate of 20 μM ferro-cytochrome *c* oxidation under aerobic conditions. The activities were normalized to the initial cell number and to cellular protein content (57). Citrate synthase catalyses the reaction between acetyl coenzyme A and oxaloacetic acid to form citric acid. Citrate synthase activity was assayed spectrophotometrically ($\varepsilon_{412nm} = 13.6\ mM^{-1}\ cm^{-1}$) measuring the reaction between CoA-SH and DTNB (5,5′-dithiobis (2-nitrobenzoic acid)) to form 5-thio-2-nitrobenzoic acid (TNB) (58).

Laser scanning confocal microscopy (LSCM) live cell imaging of mitochondrial membrane potential, ROS and $mtCa^{2+}$

Cells cultured at low density on fibronectin-coated 35-mm glass-bottom dishes were incubated for 20 min at 37°C with the either of the following probes: 2 μM tetramethylrhodamine ethyl ester (TMRE) to monitor mitochondrial membrane potential ($\Delta\Psi_m$); 10 μM 2,7-dichlorofluorescin diacetate, which is converted to dichlorofluorescein by intracellular esterases, for detection of H_2O_2; 5 μM X-Rhod-1 AM for mitochondrial Ca^{2+}. All probes were from Molecular Probes (Eugene, OR). Stained cells were washed with PBS and examined with a Nikon TE 2000 microscope [images collected using a ×60 objective (1.4 NA)] coupled to a Radiance 2100 dual-laser LSCM system (Bio-Rad). TMRE and Rhod-1 red fluorescence were elicited by exciting with the He–Ne laser beam (λex 543 nm), whereas dichlorofluorescein green fluorescence was elicited with the Ar–Kr laser beam (λex 488 nm). Acquisition, storage and analysis of data were performed with LaserSharp and LaserPix software from Bio-Rad or ImageJ version 1.37. Superimposed confocal planes were analysed by means of the 'stack' function of the LCS-Analysis Tools, which produced an *xz* intensity profile of the average value of the pixels within marked edges, including a single cell, as a function of each focal plane. The integrated value of the *xz* profile was taken as a measure of the fluorescence intensity of that individual cell relative to the selected emission channel. Correction was made for the minimal background by repeating the procedure in a cell-free field. About 100 single cells were analysed for each imaging analysis (57).

Statistics

The ANOVA test with Bonferroni *post hoc* correction was applied to evaluate the statistical significance of differences measured throughout the data sets presented. Concerning stereological investigations, the data obtained from each sample were averaged per group (N-HFF, DS-HFF, NCDS-HFF and CDS-HFF) and statistical evaluations were performed by using two nonparametric statistical tests, the Kolmogorov–Smirnov and the Kruskal–Wallis tests. The threshold for statistical significance (*P*-value) was set to 0.05.

SUPPLEMENTARY MATERIAL

Supplementary Material is available at *HMG* online.

Conflict of Interest statement. None declared.

FUNDING

This work was supported by grants from Campania Region (POR CREME to L.N.) and from the Italian Ministry of University and Research (PRIN-2008FJJHKM_001 to N.C.).

REFERENCES

1. Epstein, C.J., Korenberg, J.R., Anneren, G., Antonarakis, S.E., Ayme, S., Courchesne, E., Epstein, L.B., Fowler, A., Groner, Y., Huret, J.L *et al.* (1991) Protocols to establish genotype-phenotype correlations in Down syndrome. *Am. J. Hum. Genet.*, **49**, 207–235.
2. Park, S.C., Mathews, R.A., Zuberbuhler, J.R., Rowe, R.D., Neches, W.H. and Lenox, C.C. (1977) Down syndrome with congenital heart malformation. *Am. J. Dis. Child*, **131**, 29–33.

3. Conti, A., Fabbrini, F., D'Agostino, P., Negri, R., Greco, D., Genesio, R., D'Armiento, M., Olla, C., Paladini, D., Zannini, M *et al.* (2007) Altered expression of mitochondrial and extracellular matrix genes in the heart of human fetuses with chromosome 21 trisomy. *BMC Genomics*, **8**, 268.
4. Busciglio, J. and Yankner, B.A. (1995) Apoptosis and increased generation of reactive oxygen species in Down's syndrome neurons in vitro. *Nature*, **378**, 776–779.
5. Busciglio, J., Pelsman, A., Wong, C., Pigino, G., Yuan, M., Mori, H. and Yankner, B.A. (2002) Altered metabolism of the amyloid beta precursor protein is associated with mitochondrial dysfunction in Down's syndrome. *Neuron*, **33**, 677–688.
6. Roat, E., Prada, N., Ferraresi, R., Giovenzana, C., Nasi, M., Troiano, L., Pinti, M., Nemes, E., Lugli, E., Biagioni, O *et al.* (2007) Mitochondrial alterations and tendency to apoptosis in peripheral blood cells from children with Down syndrome. *FEBS Lett.*, **581**, 521–525.
7. Schuchmann, S. and Heinemann, U. (2000) Increased mitochondrial superoxide generation in neurons from trisomy 16 mice: a model of Down's syndrome. *Free Radic. Biol. Med.*, **28**, 235–250.
8. Shukkur, E.A., Shimohata, A., Akagi, T., Yu, W., Yamaguchi, M., Murayama, M., Chui, D., Takeuchi, T., Amano, K., Subramhanya, K.H *et al.* (2006) Mitochondrial dysfunction and tau hyperphosphorylation in Ts1Cje, a mouse model for Down syndrome. *Hum. Mol. Genet.*, **15**, 2752–2762.
9. Kim, S.H., Vlkolinsky, R., Cairns, N., Fountoulakis, M. and Lubec, G. (2001) The reduction of NADH ubiquinone oxidoreductase 24- and 75-kDa subunits in brains of patients with Down syndrome and Alzheimer's disease. *Life Sci.*, **68**, 2741–2750.
10. Bambrick, L.L. and Fiskum, G. (2008) Mitochondrial dysfunction in mouse trisomy 16 brain. *Brain Res.*, **1188**, 9–16.
11. Valenti, D., Manente, G.A., Moro, L., Marra, E. and Vacca, R.A. (2011) Deficit of complex I activity in human skin fibroblasts with chromosome 21 trisomy and overproduction of reactive oxygen species by mitochondria: involvement of the cAMP/PKA signalling pathway. *Biochem. J.*, **435**, 679–688.
12. Valenti, D., Tullo, A., Caratozzolo, M.F., Merafina, R.S., Scartezzini, P., Marra, E. and Vacca, R.A. (2010) Impairment of F1F0-ATPase, adenine nucleotide translocator and adenylate kinase causes mitochondrial energy deficit in human skin fibroblasts with chromosome 21 trisomy. *Biochem. J.*, **431**, 299–310.
13. Scarpulla, R.C. (2011) Metabolic control of mitochondrial biogenesis through the PGC-1 family regulatory network. *Biochim. Biophys. Acta*, **1813**, 1269–1278.
14. Mao, R., Wang, X., Spitznagel, E.L. Jr, Frelin, L.P., Ting, J.C., Ding, H., Kim, J.W., Ruczinski, I., Downey, T.J. and Pevsner, J. (2005) Primary and secondary transcriptional effects in the developing human Down syndrome brain and heart. *Genome Biol.*, **6**, R107.
15. Sharma, L.K., Lu, J. and Bai, Y. (2009) Mitochondrial respiratory complex I: structure, function and implication in human diseases. *Curr. Med. Chem.*, **16**, 1266–1277.
16. Bellomo, F., Piccoli, C., Cocco, T., Scacco, S., Papa, F., Gaballo, A., Boffoli, D., Signorile, A., D'Aprile, A., Scrima, R *et al.* (2006) Regulation by the cAMP cascade of oxygen free radical balance in mammalian cells. *Antioxid. Redox Signal*, **8**, 495–502.
17. Papa, S., Rasmo, D.D., Technikova-Dobrova, Z., Panelli, D., Signorile, A., Scacco, S., Petruzzella, V., Papa, F., Palmisano, G., Gnoni, A *et al.* (2012) Respiratory chain complex I, a main regulatory target of the cAMP/PKA pathway is defective in different human diseases. *FEBS Lett.*, **586**, 568–577.
18. Caviedes, P., Caviedes, R. and Rapoport, S.I. (2006) Altered calcium currents in cultured sensory neurons of normal and trisomy 16 mouse fetuses, an animal model for human trisomy 21 (Down syndrome). *Biol. Res.*, **39**, 471–481.
19. Li, H., Rao, A. and Hogan, P.G. (2011) Interaction of calcineurin with substrates and targeting proteins. *Trends Cell Biol.*, **21**, 91–103.
20. Yamato, F., Takaya, J., Yasuhara, A., Teraguchi, M., Ikemoto, Y. and Kaneko, K. (2009) Elevated intracellular calcium in neutrophils in patients with Down syndrome. *Pediatr. Int.*, **51**, 474–477.
21. De Stefani, D., Raffaello, A., Teardo, E., Szabo, I. and Rizzuto, R. (2011) A forty-kilodalton protein of the inner membrane is the mitochondrial calcium uniporter. *Nature*, **476**, 336–340.
22. Drago, I., Pizzo, P. and Pozzan, T. (2011) After half a century mitochondrial calcium in- and efflux machineries reveal themselves. *EMBO J.*, **30**, 4119–4125.
23. Peng, T.I. and Jou, M.J. (2010) Oxidative stress caused by mitochondrial calcium overload. *Ann. N. Y. Acad. Sci.*, **1201**, 183–188.
24. Chen, Y., Wang, Y., Chen, J., Chen, X., Cao, W., Chen, S., Xu, S., Huang, H. and Liu, P. (2012) Roles of transcriptional corepressor RIP140 and coactivator PGC-1alpha in energy state of chronically infarcted rat hearts and mitochondrial function of cardiomyocytes. *Mol. Cell. Endocrinol.*, **362**, 11–18.
25. Leone, T.C., Lehman, J.J., Finck, B.N., Schaeffer, P.J., Wende, A.R., Boudina, S., Courtois, M., Wozniak, D.F., Sambandam, N., Bernal-Mizrachi, C *et al.*. (2005) PGC-1alpha deficiency causes multi-system energy metabolic derangements: muscle dysfunction, abnormal weight control and hepatic steatosis. *PLoS Biol.*, **3**, e101.
26. Mitra, R., Nogee, D.P., Zechner, J.F., Yea, K., Gierasch, C.M., Kovacs, A., Medeiros, D.M., Kelly, D.P. and Duncan, J.G. (2012) The transcriptional coactivators, PGC-1alpha and beta, cooperate to maintain cardiac mitochondrial function during the early stages of insulin resistance. *J. Mol. Cell. Cardiol.*, **52**, 701–710.
27. Bersu, E.T., Ahmad, F.J., Schwei, M.J. and Baas, P.W. (1998) Cytoplasmic abnormalities in cultured cerebellar neurons from the trisomy 16 mouse. *Brain Res. Dev. Brain Res.*, **109**, 115–120.
28. John, G.B., Shang, Y., Li, L., Renken, C., Mannella, C.A., Selker, J.M., Rangell, L., Bennett, M.J. and Zha, J. (2005) The mitochondrial inner membrane protein mitofilin controls cristae morphology. *Mol. Biol. Cell*, **16**, 1543–1554.
29. Zerbes, R.M., Bohnert, M., Stroud, D.A., von der Malsburg, K., Kram, A., Oeljeklaus, S., Warscheid, B., Becker, T., Wiedemann, N., Veenhuis, M *et al.* (2012) Role of MINOS in mitochondrial membrane architecture: cristae morphology and outer membrane interactions differentially depend on mitofilin domains. *J. Mol. Biol.*, **422**, 183–191.
30. Darshi, M., Mendiola, V.L., Mackey, M.R., Murphy, A.N., Koller, A., Perkins, G.A., Ellisman, M.H. and Taylor, S.S. (2011) ChChd3, an inner mitochondrial membrane protein, is essential for maintaining crista integrity and mitochondrial function. *J. Biol. Chem.*, **286**, 2918–2932.
31. Zick, M., Rabl, R. and Reichert, A.S. (2009) Cristae formation-linking ultrastructure and function of mitochondria. *Biochim. Biophys. Acta*, **1793**, 5–19.
32. Lambert, A.J., Buckingham, J.A., Boysen, H.M. and Brand, M.D. (2008) Diphenyleneiodonium acutely inhibits reactive oxygen species production by mitochondrial complex I during reverse, but not forward electron transport. *Biochim. Biophys. Acta*, **1777**, 397–403.
33. Annerén, K.G., Korenberg, J.R. and Epstein, C.J. (1987) Phosphofructokinase activity in fibroblasts aneuploid for chromosome 21. *Hum. Genet.*, **76**, 63–65.
34. Selivanov, V.A., Votyakova, T.V., Pivtoraiko, V.N., Zeak, J., Sukhomlin, T., Trucco, M., Roca, J. and Cascante, M. (2011) Reactive oxygen species production by forward and reverse electron fluxes in the mitochondrial respiratory chain. *PLoS Comput. Biol.*, **7**, e1001115.
35. Adam-Vizi, V. and Starkov, A.A. (2010) Calcium and mitochondrial reactive oxygen species generation: how to read the facts. *J. Alzheimer Dis.*, **20**(Suppl. 2), S413–S426.
36. Feissner, R.F., Skalska, J., Gaum, W.E. and Sheu, S.S. (2009) Crosstalk signaling between mitochondrial Ca2+ and ROS. *Front. Biosci.*, **14**, 1197–1218.
37. Bush, C.R., Havens, J.M., Necela, B.M., Su, W., Chen, L., Yanagisawa, M., Anastasiadis, P.Z., Guerra, R., Luxon, B.A. and Thompson, E.A. (2007) Functional genomic analysis reveals cross-talk between peroxisome proliferator-activated receptor gamma and calcium signaling in human colorectal cancer cells. *J. Biol. Chem.*, **282**, 23387–23401.
38. Oyekan, A. (2011) PPARs and their effects on the cardiovascular system. *Clin. Exp. Hypertens*, **33**, 287–293.
39. Puigserver, P., Wu, Z., Park, C.W., Graves, R., Wright, M. and Spiegelman, B.M. (1998) A cold-inducible coactivator of nuclear receptors linked to adaptive thermogenesis. *Cell*, **92**, 829–839.
40. Gardiner, K. (2006) Transcriptional dysregulation in Down syndrome: predictions for altered protein complex stoichiometries and post-translational modifications, and consequences for learning/behavior genes ELK, CREB, and the estrogen and glucocorticoid receptors. *Behav. Genet.*, **36**, 439–453.
41. Rytinki, M.M. and Palvimo, J.J. (2009) SUMOylation attenuates the function of PGC-1alpha. *J. Biol. Chem.*, **284**, 26184–26193.
42. Powelka, A.M., Seth, A., Virbasius, J.V., Kiskinis, E., Nicoloro, S.M., Guilherme, A., Tang, X., Straubhaar, J., Cherniack, A.D., Parker, M.G *et al.* (2006) Suppression of oxidative metabolism and mitochondrial

biogenesis by the transcriptional corepressor RIP140 in mouse adipocytes. *J. Clin. Invest.*, **116**, 125–136.
43. Seth, A., Steel, J.H., Nichol, D., Pocock, V., Kumaran, M.K., Fritah, A., Mobberley, M., Ryder, T.A., Rowlerson, A., Scott, J *et al.* (2007) The transcriptional corepressor RIP140 regulates oxidative metabolism in skeletal muscle. *Cell Metab.*, **6**, 236–245.
44. Handschin, C., Rhee, J., Lin, J., Tarr, P.T. and Spiegelman, B.M. (2003) An autoregulatory loop controls peroxisome proliferator-activated receptor gamma coactivator 1alpha expression in muscle. *Proc. Natl Acad. Sci. USA*, **100**, 7111–7116.
45. Arron, J.R., Winslow, M.M., Polleri, A., Chang, C.P., Wu, H., Gao, X., Neilson, J.R., Chen, L., Heit, J.J., Kim, S.K *et al.* (2006) NFAT dysregulation by increased dosage of DSCR1 and DYRK1A on chromosome 21. *Nature*, **441**, 595–600.
46. Gittenberger-de Groot, A.C., Bartram, U., Oosthoek, P.W., Bartelings, M.M., Hogers, B., Poelmann, R.E., Jongewaard, I.N. and Klewer, S.E. (2003) Collagen type VI expression during cardiac development and in human fetuses with trisomy 21. *Anat. Rec. A Discov. Mol. Cell. Evol. Biol.*, **275**, 1109–1116.
47. Liu, C., Morishima, M., Yu, T., Matsui, S., Zhang, L., Fu, D., Pao, A., Costa, A.C., Gardiner, K.J., Cowell, J.K *et al.* (2011) Genetic analysis of Down syndrome-associated heart defects in mice. *Hum. Genet.*, **130**, 623–632.
48. Morgan, S.C., Relaix, F., Sandell, L.L. and Loeken, M.R. (2008) Oxidative stress during diabetic pregnancy disrupts cardiac neural crest migration and causes outflow tract defects. *Birth Defects Res. A Clin. Mol. Teratol.*, **82**, 453–463.
49. Miles, M.V., Patterson, B.J., Chalfonte-Evans, M.L., Horn, P.S., Hickey, F.J., Schapiro, M.B., Steele, P.E., Tang, P.H. and Hotze, S.L. (2007) Coenzyme Q10 (ubiquinol-10) supplementation improves oxidative imbalance in children with trisomy 21. *Pediatr. Neurol.*, **37**, 398–403.
50. Tiano, L., Carnevali, P., Padella, L., Santoro, L., Principi, F., Bruge, F., Carle, F., Gesuita, R., Gabrielli, O. and Littarru, G.P. (2011) Effect of Coenzyme Q10 in mitigating oxidative DNA damage in Down syndrome patients, a double blind randomized controlled trial. *Neurobiol. Aging*, **32**, 2103–2105.
51. Kerstens, H.M., Robben, J.C., Poddighe, P.J., Melchers, W.J., Boonstra, H., de Wilde, P.C., Macville, M.V. and Hanselaar, A.G. (2000) AgarCyto: a novel cell-processing method for multiple molecular diagnostic analyses of the uterine cervix. *J. Histochem. Cytochem.*, **48**, 709–718.
52. Reynolds, E.S. (1963) The use of lead citrate at high pH as an electron-opaque stain in electron microscopy. *J. Cell Biol.*, **17**, 208–212.
53. Gundersen, H.J. (2002) The smooth fractionator. *J. Microsc.*, **207**, 191–210.
54. Weibel, E.R., Kistler, G.S. and Scherle, W.F. (1966) Practical stereological methods for morphometric cytology. *J. Cell Biol.*, **30**, 23–38.
55. Marcos, R., Monteiro, R.A. and Rocha, E. (2012) The use of design-based stereology to evaluate volumes and numbers in the liver: a review with practical guidelines. *J. Anat.*, **220**, 303–317.
56. Piccoli, C., Scrima, R., Quarato, G., D'Aprile, A., Ripoli, M., Lecce, L., Boffoli, D., Moradpour, D. and Capitanio, N. (2007) Hepatitis C virus protein expression causes calcium-mediated mitochondrial bioenergetic dysfunction and nitro-oxidative stress. *Hepatology*, **46**, 58–65.
57. Cela, O., Piccoli, C., Scrima, R., Quarato, G., Marolla, A., Cinnella, G., Dambrosio, M. and Capitanio, N. (2010) Bupivacaine uncouples the mitochondrial oxidative phosphorylation, inhibits respiratory chain complexes I and III and enhances ROS production: results of a study on cell cultures. *Mitochondrion*, **10**, 487–496.
58. Barrientos, A., Fontanesi, F. and Diaz, F. (2009) Evaluation of the mitochondrial respiratory chain and oxidative phosphorylation system using polarography and spectrophotometric enzyme assays. *Curr. Protoc. Hum. Genet.*, **Chapter 19**, Unit19.13.

NRIP1/RIP140 siRNA-mediated Attenuation Counteracts Mitochondrial Dysfunction In Down Syndrome

Journal:	*Human Molecular Genetics*
Manuscript ID:	HMG-2014-D-00227.R1
Manuscript Type:	2 General Article - UK Office
Date Submitted by the Author:	n/a

Complete List of Authors:	Izzo, Antonella; University of Naples, Federico II, Molecular Medicine and Medical Biotechnology Manco, Rosanna; University of Naples, Federico II, Molecular Medicine and Medical Biotechnology Bonfiglio, Ferdinando; University of Naples, Federico II, Molecular Medicine and Medical Biotechnology Calì, Gaetano; National Research Council, Institute of Experimental Endocrinology and Oncology de Cristofaro, Tiziana; National Research Council, Institute of Experimental Endocrinology and Oncology Patergnani, Simone; University of Ferrara, Morphology, Surgery and Experimental Medicine Cicatiello, Rita; University of Naples, Federico II, Molecular Medicine and Medical Biotechnology Scrima, Rosella; University of Foggia, Clinical and Experimental Medicine Zannini, Mariastella; National Research Council, Institute of Experimental Endocrinology and Oncology Pinton, Paolo; University of Ferrara, Experimental and Diagnostic Medicine Conti, Anna; University of Naples, Federico II, Molecular Medicine and Medical Biotechnology Nitsch, Lucio; University of Naples, Molecular Medicine and Medical Biotechnology

Key Words:	Chromosome 21, Down syndrome, NRIP1/RIP140, Mitochondrial dysfunction, PGC-1alpha

NRIP1/RIP140 siRNA-MEDIATED ATTENUATION COUNTERACTS MITOCHONDRIAL DYSFUNCTION IN DOWN SYNDROME

Antonella Izzo[1#], Rosanna Manco[1#], Ferdinando Bonfiglio[1#], Gaetano Calì[2], Tiziana de Cristofaro[2], Simone Patergnani[3], Rita Cicatiello[1], Rosella Scrima[4], Mariastella Zannini[2], Paolo Pinton[3], Anna Conti[1]*, Lucio Nitsch[1].

[1]Department of Molecular Medicine and Medical Biotechnology, University of Naples Federico II, Naples, 80131, Italy; [2]Institute of Experimental Endocrinology and Oncology, National Research Council, Naples, 80131, Italy; [3]Department of Experimental and Diagnostic Medicine, University of Ferrara, Ferrara, 44100, Italy; [4]Department of Clinical and Experimental Medicine, University of Foggia, Foggia, 71100, Italy.

Footnotes

[#]The authors wish to be known that, in their opinion, the first three authors should be regarded as joint First Authors.

*** Corresponding author**

Anna Conti

Department of Molecular Medicine and Medical Biotechnology, Via Pansini 5, 80131 Naples, Italy; tel: +39-081-7463261, fax: +39-081-7463656.

E-mail: anconti@unina.it

ABSTRACT

Mitochondrial dysfunction, which is consistently observed in Down syndrome (DS) cells and tissues, might contribute to the severity of the DS phenotype. Our recent studies on DS fetal hearts and fibroblasts have suggested that one of the possible causes of mitochondrial dysfunction is the downregulation of peroxisome proliferator-activated receptor gamma, coactivator 1 alpha (*PGC-1α* or *PPARGC1A*)—a key modulator of mitochondrial function—and of several nuclear encoded mitochondrial genes (NEMGs). Reanalysis of publicly available expression data related to manipulation of Hsa21 genes suggested the nuclear receptor interacting protein 1 (*NRIP1* or *RIP140*) as a good candidate Hsa21 gene for NEMG downregulation. Indeed, *NRIP1* is known to affect oxidative metabolism and mitochondrial biogenesis by negatively controlling mitochondrial pathways regulated by *PGC-1α*. To establish whether *NRIP1* over-expression in DS downregulates both *PGC-1α* and NEMGs, thereby causing mitochondrial dysfunction, we used siRNAs to decrease *NRIP1* expression in trisomic human fetal fibroblasts. Levels of *PGC-1α* and NEMGs were increased and mitochondrial function was restored, as shown by ROS decrease, ATP production and mitochondrial activity increase.

These findings indicate that the Hsa21 gene *NRIP1* contributes to the mitochondrial dysfunction observed in DS. Furthermore, they suggest that the *NRIP1-PGC-1α* axe might represent a potential therapeutic target for restoring altered mitochondrial function in DS.

INTRODUCTION

Data from several studies show that trisomy of chromosome 21 (TS21) affects both mitochondrial function and reactive oxygen species (ROS) production. Lower levels of the mitochondrial complexes I, III, and V have been observed in the cerebellar and brain regions of subjects affected by Down syndrome (DS) **(1)**. Moreover, reduced mitochondrial redox activity and membrane potential have been observed in DS astrocytes and neuronal cultures **(2)**, **(3).** Further evidence for mitochondrial dysfunction was found in Ts1Cje mouse model for DS that shows decreased levels of ATP production **(4)**. Similarly, fetal DS fibroblasts show both a decreased efficiency of the mitochondrial energy production apparatus, involving adenine nucleotide translocators, ATP synthase, and adenylate kinase, and a selective deficit of complex I, which might contribute to ROS overproduction by DS mitochondria. These events were correlated with changes in the cAMP/PKA signaling pathway **(5)**, **(6)**. Similar research conducted on human primary lines of fibroblasts (HFFs) from TS21 fetuses has revealed that TS21 disrupts mitochondrial morphology, decreases oxygen consumption, increases $mtCa^{2+}$ load and ROS production **(7)**. Moreover, by analyzing mitochondrial defects according to the cardiac phenotype, a more severe mitochondrial dysfunction was evidenced in cardiopathic-derived TS21 fibroblasts **(7)**. A possible interpretation of these results is that a more pronounced pro-oxidative state might contribute to generating a more severe cardiac phenotype—a concept that might be extended to other phenotypic traits. Studies of genome-wide expression analysis in DS have demonstrated that nuclear encoded mitochondrial genes (NEMGs) represent the main downregulated category in fetal TS21 heart samples **(8)**. Downregulation is also manifest in DS fetal brains **(9)**. These observations led us to hypothesize that NEMG dysregulation is likely a cause of mitochondrial dysfunction in DS **(8)**. Among the dysregulated genes, the peroxisome proliferator-activated receptor gamma, coactivator 1 alpha (*PGC-1α*/*PPARGC1A*) has been found hypo-expressed at the transcriptional and protein levels in TS21 HFFs **(7)**. *PGC-1α* is indeed known to play a central role in regulating mitochondrial

biogenesis and respiratory function through the interaction with transcriptional partners, like *NRF1*, *ERRα*, *PPAR*s**,** and *YY1* **(10)**.

A known repressor of *PGC-1α* activity is the nuclear receptor interacting protein 1 (*NRIP1/RIP140*) **(11)**, **(12)**, **(13)**. This protein is coded by a highly conserved chromosome 21 (Hsa21) gene with consistent dosage effect in many studies on DS samples **(14)**. *NRIP1* acts as a scaffold protein recruiting regulatory factors, such as hystone deacetylases (HDACs) **(15)**, COOH terminal binding protein (CtBP) **(16),** and hystone metyltransferases **(17),** to exert its corepressive function. Furthermore, *NRIP1* directly interacts with some nuclear receptors including PPARs, ERRs, and ERs **(18)**, **(19)**, **(20)**. More specifically, *NRIP1* negatively controls the expression and the activity of *PGC-1α* as well as the expression of its targets. Indeed, in *PGC-1α* null mice **(21)**, **(22)**, as well as in knock-in *NRIP1* mice **(23)**, NEMG expression is decreased. Likewise, *NRIP1* is always upregulated by 1.5- to 4-fold in the heart **(8)** and fibroblasts **(7)** from DS fetuses. NRIP1 protein is also increased in the hippocampal tissue from DS subjects **(24)**.

Thus, building upon previous research, in this study we endeavored to provide new insights into the transcriptional changes influencing the molecular mechanisms associated with mitochondrial dysfunction in DS. In particular, we first investigated whether Hsa21 gene overexpression causes NEMG downregulation by focusing on those Hsa21 genes, transcription factors, and kinases that have the highest probability of affecting the expression of many genes. To this aim, we analyzed the public expression data related to the manipulation of Hsa21 genes to investigate their effects on NEMG downregulation. These analyses led us to the identification of *NRIP1* as a good candidate for the downregulation of mitochondria-related genes in DS.

Then, to determine whether *NRIP1* downregulation can effectively counteract mitochondrial dysfunction and some of its pathophysiological effects, we attenuated *NRIP1* expression in human fibroblasts from DS fetuses (DS-HFFs).

Understanding the molecular correlation between *NRIP1* expression levels, NEMG regulation, and mitochondrial function could lay the basis for the development of new therapeutic protocols for Down syndrome.

RESULTS

Analysis of public expression data suggests that *NRIP1* affects NEMG expression

Several Hsa21 genes can possibly interfere with NEMG expression. For instance, *DYRK1A* and *DSCR1/RCAN1* play key roles in the calcineurin/*NFAT* pathway, which affects mitochondrial activity and morphology during heart development **(25)**. Two more genes, *NRIP1* **(23)** and *GABPA/NRF2* **(26)** are also involved in mitochondrial pathways.

To identify which Hsa21 gene might possibly downregulate NEMG expression, we screened the Gene Expression Omnibus **(27)** repository (http://www.ncbi.nlm.nih.gov/geo) for gene expression data related to the modulation of Hsa21 genes. We selected the GEO GSE 19836 experiment **(28)**, a set of data derived from a mouse embryonic stem cell (ESC) bank in which several orthologs of Hsa21 genes, with potential regulatory role, are individually overexpressed in an inducible manner. Expression data were available for 13 transcription factors (including *NRIP1*, *RCAN1* and *GABPA*), the transcriptional activator *RCAN1,* and 6 protein kinases (including *DYRK1A*) (for details see Materials and Methods). We reanalyzed this series of data by focusing on the mitochondria-related categories and pathways dysregulated by the overexpression of each gene looking for Hsa21genes that when overexpressed would induce NEMG downregulation. Among the 20 analyzed Hsa21 genes, only *NRIP1*, one of the 7 genes that are considered "effective" for the expression perturbation in the manipulated cells **(28)**, was able to cause NEMG downregulation when overexpressed. Our analysis showed that *NRIP1* overexpression caused a significant enrichment of NEMGs among 298 downregulated genes. The "Mitochondrion" was the most affected Cell Component Gene Ontology (GO) category ($p< 0.0001$) (**Table 1** and **Suppl. Fig. 1**), with a cluster of 37 downregulated genes. Motif enrichment analysis, by clustering downregulated genes on the basis of their promoter regions, revealed a significant enrichment ($p<0.005$) in genes with the *ERR*α motif. Twenty-five downregulated genes, instead of the expected 10, showed promoter regions around the transcription start site containing the *ERR*α motif.

Neither *DYRK1A,* nor *RCAN1,* nor *GABPA*, all considered "silent" genes **(28)**, caused NEMG downregulation when overexpressed.

Modulation of *NRIP1* and *PGC-1α* expression dysregulates the same NEMGs downregulated in DS fetal hearts

To investigate whether the sets of genes regulated by *NRIP1* and/or *PGC-1α* showed any overlapping to the NEMGs downregulated in DS fetal hearts **(8)**, we performed a meta-analysis comparing 3 sets of gene expression data, SET1, SET2 and SET3. SET1 included 123 genes which were both upregulated after *NRIP1* silencing and downregulated after *NRIP1* re-expression in mouse adipocytes **(29)**. SET2 included 129 genes which were upregulated after *PGC-1α* induction in SAOS2 cells (human osteoblast-like cells) **(30)**. SET3 included the 70 genes downregulated in DS fetal heart tissues **(8)** belonging to the "mitochondrion" GO category (**Suppl. Table 1**). The comparison was aimed at identifying genes consistently dysregulated across these studies.
The Venn Diagram shows that NEMGs in SET3, which were downregulated in DS fetal hearts, overlap with both SET1 and SET2 (**Fig. 1A**). The three sets of genes overlap each other for at least 25 genes. Fifteen genes are consistently dysregulated across all 3 experiments (**Fig. 1B**). Most of these genes are included in the electron transport chain, mainly in complex I, and in oxidative phosphorylation pathways. It is also interesting to note that 42 genes overlap between the sets of genes inversely regulated by *NRIP1* and *PGC-1α* (SET1 and SET2), in agreement with the antagonistic functions of the two coregulators **(19)**.

***NRIP1* attenuation by siRNA affects NEMG expression in DS-HFFs**

We previously demonstrated that *NRIP1* is upregulated in human fetal fibrobasts from DS fetuses (DS-HFFs) in which Hsa21 trisomy negatively regulates NEMGs and impairs mitochondrial function **(7)**.

To test the hypothesis that *NRIP1* overexpression perturbs mitochondrial function and that this effect is associated with *PGC-1α* downregulation, we performed silencing experiments of *NRIP1* gene in DS-HFFs. In brief, after re-analyzing all DS-HFF lines used for silencing experiments, we demonstrated that *NRIP1* is significantly upregulated in all trisomic samples if compared to euploid controls (**Fig. 2A**). Seventy-two hours after transfection of a specific SMART pool of siRNAs in DS-HFFs, an inverse correlation between *NRIP1* and *PGC-1α* expression, in a siRNA dosage-dependent way, was demonstrated by qRT-PCR (**Fig. 2B**). By mmunofluorescence analysis we demonstrated that the NRIP1 protein localizes to the cell nucleus, as expected for a corepressor protein, both in euploid and in trisomic fibroblasts **(Fig. 3)**. Fluorescent signal was more intense over nuclei of DS-HFFs **(Fig. 3B)** with respect to euploid HFFs **(Fig. 3A)** indicating a higher concentration of the NRIP1 protein in trisomic cells. In these cells some fluorescent signal was also present over the cytoplasm **(Fig. 3B)** likely due to the overexpression of the NRIP1 protein. In DS-HFFs treated with siRNAs to attenuate *NRIP1* mRNA expression, NRIP1 fluorescent signal was significantly decreased in a siRNA dosage-dependent way (**Fig. 3**). Quantitative evaluation of fluorescence intensities in euploid, trisomic, and siRNA transfected cells (**Fig. 3F**) indicated that siRNA transfection reduces NRIP1 protein levels of trisomic cells down to the range of diploid cells or even lower (**Fig. 3D-E**).

To determine the effects of *NRIP1* attenuation by siRNA on other mitochondria-related genes, we compared the expression of 7 genes in silenced vs scrambled cells using qRT-PCR. Three genes, *i.e., COX5A*, *NDUFA1* and *NDUFS3*, were chosen from the list of 15 genes that resulted consistently dysregulated across the 3 sets compared in the meta-analysis (**Fig. 1**). The fourth gene, *NRF1*, which is downregulated in DS hearts **(8)** and fibroblasts **(7)**, was chosen because of its role both as a *PGC-1α* partner and as its target. Finally, three other genes, *i.e.*, *ANT1/SLC25A4*, *ANT2/SLC25A5* and *ANT3/SLC25A6*, which are downregulated in DS fetal fibroblasts (our unpublished data), were also chosen as *PGC-1α* targets (SET2, **Suppl. Table 1**) **(30)**. *ANT1/SLC25A4* is downregulated in SET3 and after *NRIP1* overexpression in the De Cegli's data

set **(28)**. The expression ratio of these genes in *NRIP1*-silenced DS-HFFs versus scrambled transfected DS-HFFs demonstrated that 5 out of 7 analyzed genes were significantly upregulated after *NRIP1* attenuation by siRNA (**Fig. 4**).

Further, to verify the effect of *NRIP1* attenuation and consequent *PGC-1α* upregulation on the mitochondrial biogenesis, we used qRT-PCR to quantify *D-LOOP* and *ACTIN* gene expression in scrambled and silenced cells, as mitochondrial and nuclear markers, respectively. The average of *D-LOOP/ACTIN* ratio increased by 2.5 fold in silenced trisomic cells (**Fig. 5**), thereby suggesting that mtDNA content does increase after *NRIP1* attenuation by siRNA and consequent *PGC-1α* overexpression.

Mitochondrial function is improved in DS-HFFs after *NRIP1* attenuation by siRNA

We verified whether *NRIP1* attenuation by siRNA, along with the consequent increases in *PGC-1α* and other mitochondrial genes, might counteract the mitochondrial dysfunction in trisomic cells. For this study, intracellular ROS production, mitochondrial activity, mitochondrial calcium, and ATP content were evaluated in DS-HFFs after transient *NRIP1* siRNA-mediated attenuation.

ROS production was measured by confocal microscopy imaging of cells treated with the redox-sensitive fluorescent probe dichlorofluorescein (DCF). Seventy-two hours after transfection with *NRIP1* siRNA, DCF-related fluorescence was lower with respect to scrambled DS-HFFs. Semiquantitative analysis of fluorescent signals demonstrated that, on an average basis, the ROS-related DCF fluorescence decreased up to 50% in a siRNA dosage-dependent manner (**Fig. 6**).

We then established whether decreases in ROS could depend on a rescue of respiratory chain complex activities. To this aim, we incubated silenced DS-HFFs with the specific mitochondrial superoxide indicator, MitoSOX Red. This reagent is a live-cell permeant that is rapidly and selectively targeted to mitochondria. Once in the mitochondria, MitoSOX Red reagent is oxidized by superoxide and exhibits red fluorescence. In experiments performed in *NRIP1*-silenced DS-

HFFs, a reduction of the MitoSOX Red signal was demonstrated thus suggesting that the decrease in ROS was partially associated with mitochondrial activity (**Fig. 7**).

Then, to confirm even further that *NRIP1* attenuation by siRNA improves mitochondrial function, we incubated trisomic silenced cells with the MitoTracker Red dye, a reagent that stains mitochondria in live cells and whose accumulation is dependent upon membrane potential. A significant 50% increase of the MitoTracker Red-related fluorescence was observed in *NRIP1*-silenced cells when compared with scrambled controls, thus indicating an increase in respiratory activity (**Fig. 8**).

***NRIP1* attenuation by siRNA does not affect mitochondrial Ca^{2+} homeostasis**

In DS-HFFs the mitochondrial Ca^{2+} concentration is significantly greater than that of euploid fetal fibroblasts **(7)**. Many extracellular stimuli exert their effect through an increase in cytosolic Ca^{2+} concentration ($[Ca^{2+}]_c$) mediated by the influx of extracellular Ca^{2+} and/or the release of Ca^{2+} from intracellular stores, predominantly the endoplasmic reticulum (ER). When $[Ca^{2+}]_c$ increases, mitochondria undergo a major rise in the matrix Ca^{2+} concentration ($[Ca^{2+}]_m$). The amplitude of this rise largely exceeds that observed in the cytosol thanks to electrochemical potential across the cation-impermeant inner mitochondrial membrane that provides the driving force for mitochondrial Ca^{2+} accumulation **(31)**.

Variations in $[Ca^{2+}]_m$ were measured as previously described **(7)**. In brief, DS-HFFs were transfected with a mitochondrially targeted aequorin **(32)** and then stimulated with histamine. This agonist elicited the production of inositol 1,4,5 trisphosphate (IP3) and the consequent release of Ca^{2+} from the ER, through the IP3 receptor (IP3R).

We found no significant differences in the mitochondrial $[Ca^{2+}]_m$ uptake in *NRIP1*-silenced DS-HFFs compared to control cells transfected with the non-targeting scrambled siRNA (42.0±2.6 μM vs. 38.7±3.9 μM, p=0.5) (**Fig. 9**).

NRIP1 attenuation by siRNA strongly increases cellular ATP content

Levels of phosphorylated adenosine nucleotides, including the universal energy carrier adenosine 5′-triphosphate (ATP), define the energy state in living cells and depend mainly on mitochondrial function **(33)**. In *NRIP1*-silenced DS-HFFs, we investigated the intramitochondrial ATP concentration ($[ATP]_m$). For this purpose, we used a chimera of the ATP-sensitive photoprotein luciferase specifically targeted to mitochondria (mtLuc) to obtain a dynamic monitoring of $[ATP]_m$. Luciferase has been widely employed to measure ATP content both in isolated mitochondria and in intact cells; its reaction with luciferin produces a flash of yellow-green light with a peak emission at 560 nm, the intensity of which is proportional to the amount of substrates in the reaction mixture.

We found that silenced DS-HFFs showed a very strong increase (+50%, $p=10^{-4}$) in basal ATP content, calculated by the luminescence values of the plateau generated after addition of luciferin (**Fig. 10**). Since basal ATP content is highly dependent on the abundance of transfected luciferase, we determined the exact amount of the luciferase transduced under our experimental conditions through an immunoblot assay. We found that the levels of luciferase protein transduced in *NRIP1*-silenced DS-HFFs were comparable with those detected in control cells transfected with the non-targeting scrambled siRNA (**Fig. 11**).

In parallel, *NRIP1*-silenced cells were slightly decreased in mitochondrial ATP production 72h after transfection. This was calculated by subtracting the basal cellular luminescence plateau, generated after addition of luciferin, from the luminescence values of the second plateau, generated after addition of the Ca^{2+} mobilizing agent histamine (**Fig. 10**).

DISCUSSION

This study originates from previous analyses demonstrating a global mitochondrial dysfunction in several DS models **(1)**, **(2)**, **(3)**, **(4)** and a significant dysregulation of NEMGs in the heart **(8)**, brain **(9)**, and fibroblasts **(7)** from human fetuses with DS. From these studies it emerged that genes and transcription factors responsible for the activity of respiratory complexes and mitochondrial biogenesis are globally repressed. Thus we speculated that most of the underexpressed NEMGs might be under the same regulatory control and that this control might be affected by the trisomy of Hsa21. In the present study, we looked for a regulator of NEMGs that maps to Hsa21 and that is upregulated in DS samples, by virtue of a gene dosage effect. To this aim, we re-evaluated the expression data from the GEO repository (http://www.ncbi.nlm.nih.gov/geo) by focusing on an experiment in which regulatory genes mapping to Hsa21 were individually overexpressed in mouse ESCs **(28)**. Our analysis demonstrated that only one gene is able to cause NEMG downregulation and that no other Hsa21 tested gene exerts such an effect. This gene is *NRIP1* which encodes for a corepressor protein. Although the mean dysregulation of each NEMG elicited by *NRIP1* overexpression was not very strong, the number of affected genes was significantly enriched ($p<0.001$). The role of *NRIP1* in mitochondrial dysfunction is supported by previous findings demonstrating that both in cellular and in animal models *NRIP1* silencing upregulates the expression of genes responsible for mitochondrial biogenesis and oxidative phosphorylation whereas, *NRIP1* re-expression downregulates them **(29)**, **(23)**. Experiments of *NRIP1* manipulation, performed in transgenic mice and human cells, have actually demonstrated that even mild variations in *NRIP1* expression can significantly affect oxidative metabolism and mitochondrial biogenesis **(29), (23), (34), (11)**.

We also considered the possible effects of the overexpression of other Hsa21 genes that have previously been implicated in the regulation of mitochondrial function such as *DYRK1A*, *DSCR1,* and *GABPA*, but none of these genes turned out to regulate *per se* NEMG expression. *GABPA*, in particular, is a nuclear respiratory factor that would be expected to downregulate mitochondria-

related genes when it is downregulated. However, *GABPA* is never downregulated in DS samples. Indeed it was normoregulated in DS fetal hearts **(8)**, upregulated in DS fetal fibroblasts **(7)** and inconsistently dysregulated in Vilardell's meta-analysis **(14)**.

On the other hand, the effect of *NRIP1* on NEMG expression could be further reinforced by another Hsa21 gene, *SUMO3*, as sumoylation modulates *NRIP1* activity **(35)**. We thus speculate that the simultaneous upregulation of both *NRIP1* and *SUMO3* exerts a synergistic effect on mitochondrial dysfunction.

NRIP1 is supposed to exert a repression of mitochondrial biogenesis by either interacting with nuclear receptors **(19)**, **(18)** or regulating *PGC-1α* activity **(10)**, **(12)**, **(13)**. *PGC-1α* knockout mice show not only a decreased number of mitochondria but also a decreased respiratory capacity in skeletal muscle **(21)**. In particular, under physiological conditions, *PGC-1α*, by coactivating several transcription factors, including nuclear receptors such as *PPARγ*, *PPARα* and *ERRα*, promotes mitochondrial biogenesis and regulates mitochondrial respiratory efficiency **(21)**, **(10)**, **(36)**.

Interestingly among the 37 NEMGs downregulated after *NRIP1* induction in the GEO GSE 19836 experiment **(28)**, we observed an enrichment both of genes involved in *PPAR*s pathways (8 genes) and of genes containing the *ERRα* motif in their promoter regions (25 genes) ($p<0.0005$). Notably, the known targets of *PGC-1α*, namely, *CIDEA* **(12)** and *ANT1/SLC25A4* **(30)**, are included in the list of genes that are downregulated following *NRIP1* overexpression **(28)**.

Moreover, to investigate whether the NEMGs repressed by *NRIP1* and induced by *PGC-1α* corresponded to the NEMGs downregulated genes in DS fetal hearts **(8)**, we performed a meta-analysis by comparing our microarray data with the results of 2 experiments in which the gene expression of *NRIP1* or *PGC-1α* was modulated. We found that the correspondence between the 3 sets of genes was remarkably high, considering that they all derived from different species, tissues, and experimental approaches. The high number of overlapping genes in SET1 and SET2 is in

agreement with previous research indicating an interrelationship between *PGC-1α* and *NRIP1* activity on mitochondrial pathways **(11)**.

These results, combined with the data from previous research, finally led us to verify the potential role of *NRIP1* in mitochondrial dysfunction in DS. When we transiently attenuated *NRIP1* in trisomic fibroblasts, we demonstrated an inverse correlation between *NRIP1* and *PGC-1α* expression. Accordingly, we found that this attenuation induced the upregulation of 5 out of 7 genes randomly chosen in SET3, all of which overlapped with the lists of genes regulated by *NRIP1* (SET1) and/or *PGC-1α* (SET2). Moreover *NRIP1* siRNA-mediated attenuation in DS-HFFs, and the consequent *PGC-1α* and *NRF1* upregulation, elicited a significant increase in mtDNA. This result fully corroborates similar experiments performed in cardiomyocytes **(11)**.

In the same trisomic fibroblasts, ROS production was decreased and mitochondrial activity was increased, demonstrating that the induction of NEMG expression in silenced DS-HFFs counteracts mitochondrial impairment and partially rescues mitochondrial function. However, no significant alterations of mitochondrial [Ca^{2+}] were observed after *NRIP1* attenuation by siRNA. A possible explanation to this phenomenon is either that 72-hours is not a sufficient time to determine detectable differences in Ca^{2+} uptake or that many other mechanisms affect calcium uptake in TS21 cells, e.g. the trisomy of genes involved in the calcineurin pathway (*DYRK1A* and *DSCR1*) **(25)**. Other Ca^{2+} regulators could play a role.

Interestingly, in *NRIP1*-silenced trisomic cells, we found a significant 50% increase in basal ATP content. These results, together with the finding that *NRIP1* attenuation by siRNA leads to an increase in the adenine nucleotide translocators *ANT1/SLC25A4* and *ANT2/SLC25A5* (**Fig. 4**), suggest that a more efficient exchange of adenosine 5′-triphosphate is induced, thus benefitting the mitochondrial activity and function of these cells, as demonstrated by the reduction in ROS production at the mitochondrial level (**Fig. 7**).

Supporting evidence for the opposite effects of *NRIP1* and *PGC-1α* on mitochondrial function and NEMG regulation is that in neonatal rat cardiomyocytes *NRIP1* mediates an antagonistic role versus *PGC-1α* in the regulation of mitochondrial energy metabolism **(11)**. Indeed, overexpressed *NRIP1* abrogates *PGC-1α*-mediated induction of mitochondrial membrane potential and mitochondrial biogenesis **(11)**. Furthermore, the *NRIP1*-dependent repression of genes involved in mitochondrial function is closely linked with post-natal impaired cardiac function as a result of reduced mitochondrial electron-transport chain activity and oxygen consumption. *NRIP1* hyperexpressing mice are indeed affected by cardiac hypertrophy **(34)**.

NRIP1 and *PGC-1α* are also involved in glucose uptake and therefore in the physiopathology of diabetes through the regulation of the insulin sensitive glucose transporter *GLUT4* expression and its sub-cellular localization **(37)**. These findings correlate with the fact that cardiac hypertrophy and diabetes are two important post-natal complications of DS.

Mitochondrial dysfunction might also contribute to determining DS mental retardation and other DS associated post-natal pathologies, like Alzheimer's disease (AD) and obesity. It is known that mitochondria also play a central role in many neurodegenerative diseases such as AD, Parkinson's disease, Huntington's disease, and amyotrophic lateral sclerosis. Impaired energy metabolism, defective mitochondrial enzymatic activity, abnormal mitochondrial respiration, mutated mtDNAs, and oxidative stress are all common features of these neurodegenerative conditions **(38)**.

It is interesting to note that the bioinformatic functional analysis of the 25 genes overlapping SET1 (genes regulated by *NRIP1*) and SET3 (genes downregulated in DS fetal hearts) showed that 16 out of 25 genes characterized the mitochondrial dysfunction pathways described in neurodegenerative diseases such as AD and Parkinson's disease (KEGG Pathways http://www.genome.jp/kegg/ **(39)**). However, given that there is a high prevalence of AD in DS patients, we cannot neglect the possibility that the overexpression of the Hsa21 gene *APP* might have a main role in the development of AD in DS patients.

Taken all together our study indicates that *NRIP1* is a key gene in the regulation of the mitochondrial pathways and that it is linked to mitochondrial dysfunction in DS. Accordingly, this should be taken into account when planning therapeutic approaches aimed at improving functions and cognitive performance in DS mouse models. Many of these models are indeed inadequate since they are not trisomic for all Hsa21 genes and may also have duplications of regions non syntenic to Hsa21. This is true, for instance, for the very popular Ts65Dn mouse that, among other Hsa21 genes, is not trisomic for either *NRIP1* or *SUMO3*. Thus, preclinical models of Ts65Dn will be unable to address all phenotypic problems and we speculate that clinical trial oftentimes fail because the overexpression of important genes like *NRIP1* is not taken into account.

Our results do highlight that *NRIP1* plays a relevant role in DS mitochondrial dysfunction, as evidenced by the ability of *NRIP1* inhibition to counteract mitochondrial dysfunction. However, we cannot rule out the likelihood that other genes may, in fact, be involved. A case in point is that the DS mouse model Ts1Cje manifests mitochondrial dysfunction even though it is not trisomic for either *NRIP1* or for *SUMO3*. Thus, further studies are indeed warranted to identify additional genes possibly responsible for DS mitochondrial alterations.

Finally, these results provide the basis for clinical trials aimed at restoring mitochondrial function in DS subjects to counteract specific phenotypic features such as neurodegeneration, cardiac hypertrophy, diabetes, and obesity. Such therapeutic approach would be highly desirable considering that the very few therapeutic approaches undertaken so far in this direction using antioxidants and nutraceutics have yielded either poor or discordant outcomes **(40)**, **(41)**.

Thus we speculate that a possible therapeutic approach in DS could be based either on *PGC-1α* activators, which have been tested in other disease mouse models **(42)**, **(43)**, **(44)**, **(45)**, or on *PPARγ* agonists, which attenuate mitochondrial dysfunction in AD mouse models **(46)**, **(47)**, **(48)**, **(49)**, **(50)**, **(51)**. Such drugs are already routinely used in clinical practice for the treatment of metabolic syndromes, type 2 diabetes, and neurodegenerative diseases such as AD **(52)**, **(53)**, **(54)**.

In conclusion, our study has provided further insights into the transcription factors that influence mitochondrial dysfunction in DS. Our findings could indeed pave the way for the development of new and more effective drugs capable of selectively targeting the intricate set of molecular mechanisms underlying the pathogenesis of this disease.

MATERIALS AND METHODS

Analysis of public expression data. A set of expression data from GSE 19836 series **(28)** was obtained from Gene Expression Omnibus repository GEO (http://www.ncbi.nlm.nih.gov/geo). This set of data, derived from the analysis of a mouse embryonic stem cell bank in which 32 orthologs of human chromosome 21 genes, including transcription factors and protein kinases, were individually overexpressed in an inducible manner. A set of clones individually overexpressing 20 of the 32 genes, namely 13 transcription factors (*Aire*, *Bach1*, *Erg*, *Ets2*, *Gabpa*, *Nrip1*, *Olig1*, *Olig2*, *Pknox1*, *Runx1*, *Sim2*, *ZFP295*, *1810007M14Rik*), one transcriptional activator (*Dscr1-Rcan1*) and 6 protein kinases (*DYRK1A, SNF1LK*, *Hunk*, *Pdxk*, *Pfkl*, *Ripk4*), was transcriptionally profiled under inducing and non-inducing conditions with Affymetrix Gene Chip Mouse 430_2. Specifically, RNAs from 3 induced mouse ESCs and 3 controls were profiled for each inducible Hsa21 gene **(28)**. In our analysis, we used GeneSpring software vers. 11.5 Multi−Omic Analysis (Agilent technologies Inc.) for data interpretation; however our criteria were different from those used by the authors of the gene expression data set, focusing on downregulated genes. We considered genes differentially expressed with a Fold change (LogFC) >0.3 and <−0.3 with $p<0.05$, thus producing 2 lists of dysregulated genes: 511 upregulated genes and 298 downregulated genes. Gene ontology (GO) functional class scoring of all the lists of significantly upregulated or downregulated genes was performed using the Web−based Gene Set Analysis Toolkit V2 (http://bioinfo.vanderbilt.edu/webgestalt/) **(55)**, **(56)**. Special attention was given to mitochondria-related categories and pathways.

Meta-analysis. We compared 3 sets of gene expression data from different experiments, to identify genes consistently dysregulated across the 3 studies. The first set, SET 1,included genes dysregulated by *Nrip1* modulation in mouse adipocytes **(29)**. The second set, SET2, included genes upregulated after *PGC-1α* induction in SAOS2 cells (human osteoblast like cells) **(30)**. The third

set included mitochondria-related genes, downregulated in DS fetal heart tissue **(8)** The 3 sets were filtered according to the GO cell component category "mitochondrion" with the above mentioned Web−based Gene Set Analysis Toolkit V2. The resulting genes – 123 genes in SET1, 129 in SET2 and 70 in SET3 (Suppl. Table 1) – were intersected using the R software (http://www.R-project.org/). A Venn Diagram was built, which shows overlapping genes across the 3 sets.

Ethics Statement. Human primary lines of fetal fibroblasts (HFFs) were obtained from the "Telethon Bank of Fetal Biological Samples" at the University of Naples. All experimental protocols were approved by the local Institutional Ethics Committee.

Samples. Eight skin biopsies were explanted from human fetuses with trisomy of Hsa21 (DS-HFF) after therapeutic abortion at 18–22 gestational weeks. Fibroblasts from biopsies were cultured in T25 flasks (BD Falcon) with Chang medium B+C (Irvine Scientific) supplemented with 1% penicillin/streptomycin (Gibco) at 37°C in 5% CO_2 atmosphere; all the analyses described throughout this study were carried out at cell culture passages 4–5.

Transfection protocol. *NRIP1* was transiently silenced in 8 DS-HFF lines using a pool of specific *NRIP1*-siRNAs (ON-TARGETplus SMARTpool, Dharmacon), with negative (ON-TARGETplus SMARTpool Non targeting siRNAs control, Dharmacon) and positive controls (ON-TARGETplus SMARTpool, GAPDH siRNAs, Dharmacon). Interferin transfection reagent (Polyplus transfection) was used. Cells were plated on 12 well plates (50000 cells/well) for RNA collection, on 35 mm diameter plates with 20 mm slides (Delchimica) (50000 cells/well) for ROS production analysis and on 24 well plates (30000 cells/well) (BD Falcon) for immunofluorescence and mitochondrial activity assays. DS-HFFs were transfected with 5nM and 20nM siRNA according to the manufacturer's protocol (Polyplus transfection). Seventy-two hours after transfection, the effects of *NRIP1* siRNA-mediated attenuation were evaluated.

NRIP1 immunofluorescence. For the evaluation of NRIP1 protein by immunofluorescence, 30,000 cells were plated in 24 well plates on 12 mm diameter round glass coverslips. Cells were fixed in 3:1 methanol: acetic acid for 15 min, washed twice with PBS, and then incubated twice in 0.1M Borate Buffer pH 8.5 for 10 minutes to neutralize the pH. After two washes with PBS, the cells were incubated with DNase 1:10 in RDD Buffer (Qiagen) at 37°C for 1h and then treated with 2% BSA in PBS to block non-specific protein-protein interactions. The cells were then incubated with the antibody anti-NRIP1 (30µg/ml, ab42126 Abcam, Cambridge Science Park, Cambridge, UK) overnight at +4°C. The secondary antibody (green) was Alexa Fluor® 488 goat anti-rabbit IgG (H+L) used at a 1/200 dilution for 1h **(57)**. Cells were finally mounted in 50% glycerol in PBS. Immunofluorescence analysis was performed at a confocal laser scanning microscope LSM 510 (Zeiss, Gottingen, Germany) equipped with an Argon ionic laser whose λ was set at 488nm, and an HeNe laser whose λ was set at 633nm. Emission of fluorescence was revealed by a BP 505-530 band pass filter for Alexa Fluor 488 and by a 615 long pass filter for DRAQ5. Images were acquired at a resolution of 1024x1024 pixels. Analysis of data were performed with ImageJ software, version 1.37 **(58)**. Fifty random single cells were analyzed for each imaging analysis.

Laser scanning confocal microscopy (LSCM) live cell imaging of ROS production. For the evaluation of ROS production after *NRIP1* siRNA transfection, 50,000 cells were plated on 25 mm diameter round glass coverslips in an Attofluor cell chamber (Molecular Probe, Leiden, NL). Seventy-two hours later, the cells were incubated for 15 minutes at 37°C with 10µM of 2,7-dichlorofluorescin diacetate (DCF-DA) which is converted to dichlorofluorescein by intracellular esterases, for detection of H_2O_2, or with 5µM of MitoSOX™ Red reagent (Life Technologies, Molecular Probes), which is a live-cell permeant and is rapidly and selectively targeted to the mitochondria. Once in the mitochondria, MitoSOX™ Red reagent is oxidized by superoxide and exhibits red fluorescence. After incubation cells were washed three times with medium w/o serum.

To maintain the cells alive during observation and to create the proper environmental conditions, the specimen was placed in an Oko Lab (Na, Italy) Water Jacket Top Stage Incubator, kept at 37°C, under humidified condition of 5% CO_2 and 95% air by means of temperature controllers, gas mixers, and humidifiers right on the microscope.

The analysis of immunofluorescence was performed with a confocal laser scanner microscopy Zeiss LSM 510 (Carl Zeiss, Gottingen, Germany), equipped with Argon ionic laser whose λ was set at 488nm, an HeNe laser whose λ was set at 546nm, and an immersion oil objective 63x/1.4f. Emission of fluorescence was revealed by BP 505-530 band pass filter for DCF and 560 Long Pass for MitoSOX Red. Images were acquired in the green or in the red channels and then saved in TIFF format to prevent the loss of information. They were acquired with a resolution of 1024x1024 pixel with the confocal pinhole set to one Airy unit.

Analysis of data were performed with ImageJ software, version 1.37. Fifty random single cells were analyzed for each imaging analysis.

Mitotracker immunofluorescence. For the evaluation of mitochondrial activity MitoTracker® Red CMXRos (Molecular Probes) was chosen. MitoTracker® probes passively diffuse across the plasma membrane and accumulate in actively respiring mitochondria. Thirty-thousand cells were plated on 24 well plates on 12 mm diameter round glass coverslips and then incubated with 150nM of Mitotracker Red for 30 minutes. After incubation cells were fixed for 20 minutes in PBS containing 4% paraformaldehyde (Sigma) and then washed once with PBS 1X. Nuclei were stained with the DNA intercalant DRAQ5 (Bio status, Alexis Corporation). Cells were finally mounted in 50% glycerol in PBS. Immunofluorescence analysis was performed with a confocal laser scanning microscope LSM 510 (Zeiss, Gottingen, Germany). The lambda of the two HeNe lasers was set at 546nm and at 633nm. Fluorescence emission was revealed by BP 560–615 band pass filter for Mitotracker Red and by 615 long pass filter for DRAQ5. Double staining immunofluorescence images were acquired separately in the red and infrared channels at a resolution of 1024x1024

pixels, with the confocal pinhole set to one Airy unit, and then saved in TIFF format. Fifty random single cells were analyzed for each imaging analysis using the ImageJ version 1.37.

RNA extraction and Quantitative Real-time PCR. Total RNA from each sample was extracted using TRIzol reagent (Gibco/BRL Life Technologies, Inc., Gaithersburg, MD) and was reverse transcribed using the iScript cDNA Synthesis kit (Bio-Rad Laboratories Inc., Hercules, CA, USA). Real-time PCR was performed using iQ Supermix SYBR Green 2X on a Bio-Rad iCycler according to the manufacturer's protocols. PCR reactions were performed in triplicate. Primer pairs (MWG Biotech, Ebersberg, Germany) were designed using the Primer 3 software (http://frodo.wi.mit.edu/primer3) to obtain amplicons ranging from 100 to 150 base pairs. Expression values were normalized either versus scrambled transfected cells or versus scrambled transfected euploid cells. *ABELSON* and *GAPDH* housekeeping genes were chosen as reference genes.

mtDNA quantification. To quantify the mtDNA content, we selected two genes: *D-LOOP* as the mitochondrial target and *ACTIN* as the nuclear target. Both targets were quantified by qRT-PCR using cDNA reverse-transcribed from RNA of 3 *NRIP1*-silenced trisomic samples and scrambled control. Normalization of gene expression was obtained using *ABELSON* gene as housekeeping. The ratio between *D-LOOP* and *ACTIN* expression under each condition (*NRIP1*-silenced or scrambled trisomic cells) was calculated.

Aequorin measurement. A chimeric aequorin targeted to the mitochondria (mtAEQmut) was used as probe. For the experiments with mtAEQmut, cells were incubated with 5 mM coelenterazine (Fluka, 7372) for 1–2 h in DMEM supplemented with 1% FBS. A coverslip with transfected cells was placed in a perfused thermostated chamber located in close proximity to a low-noise photomultiplier with a built-in amplifier/discriminator. All aequorin measurements were performed

in KRB supplemented with 1 mM $CaCl_2$. Agonist was added to the same medium as specified in figure legends. The experiments were terminated by lysing cells with 100 mM digitonin in a hypotonic Ca^{2+}-containing solution (10 mM $CaCl_2$ in H_2O), thus discharging the remaining aequorin pool. The output of the discriminator was captured by a Thorn EMI photon-counting board and stored in an IBM-compatible computer for further analyses. The aequorin luminescence data were calibrated offline into [Ca^{2+}] values using a computer algorithm based on the Ca^{2+} response curve of mutant aequorins.

Immunoblotting. For immunoblotting, cells were scraped into ice cold phosphate-buffered saline and lysed in a modified 10 mM Tris buffer pH 7.4 containing 150 mM NaCl, 1% Triton X-100, 10% glycerol, 10 mM EDTA and protease inhibitor cocktail. After 30 min of incubation on ice, the lysates were cleared via centrifugation at 12,000 g at 4°C for 10 min. Protein concentrations were determined by the Lowry procedure. Protein extracts (18 µg) were separated on 4–12% Bis-Tris acrylamide Gel (Life Technologies, NP0323) and electron-transferred to PVDF or nitrocellulose membrane according to standard procedures. Unspecific binding sites were saturated by incubating membranes with TBS-Tween 20 (0.05%) supplemented with 5% nonfat powdered milk for 1 h. Next, the membranes were incubated overnight with primary antibodies [GAPDH (Cell Signaling, 2118); LUCIFERASE (Invitrogen, 356700)] and the detection was assessed by appropriate HRP-labeled secondary antibodies [Santa Cruz, sc-2004 (goat anti-rabbit) and sc-2005 (goat anti-mouse)] plus a chemiluminescent substrate (Thermo Scientific, 34080). Equal loading of lanes was confirmed by incubation with an anti-GAPDH antibody.

Luciferase measurements. Cells were seeded on glass coverslips (13 mm in diameter) for single sample luminescence measurements and allowed to grow until 50% confluence. The cells were then transfected with a cytosolic (untargeted) firefly luciferase (cytLuc) and a mitochondrially targeted luciferase (mtLuc) **(59)**, **(60)**.

Cell luminescence was measured in the same purpose-built luminometer used for the aequorin measurements, constantly perfused with KRB, supplemented with 1 mM $CaCl_2$ and 20 mM luciferin. The light output of a coverslip of infected cells was in the range of 1,000 –10,000 counts per second (cps) versus a background lower than 10 cps. All compounds employed in the experiments were tested for non-specific effects on the luminescence, but none was observed.

Statistics. The ANOVA test, with Bonferroni *post hoc* correction in case of multiple comparisons, was applied to evaluate the statistical significance of differences measured throughout the data sets presented. The threshold for statistical significance (p-value) was set at 0.05.

ACKNOWLEDGEMENTS

We thank Paola Merolla for language revision and editing. This work has been supported by POR Campania FSE 2007-2013, Project CREME from Campania Region to L.N.

CONFLICT OF INTEREST STATEMENT

None declared

REFERENCES

1 Kim, S.H., Vlkolinsky, R., Cairns, N., Fountoulakis, M. and Lubec, G. (2001) The reduction of NADH ubiquinone oxidoreductase 24- and 75-kDa subunits in brains of patients with Down syndrome and Alzheimer's disease. *Life Sci.*, **68**, 2741-2750.

2 Busciglio, J., Pelsman, A., Wong, C., Pigino, G., Yuan, M., Mori, H. and Yankner, B.A. (2002) Altered metabolism of the amyloid beta precursor protein is associated with mitochondrial dysfunction in Down's syndrome. *Neuron*, **33**, 677-688.

3 Helguera, P., Seiglie, J., Rodriguez, J., Hanna, M., Helguera, G. and Busciglio, J. (2013) Adaptive downregulation of mitochondrial function in down syndrome. *Cell. Metab.*, **17**, 132-140.

4 Shukkur, E.A., Shimohata, A., Akagi, T., Yu, W., Yamaguchi, M., Murayama, M., Chui, D., Takeuchi, T., Amano, K., Subramhanya, K.H. *et al.* (2006) Mitochondrial dysfunction and tau hyperphosphorylation in Ts1Cje, a mouse model for Down syndrome. *Hum. Mol. Genet.*, **15**, 2752-2762.

5 Valenti, D., Tullo, A., Caratozzolo, M.F., Merafina, R.S., Scartezzini, P., Marra, E. and Vacca, R.A. (2010) Impairment of F1F0-ATPase, adenine nucleotide translocator and adenylate kinase causes mitochondrial energy deficit in human skin fibroblasts with chromosome 21 trisomy. *Biochem. J.*, **431**, 299-310.

6 Valenti, D., Manente, G.A., Moro, L., Marra, E. and Vacca, R.A. (2011) Deficit of complex I activity in human skin fibroblasts with chromosome 21 trisomy and overproduction of reactive oxygen species by mitochondria: involvement of the cAMP/PKA signalling pathway. *Biochem. J.*, **435**, 679-688.

7 Piccoli, C., Izzo, A., Scrima, R., Bonfiglio, F., Manco, R., Negri, R., Quarato, G., Cela, O., Ripoli, M., Prisco, M. *et al.* (2013) Chronic pro-oxidative state and mitochondrial dysfunctions are more pronounced in fibroblasts from Down syndrome foeti with congenital heart defects. *Hum. Mol. Genet.*, **22**, 1218-1232.

8 Conti, A., Fabbrini, F., D'Agostino, P., Negri, R., Greco, D., Genesio, R., D'Armiento, M., Olla, C., Paladini, D., Zannini, M. *et al.* (2007) Altered expression of mitochondrial and extracellular matrix genes in the heart of human fetuses with chromosome 21 trisomy. *BMC Genomics*, **8**, 268.

9 Mao, R., Wang, X., Spitznagel, E.L., Jr., Frelin, L.P., Ting, J.C., Ding, H., Kim, J.W., Ruczinski, I., Downey, T.J. and Pevsner, J. (2005) Primary and secondary transcriptional effects in the developing human Down syndrome brain and heart. *Genome Biol.*, **6**, R107.

10 Scarpulla, R.C. (2011) Metabolic control of mitochondrial biogenesis through the PGC-1 family regulatory network. *Biochim. Biophys. Acta*, **1813**, 1269-1278.

11 Chen, Y., Wang, Y., Chen, J., Chen, X., Cao, W., Chen, S., Xu, S., Huang, H. and Liu, P. (2012) Roles of transcriptional corepressor RIP140 and coactivator PGC-1alpha in energy state of chronically infarcted rat hearts and mitochondrial function of cardiomyocytes. *Mol. Cell. Endocrinol.*, **362**, 11-18.

12 Hallberg, M., Morganstein, D.L., Kiskinis, E., Shah, K., Kralli, A., Dilworth, S.M., White, R., Parker, M.G. and Christian, M. (2008) A functional interaction between RIP140 and PGC-1alpha regulates the expression of the lipid droplet protein CIDEA. *Mol. Cell. Biol.*, **28**, 6785-6795.

13 Rytinki, M.M. and Palvimo, J.J. (2009) SUMOylation attenuates the function of PGC-1alpha. *J. Biol. Chem.*, **284**, 26184-26193.

14 Vilardell, M., Rasche, A., Thormann, A., Maschke-Dutz, E., Perez-Jurado, L.A., Lehrach, H. and Herwig, R. (2011) Meta-analysis of heterogeneous Down Syndrome data reveals consistent genome-wide dosage effects related to neurological processes. *BMC Genomics*, **12**, 229.

15 Wei, L.N., Hu, X., Chandra, D., Seto, E. and Farooqui, M. (2000) Receptor-interacting protein 140 directly recruits histone deacetylases for gene silencing. *J. Biol. Chem.*, **275**, 40782-40787.

16 Vo, N., Fjeld, C. and Goodman, R.H. (2001) Acetylation of nuclear hormone receptor-interacting protein RIP140 regulates binding of the transcriptional corepressor CtBP. *Mol. Cell. Biol.*, **21**, 6181-6188.
17 Kiskinis, E., Hallberg, M., Christian, M., Olofsson, M., Dilworth, S.M., White, R. and Parker, M.G. (2007) RIP140 directs histone and DNA methylation to silence Ucp1 expression in white adipocytes. *Embo J.*, **26**, 4831-4840.
18 Nautiyal, J., Christian, M. and Parker, M.G. (2013) Distinct functions for RIP140 in development, inflammation, and metabolism. *Trends Endocrinol. Metab.*, **24**, 451-459.
19 Fritah, A., Christian, M. and Parker, M.G. (2010) The metabolic coregulator RIP140: an update. *Am. J. Physiol. Endocrinol. Metab.*, **299**, E335-340.
20 Christian, M., White, R. and Parker, M.G. (2006) Metabolic regulation by the nuclear receptor corepressor RIP140. *Trends Endocrinol. Metab.*, **17**, 243-250.
21 Leone, T.C., Lehman, J.J., Finck, B.N., Schaeffer, P.J., Wende, A.R., Boudina, S., Courtois, M., Wozniak, D.F., Sambandam, N., Bernal-Mizrachi, C. *et al.* (2005) PGC-1alpha deficiency causes multi-system energy metabolic derangements: muscle dysfunction, abnormal weight control and hepatic steatosis. *PLoS Biol.*, **3**, e101.
22 Mitra, R., Nogee, D.P., Zechner, J.F., Yea, K., Gierasch, C.M., Kovacs, A., Medeiros, D.M., Kelly, D.P. and Duncan, J.G. (2012) The transcriptional coactivators, PGC-1alpha and beta, cooperate to maintain cardiac mitochondrial function during the early stages of insulin resistance. *J. Mol. Cell. Cardiol.*, **52**, 701-710.
23 Seth, A., Steel, J.H., Nichol, D., Pocock, V., Kumaran, M.K., Fritah, A., Mobberley, M., Ryder, T.A., Rowlerson, A., Scott, J. *et al.* (2007) The transcriptional corepressor RIP140 regulates oxidative metabolism in skeletal muscle. *Cell. Metab.*, **6**, 236-245.
24 Gardiner, K. (2006) Transcriptional dysregulation in Down syndrome: predictions for altered protein complex stoichiometries and post-translational modifications, and consequences for learning/behavior genes ELK, CREB, and the estrogen and glucocorticoid receptors. *Behav. Genet.*, **36**, 439-453.
25 Arron, J.R., Winslow, M.M., Polleri, A., Chang, C.P., Wu, H., Gao, X., Neilson, J.R., Chen, L., Heit, J.J., Kim, S.K. *et al.* (2006) NFAT dysregulation by increased dosage of DSCR1 and DYRK1A on chromosome 21. *Nature*, **441**, 595-600.
26 O'Leary, D.A., Pritchard, M.A., Xu, D., Kola, I., Hertzog, P.J. and Ristevski, S. (2004) Tissue-specific overexpression of the HSA21 gene GABPalpha: implications for DS. *Biochim. Biophys. Acta*, **1739**, 81-87.
27 Sturgeon, X., Le, T., Ahmed, M.M. and Gardiner, K.J. (2012) Pathways to cognitive deficits in Down syndrome. *Prog. Brain Res.*, **197**, 73-100.
28 De Cegli, R., Romito, A., Iacobacci, S., Mao, L., Lauria, M., Fedele, A.O., Klose, J., Borel, C., Descombes, P., Antonarakis, S.E. *et al.* (2010) A mouse embryonic stem cell bank for inducible overexpression of human chromosome 21 genes. *Genome Biol.*, **11**, R64.
29 Powelka, A.M., Seth, A., Virbasius, J.V., Kiskinis, E., Nicoloro, S.M., Guilherme, A., Tang, X., Straubhaar, J., Cherniack, A.D., Parker, M.G. *et al.* (2006) Suppression of oxidative metabolism and mitochondrial biogenesis by the transcriptional corepressor RIP140 in mouse adipocytes. *J. Clin. Invest.*, **116**, 125-136.
30 Schreiber, S.N., Emter, R., Hock, M.B., Knutti, D., Cardenas, J., Podvinec, M., Oakeley, E.J. and Kralli, A. (2004) The estrogen-related receptor alpha (ERRalpha) functions in PPARgamma coactivator 1alpha (PGC-1alpha)-induced mitochondrial biogenesis. *Proc. Natl. Acad. Sci. U S A*, **101**, 6472-6477.
31 Patergnani, S., Suski, J.M., Agnoletto, C., Bononi, A., Bonora, M., De Marchi, E., Giorgi, C., Marchi, S., Missiroli, S., Poletti, F. *et al.* (2011) Calcium signaling around Mitochondria Associated Membranes (MAMs). *Cell Commun. Signal*, **9**, 19.

32 Bonora, M., Giorgi, C., Bononi, A., Marchi, S., Patergnani, S., Rimessi, A., Rizzuto, R. and Pinton, P. (2013) Subcellular calcium measurements in mammalian cells using jellyfish photoprotein aequorin-based probes. *Nat. Protoc.*, **8**, 2105-2118.
33 Bonora, M., Patergnani, S., Rimessi, A., De Marchi, E., Suski, J.M., Bononi, A., Giorgi, C., Marchi, S., Missiroli, S., Poletti, F. *et al.* (2012) ATP synthesis and storage. *Purinergic Signal.*, **8**, 343-357.
34 Fritah, A., Steel, J.H., Nichol, D., Parker, N., Williams, S., Price, A., Strauss, L., Ryder, T.A., Mobberley, M.A., Poutanen, M. *et al.* (2010) Elevated expression of the metabolic regulator receptor-interacting protein 140 results in cardiac hypertrophy and impaired cardiac function. *Cardiovasc. Res.*, **86**, 443-451.
35 Rytinki, M.M. and Palvimo, J.J. (2008) SUMOylation modulates the transcription repressor function of RIP140. *J. Biol. Chem.*, **283**, 11586-11595.
36 Scarpulla, R.C., Vega, R.B. and Kelly, D.P. (2012) Transcriptional integration of mitochondrial biogenesis. *Trends Endocrinol. Metab.*, **23**, 459-466.
37 Fritah, A., Steel, J.H., Parker, N., Nikolopoulou, E., Christian, M., Carling, D. and Parker, M.G. (2012) Absence of RIP140 reveals a pathway regulating glut4-dependent glucose uptake in oxidative skeletal muscle through UCP1-mediated activation of AMPK. *PLoS One*, **7**, e32520.
38 Petrozzi, L., Ricci, G., Giglioli, N.J., Siciliano, G. and Mancuso, M. (2007) Mitochondria and neurodegeneration. *Biosci. Rep.*, **27**, 87-104.
39 Kanehisa, M. and Goto, S. (2000) KEGG: kyoto encyclopedia of genes and genomes. *Nucleic Acids Res.*, **28**, 27-30.
40 de la Torre, R. and Dierssen, M. (2012) Therapeutic approaches in the improvement of cognitive performance in Down syndrome: past, present, and future. *Prog. Brain Res.*, **197**, 1-14.
41 Costa, A.C. and Scott-McKean, J.J. (2013) Prospects for improving brain function in individuals with Down syndrome. *CNS Drugs*, **27**, 679-702.
42 Rodgers, J.T., Lerin, C., Haas, W., Gygi, S.P., Spiegelman, B.M. and Puigserver, P. (2005) Nutrient control of glucose homeostasis through a complex of PGC-1alpha and SIRT1. *Nature*, **434**, 113-118.
43 Dong, W., Gao, D. and Zhang, X. (2007) Mitochondria biogenesis induced by resveratrol against brain ischemic stroke. *Med. Hypotheses*, **69**, 700-701.
44 Lagouge, M., Argmann, C., Gerhart-Hines, Z., Meziane, H., Lerin, C., Daussin, F., Messadeq, N., Milne, J., Lambert, P., Elliott, P. *et al.* (2006) Resveratrol improves mitochondrial function and protects against metabolic disease by activating SIRT1 and PGC-1alpha. *Cell*, **127**, 1109-1122.
45 Jager, S., Handschin, C., St-Pierre, J. and Spiegelman, B.M. (2007) AMP-activated protein kinase (AMPK) action in skeletal muscle via direct phosphorylation of PGC-1alpha. *Proc. Natl. Acad. Sci. U S A*, **104**, 12017-12022.
46 Bastin, J., Aubey, F., Rotig, A., Munnich, A. and Djouadi, F. (2008) Activation of peroxisome proliferator-activated receptor pathway stimulates the mitochondrial respiratory chain and can correct deficiencies in patients' cells lacking its components. *J. Clin. Endocrinol. Metab.*, **93**, 1433-1441.
47 Nicolakakis, N., Aboulkassim, T., Ongali, B., Lecrux, C., Fernandes, P., Rosa-Neto, P., Tong, X.K. and Hamel, E. (2008) Complete rescue of cerebrovascular function in aged Alzheimer's disease transgenic mice by antioxidants and pioglitazone, a peroxisome proliferator-activated receptor gamma agonist. *J. Neurosci.*, **28**, 9287-9296.
48 Escribano, L., Simon, A.M., Perez-Mediavilla, A., Salazar-Colocho, P., Del Rio, J. and Frechilla, D. (2009) Rosiglitazone reverses memory decline and hippocampal glucocorticoid receptor down-regulation in an Alzheimer's disease mouse model. *Biochem. Biophys. Res. Commun.*, **379**, 406-410.
49 Johri, A., Calingasan, N.Y., Hennessey, T.M., Sharma, A., Yang, L., Wille, E., Chandra, A. and Beal, M.F. (2012) Pharmacologic activation of mitochondrial biogenesis exerts widespread

beneficial effects in a transgenic mouse model of Huntington's disease. *Hum. Mol. Genet.*, **21**, 1124-1137.
50 Sauerbeck, A., Gao, J., Readnower, R., Liu, M., Pauly, J.R., Bing, G. and Sullivan, P.G. (2011) Pioglitazone attenuates mitochondrial dysfunction, cognitive impairment, cortical tissue loss, and inflammation following traumatic brain injury. *Exp. Neurol.*, **227**, 128-135.
51 Yamaguchi, S., Li, H., Purevsuren, J., Yamada, K., Furui, M., Takahashi, T., Mushimoto, Y., Kobayashi, H., Hasegawa, Y., Taketani, T. *et al.* (2012) Bezafibrate can be a new treatment option for mitochondrial fatty acid oxidation disorders: evaluation by in vitro probe acylcarnitine assay. *Mol. Genet. Metab.*, **107**, 87-91.
52 Watson, G.S., Cholerton, B.A., Reger, M.A., Baker, L.D., Plymate, S.R., Asthana, S., Fishel, M.A., Kulstad, J.J., Green, P.S., Cook, D.G. *et al.* (2005) Preserved cognition in patients with early Alzheimer disease and amnestic mild cognitive impairment during treatment with rosiglitazone: a preliminary study. *Am. J. Geriatr. Psychiatry*, **13**, 950-958.
53 Sato, T., Hanyu, H., Hirao, K., Kanetaka, H., Sakurai, H. and Iwamoto, T. (2011) Efficacy of PPAR-gamma agonist pioglitazone in mild Alzheimer disease. *Neurobiol. Aging*, **32**, 1626-1633.
54 Marciano, D.P., Chang, M.R., Corzo, C.A., Goswami, D., Lam, V.Q., Pascal, B.D. and Griffin, P.R. (2014) The Therapeutic Potential of Nuclear Receptor Modulators for Treatment of Metabolic Disorders: PPARgamma, RORs, and Rev-erbs. *Cell Metab.*, **19**, 193-208.
55 Zhang, B., Kirov, S. and Snoddy, J. (2005) WebGestalt: an integrated system for exploring gene sets in various biological contexts. *Nucleic Acids Res.*, **33**, W741-748.
56 Wang, J., Duncan, D., Shi, Z. and Zhang, B. (2013) WEB-based GEne SeT AnaLysis Toolkit (WebGestalt): update 2013. *Nucleic Acids Res.*, **41**, W77-83.
57 Cali, G., Gentile, F., Mogavero, S., Pallante, P., Nitsch, R., Ciancia, G., Ferraro, A., Fusco, A. and Nitsch, L. (2012) CDH16/Ksp-cadherin is expressed in the developing thyroid gland and is strongly down-regulated in thyroid carcinomas. *Endocrinology*, **153**, 522-534.
58 Cali, G., Zannini, M., Rubini, P., Tacchetti, C., D'Andrea, B., Affuso, A., Wintermantel, T., Boussadia, O., Terracciano, D., Silberschmidt, D. *et al.* (2007) Conditional inactivation of the E-cadherin gene in thyroid follicular cells affects gland development but does not impair junction formation. *Endocrinology*, **148**, 2737-2746.
59 Jouaville, L.S., Pinton, P., Bastianutto, C., Rutter, G.A. and Rizzuto, R. (1999) Regulation of mitochondrial ATP synthesis by calcium: evidence for a long-term metabolic priming. *Proc. Natl. Acad. Sci. U S A*, **96**, 13807-13812.
60 Porcelli, A.M., Pinton, P., Ainscow, E.K., Chiesa, A., Rugolo, M., Rutter, G.A. and Rizzuto, R. (2001) Targeting of reporter molecules to mitochondria to measure calcium, ATP, and pH. *Methods Cell Biol.*, **65**, 353-380.

LEGENDS TO FIGURES

Figure 1. Comparison of NEMGs downregulated in DS fetal hearts with those dysregulated by *NRIP1* and/or *PGC-1α*.

A. Venn Diagram showing overlapping amongst the 3 sets of data. Out of the 70 mitochondrial genes that are downregulated in DS fetal hearts (SET3) **(8)**, 25 overlap the list of *NRIP1* regulated genes (SET1) **(29)**, and 29 overlap the list of *PGC-1α* regulated genes (SET2) **(30)**.

B. List of mitochondria-related genes overlapping in the 3 sets of data. The complete lists of genes are in Suppl. Table 1.

Figure 2. *NRIP1* modulates *PGC-1α* expression in HFFs.

A. *NRIP1* mRNA expression level in euploid cells (N1-N5), and in trisomic (DS1-DS8) HFF lines used for silencing experiments. For each sample, values represent the average determination ± SEM for 3 qRT-PCR experiments. A pool of euploid cells was used as a calibrator.

** = $p<10^{-4}$. P-values express statistical significance for euploid vs trisomic comparisons.

B. *NRIP1* and *PGC-1α* expression levels in trisomic cells transfected with a scrambled siRNA and with a *NRIP1*-specific SMART pool of siRNAs. A decrease in *NRIP1* expression level corresponds to an increase on *PGC-1α* expression level in a siRNA-dependent way.

Values represent the average determination ± SEM for 8 *NRIP1*-silenced DS-HFFs carried out in triplicate.

* = $p<0.05$, ** = $p<0.01$. P-values express statistical significance for *NRIP1*-silenced vs scrambled comparisons.

Figure 3. NRIP1 immunofluorescence in *NRIP1*-silenced DS-HFFs.

Representative images of NRIP1 immunofluorescence analysis in (**A**) euploid cells, (**B**) trisomic cells, and trisomic cells transfected (**C**) with a scrambled siRNA, (**D**) with 5nM *NRIP1* siRNA and

(**E**) 20nM *NRIP1* siRNA.

F. Semiquantitative analysis of the immunodetected signals, by ImageJ software (means±SEM of 3 assayed samples). Fifty randomly selected, different cells for each sample/experimental condition were analyzed. A decrease of the fluorescent signal is observed in silenced vs scrambled DS-HFFs. Signal from 5nM *NRIP1* siRNA transfected cells is comparable with euploid HFFs.

Statistical significance: ** = $p<0.01$ for trisomic vs euploid comparisons; # = $p<0.05$ for *NRIP1*-silenced vs scrambled comparisons.

Figure 4. Mitochondria-related gene expression in *NRIP1*-silenced DS-HFFs.

Relative mRNA expression of 7 mitochondria-related genes was measured in *NRIP1*-silenced DS-HFFs vs scrambled transfected DS-HFFs. Five out of the 7 genes show a significant increase in their expression level.

Values represent the average determination ± SEM for 3 DS-HFF samples carried out in triplicate. A pool of scrambled transfected euploid cells was used as calibrator.

* = $p<0.05$. P-value express statistical significance for *NRIP1*-silenced vs scrambled comparisons.

Figure 5. mtDNA content in *NRIP1*-silenced DS-HFFs.

Ratio between the mtDNA marker *D-LOOP* and the nuclear DNA marker *ACTIN* indicates an increase after *NRIP1* attenuation by siRNA. The ratio was calculated upon normalization to a reference gene (*ABELSON*) by qRT-PCR.

Values represent the average determination ± SEM for 3 *NRIP1*-silenced trisomic samples carried out in triplicate.

* = $p<0.05$. P-value express statistical significance for *NRIP1*-silenced vs scrambled comparisons.

Figure 6. ROS decrease in *NRIP1*-silenced DS-HFFs.

Confocal microscopy live cell imaging of the DCF fluorescence in transfected DS-HFFs: (**A**)

scrambled, (**B**) 5nM *NRIP1* siRNA and (**C**) 20nM *NRIP1* siRNA.

D. Semiquantitative analysis of the DCF-related fluorescence, by ImageJ software (means±SEM of 3 assayed samples). Fifty randomly selected, different cells for each sample/experimental condition were analyzed. A significant decrease of DCF-related fluorescence is observed after *NRIP1* attenuation in a siRNA-dependent way.

** = $p<10^{-4}$. P-value express statistical significance for *NRIP1*-silenced vs scrambled comparisons.

Figure 7. Intra-mitochondrial superoxide decrease in *NRIP1*-silenced DS-HFFs.

Confocal microscopy live cell imaging of the MitoSOX Red fluorescence in transfected DS-HFFs: (**A**) scrambled, and (**B**) 20nM *NRIP1* siRNA. Note that the distribution of MitoSOX Red signal resembles the mitochondrial network.

C. Semiquantitative analysis of the MitoSOX-related fluorescence, by ImageJ software (means±SEM of 3 assayed samples). Fifty randomly selected, different cells for each sample/experimental condition were analyzed. A reduction of the fluorescent signal over the mitochondrial network is detected.

** = $p<0.01$. P-value express statistical significance for *NRIP1*-silenced vs scrambled comparisons.

Figure 8. Mitochondrial activity in DS *NRIP1*-silenced DS-HFFs.

Confocal microscopy live cell imaging of the Mitotracker fluorescence in transfected DS-HFFs: (**A**) scrambled and (**B**) with 20nM *NRIP1* siRNA.

C. Semiquantitative analysis of the Mitotracker-related fluorescence, by ImageJ software (means±SEM of 5 assayed samples). Fifty randomly selected, different cells for each sample/experimental condition were analyzed. An increase of Mitotracker related fluorescence is observed in *NRIP1*-silenced DS-HFFs.

** = $p<0.005$. P-value express statistical significance for *NRIP1*-silenced vs scrambled comparisons.

Figure 9. Mitochondrial calcium measurement.

A. Barplot of the $[Ca^{2+}]_m$ in scrambled and *NRIP1* siRNA transfected DS-HFFs. The light signal was collected and calibrated into $[Ca^{2+}]$ values, as described in Materials and Methods. Results are shown as the average of measurements from 4 different *NRIP1*-silenced DS-HFFs ± SEM.

B. Effect of histamine on $[Ca^{2+}]_m$. The traces show the average $[Ca^{2+}]_m$ in DS-HFFs transfected with the mitochondrially targeted aequorin. Where indicated, the cells were treated with 100µM histamine added to KRB.

No significant variation in $[Ca^{2+}]_m$ is observed in the 2 conditions.

Figure 10. Mitochondrial ATP measurement.

A. Barplot of the mitochondrial ATP content and of the basal ATP content in scrambled and *NRIP1* siRNA-transfected DS-HFFs.

B. The traces show mitochondrial $[ATP]_m$ changes elicited by mitochondrial $[Ca^{2+}]$ increase in cells perfused with 100µM histamine as agonist. mtLuc luminescence data are expressed as a percentage of the initial value ±SEM (n=4). The traces are representative of four independent experiments.

* = p=0.05, ** = $p=10^{-4}$. P-values express statistical significance for *NRIP1*-silenced vs scrambled comparisons.

Figure 11. Luciferase expression following *NRIP1* attenuation by siRNA.

A. Representative immunoblot of luciferase protein in 3 *NRIP1*-silenced or scrambled DS-HFFs transfected with a luciferase–encoding plasmid specifically targeted to mitochondria (mtLuc) and cultured in complete medium for 72h.

B. Quantification of luciferase accumulation by LUCIFERASE/GAPDH ratio.

TABLES

Table 1. Gene Ontology categories affected by *NRIP1* overexpression in GSE 19836 series with a p-value < 0.05.

The "Mitochondrion" is the category most affected by *NRIP1* upregulation (enrichment = 37 observed genes instead of 17.7 expected genes with p< 0.001).

Biological Process	GO category	Genes in category	Observed	Expected	O/R Ratio	pvalue
carboxylic acid metabolic process	GO:0019752	630	20	7.51	2.66	0.0089
cellular carbohydrate metabolic process	GO:0044262	198	11	2.36	4.66	0.0089
monocarboxylic acid metabolic process	GO:0032787	339	14	4.04	3.47	0.0089
carboxylic acid catabolic process	GO:0046395	139	8	1.66	4.83	0.0100
organic acid catabolic process	GO:0016054	139	8	1.66	4.83	0.0100
regulation of transmembrane receptor protein serine/threonine kinase signaling pathway	GO:0090092	137	8	1.63	4.9	0.0100
carbohydrate metabolic process	GO:0005975	527	17	6.28	2.71	0.0100
lipid metabolic process	GO:0006629	881	23	10.5	2.19	0.0100
oxoacid metabolic process	GO:0043436	667	20	7.95	2.52	0.0100
organic acid metabolic process	GO:0006082	680	20	8.1	2.47	0.0100
Molecular function						
kinase activity	GO:0016301	736	21	9.07	2.32	0.0219
transferase activity	GO:0016740	1574	34	19.4	1.75	0.0328
transferase activity. transferring phosphorus-containing groups	GO:0016772	857	21	10.56	1.99	0.0511
cofactor binding	GO:0048037	244	9	3.01	2.99	0.0602
Cellular component						
mitochondrion	GO:0005739	1480	37	17.7	2.09	0.0009
mitochondrial envelope	GO:0005740	446	17	5.34	3.19	0.0010
mitochondrial membrane	GO:0031966	424	16	5.07	3.15	0.0013
organelle inner membrane	GO:0019866	330	13	3.95	3.29	0.0036
mitochondrial part	GO:0044429	548	17	6.56	2.59	0.0043
mitochondrial inner membrane	GO:0005743	312	12	3.73	3.22	0.0047
organelle envelope	GO:0031967	671	18	8.03	2.24	0.0122
envelope	GO:0031975	683	18	8.17	2.2	0.0133
mitochondrial outer membrane	GO:0005741	111	6	1.33	4.52	0.0174
organelle outer membrane	GO:0031968	125	6	1.5	4.01	0.0277

ABBREVIATIONS

DS, Down Syndrome; TS21, Trisomy of chromosome 21; ROS, reactive oxygen species; cAMP, cyclic Adenosine Monophosphate; *PKA*, Protein Kinase A; HFF, human fetal fibroblasts; *PGC-1α/PPARGC1A*, peroxisome proliferator-activated receptor gamma coactivator 1-alpha; *NRF1*, Nuclear respiratory factor 1; *ERRα*, Estrogen-related receptor alpha; *PPAR*, peroxisome proliferator-activated receptor; *YY1*, Yin Yang 1; NEMGs, Nuclear encoded mitochondrial genes; *NRIP1/RIP140*, Nuclear receptor interacting protein 1/Receptor interacting protein 140; Hsa21, Homo sapiens chromosome 21; DS-HFFs, Down syndrome-human fetal fibroblasts; *DYRK1A*, dual specificity tyrosine-phosphorylation-regulated kinase 1; *DSCR1/RCAN1*, down syndrome critical region 1/regulator of calcineurin 1; *NFAT*, nuclear factor of activated T-cells; *APP*, amyloid beta (A4) precursor protein; *GABPA/NRF2*, GA-binding protein alpha chain/Nuclear respiratory factor 2; GEO, Gene Expression Omnibus; GO, Gene Ontology; qRT-PCR, quantitative Real-Time PCR; siRNA, short interfering RNA; *COX5A*, Cytochrome c oxidase subunit Va; *NDUFA1*, NADH dehydrogenase (ubiquinone) 1 alpha subcomplex; *NDUFS3*, NADH dehydrogenase (ubiquinone) Fe-S protein 3; *ANT1*, adenine nucleotide translocator 1; *ANT2*, adenine nucleotide translocator 2; *ANT3*, adenine nucleotide translocator 3; DCF, dichlorofluorescein; ER, endoplasmic reticulum; IP3, inositol 1,4,5 trisphosphate; IP3R, inositol 1,4,5 trisphosphate receptor; ESCs, embyonic stem cells; *SUMO3,* small ubiquitin-like modifier 3; *GLUT4*, Glucose transporter type 4*; GAPDH,* glyceraldehyde-3-phosphate dehydrogenase; BSA, bovine serum albumin; PBS, Phosphate buffered saline; DCF-DA, dichlorofluorescein diacetate; LSCM, laser scanning confocal microscopy; H_2O_2, hydrogen peroxide; EDTA, Ethylenediaminetetraacetic acid; TBS, Tris-buffered saline; KRB, Krebs-Ringer buffer; AD, Alzheimer's disease.

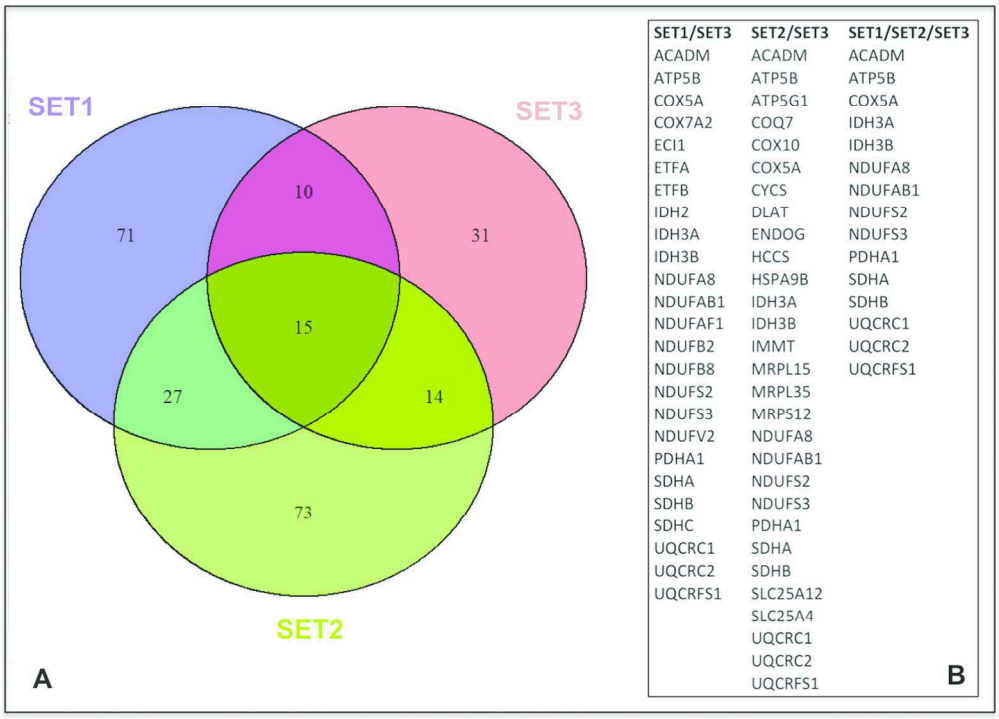

SET1/SET3	SET2/SET3	SET1/SET2/SET3
ACADM	ACADM	ACADM
ATP5B	ATP5B	ATP5B
COX5A	ATP5G1	COX5A
COX7A2	COQ7	IDH3A
ECI1	COX10	IDH3B
ETFA	COX5A	NDUFA8
ETFB	CYCS	NDUFAB1
IDH2	DLAT	NDUFS2
IDH3A	ENDOG	NDUFS3
IDH3B	HCCS	PDHA1
NDUFA8	HSPA9B	SDHA
NDUFAB1	IDH3A	SDHB
NDUFAF1	IDH3B	UQCRC1
NDUFB2	IMMT	UQCRC2
NDUFB8	MRPL15	UQCRFS1
NDUFS2	MRPL35	
NDUFS3	MRPS12	
NDUFV2	NDUFA8	
PDHA1	NDUFAB1	
SDHA	NDUFS2	
SDHB	NDUFS3	
SDHC	PDHA1	
UQCRC1	SDHA	
UQCRC2	SDHB	
UQCRFS1	SLC25A12	
	SLC25A4	
	UQCRC1	
	UQCRC2	
	UQCRFS1	

180x129mm (300 x 300 DPI)

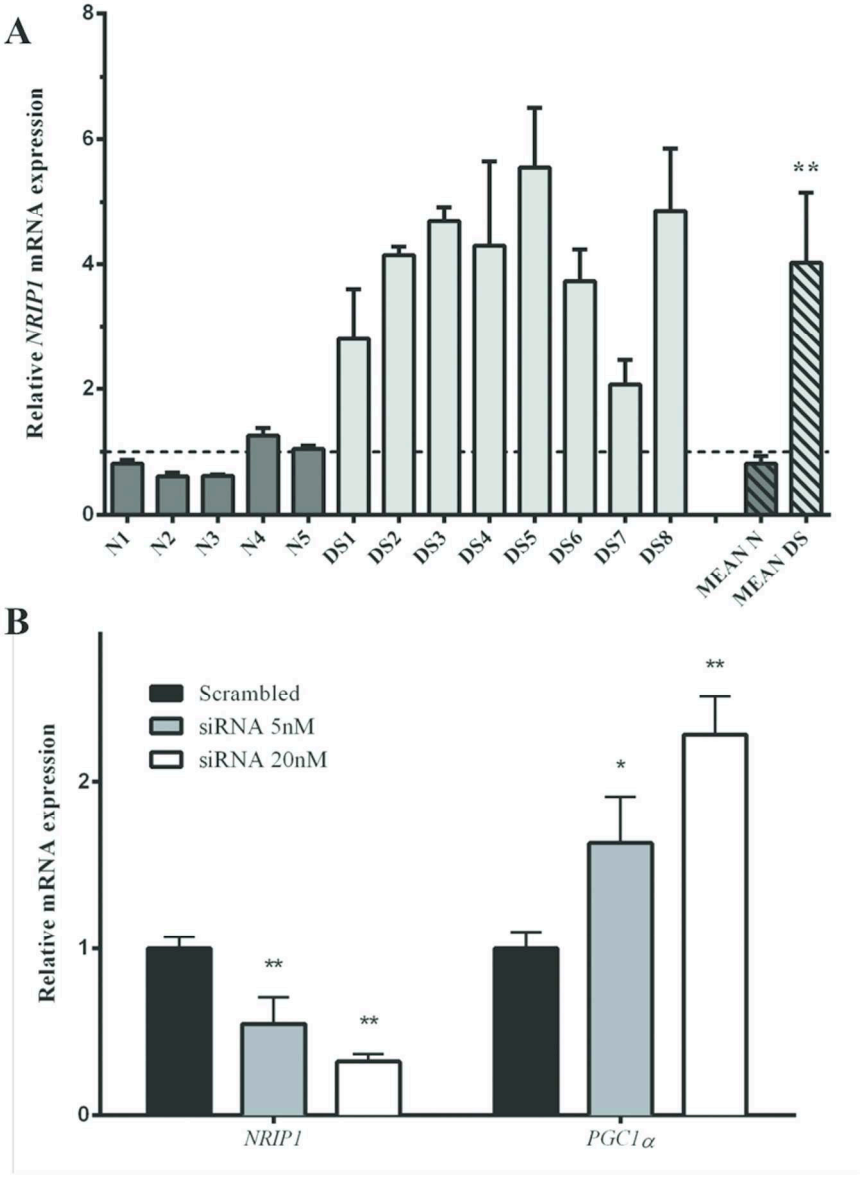

86x118mm (300 x 300 DPI)

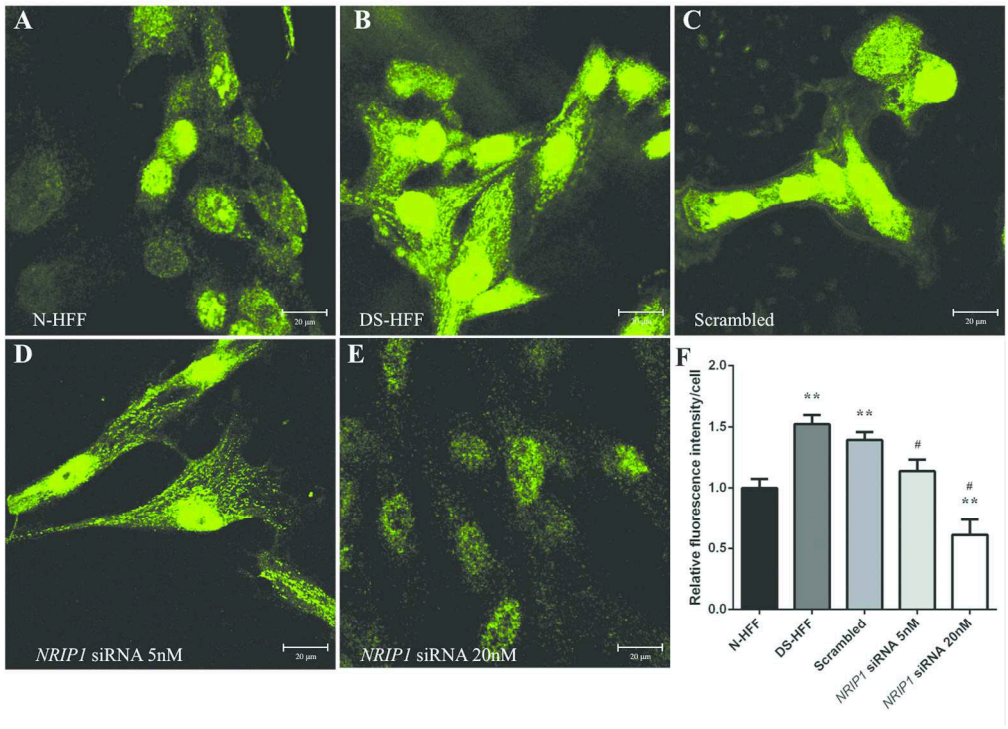

180x131mm (300 x 300 DPI)

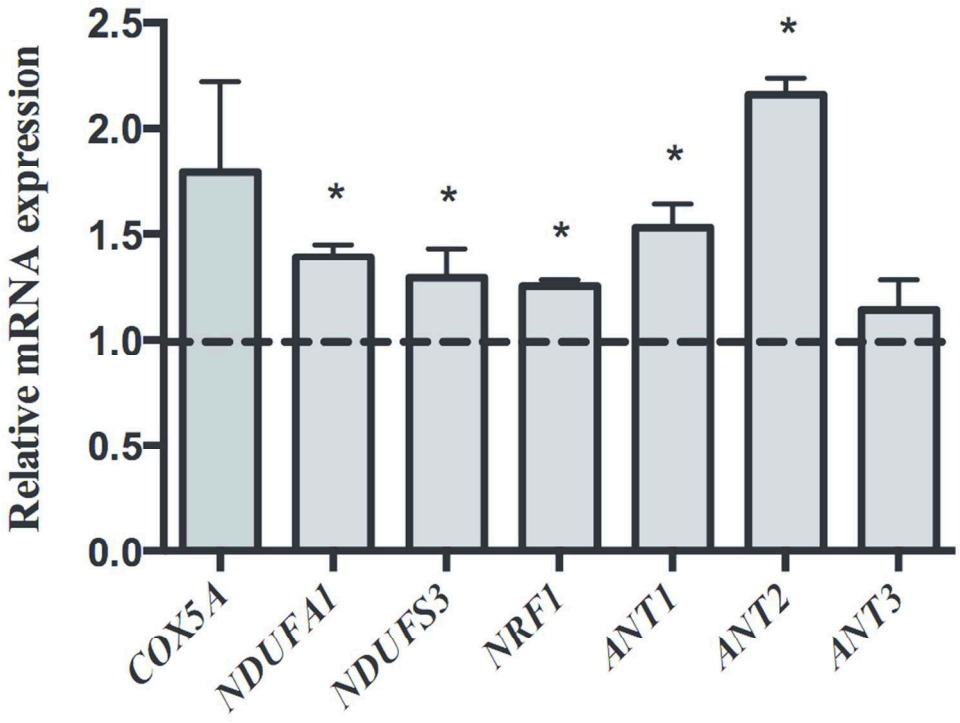

86x65mm (300 x 300 DPI)

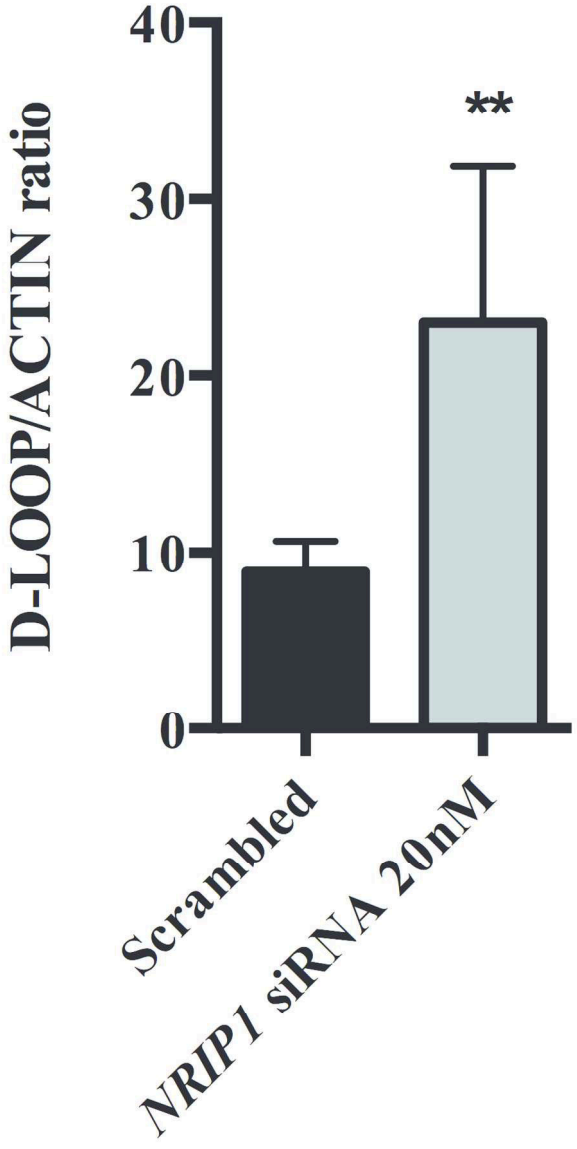

86x164mm (300 x 300 DPI)

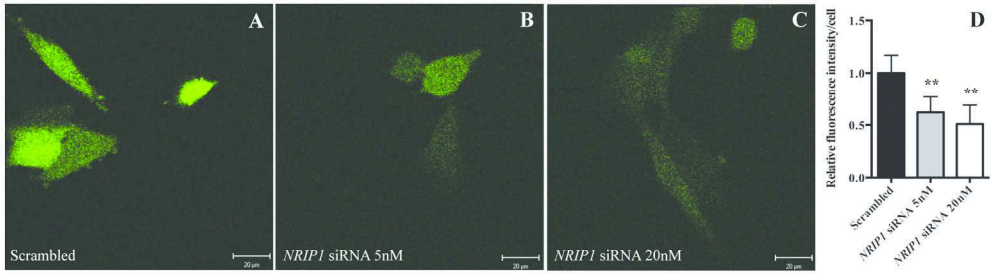

180x49mm (300 x 300 DPI)

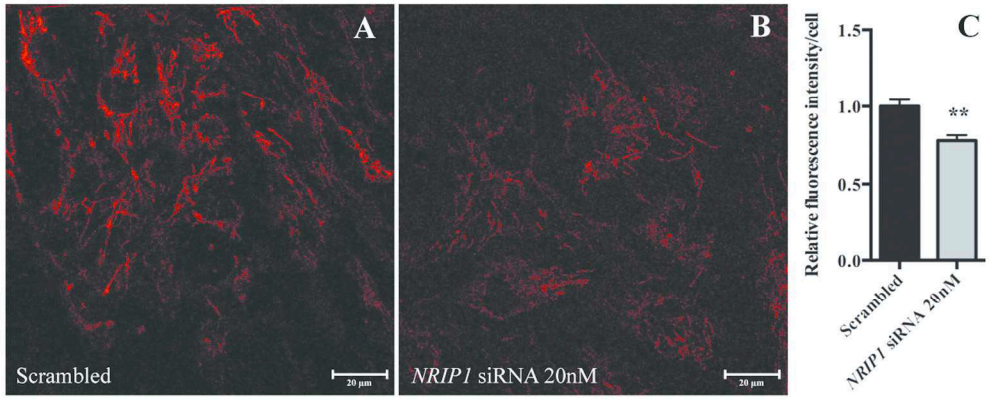

180x71mm (300 x 300 DPI)

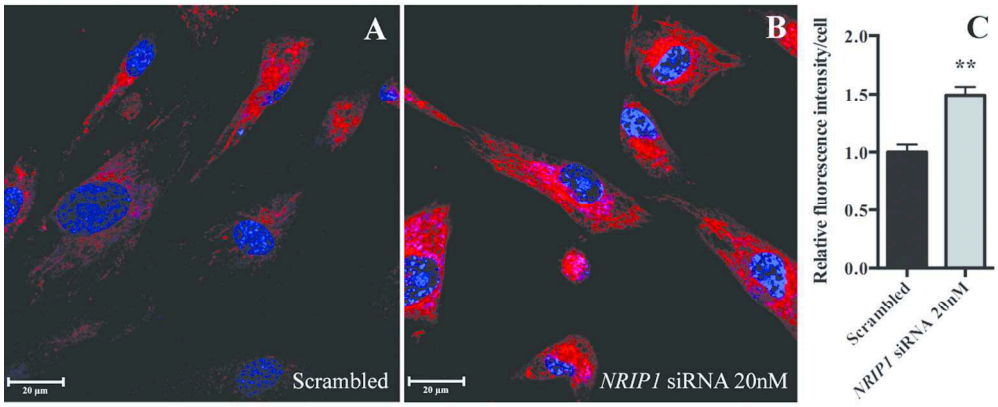

180x73mm (300 x 300 DPI)

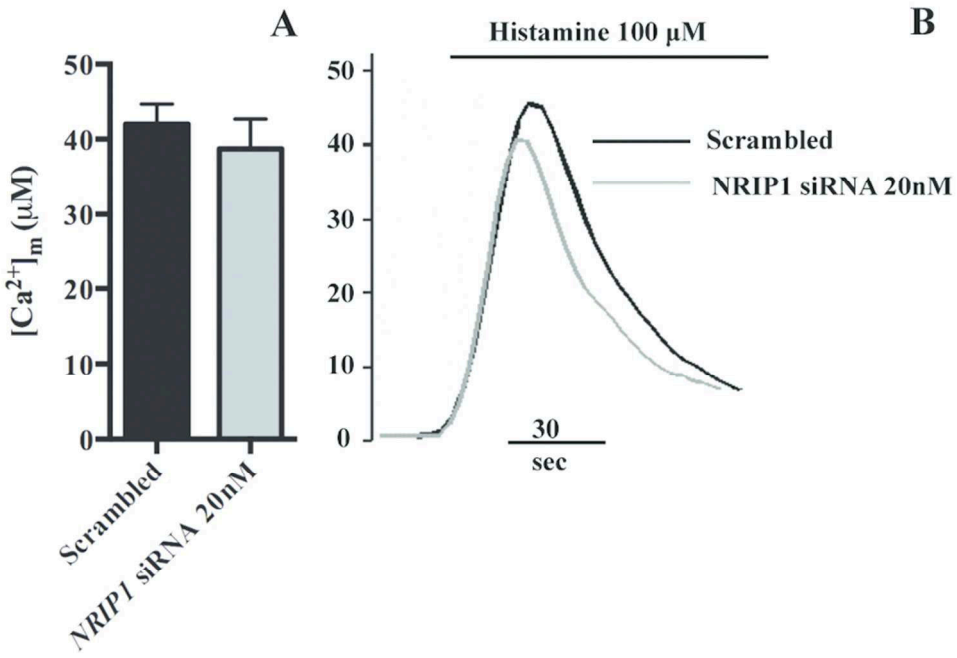

86x58mm (300 x 300 DPI)

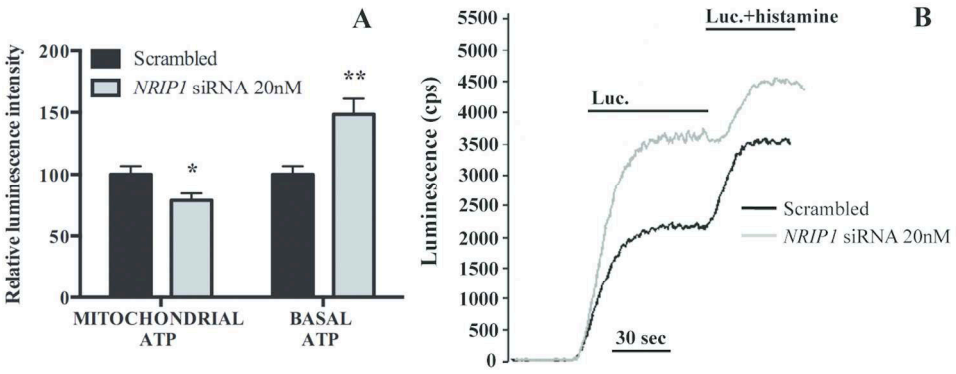

180x69mm (300 x 300 DPI)

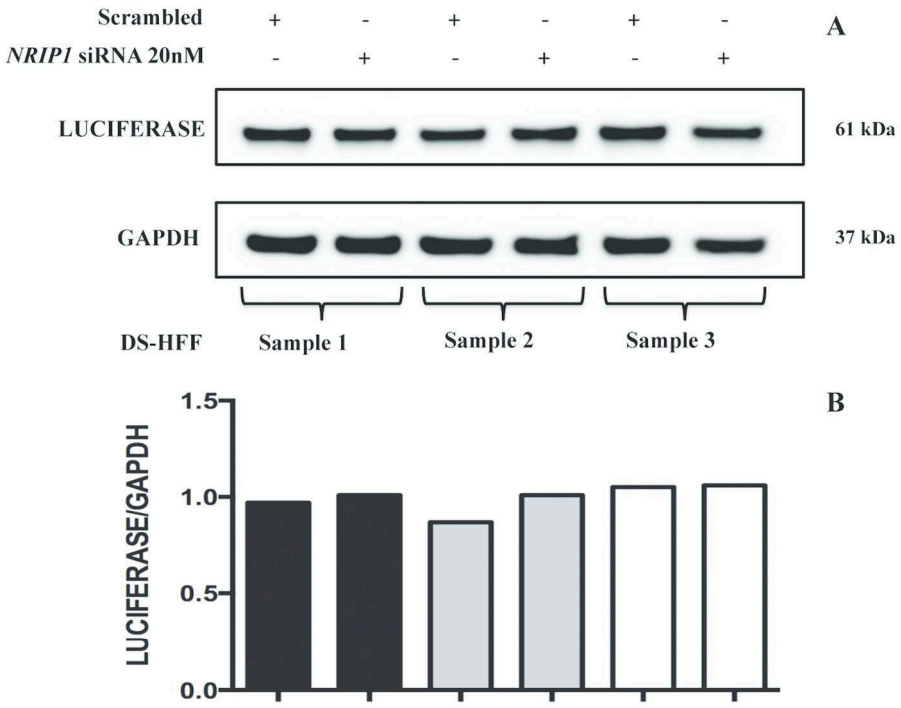

180x135mm (300 x 300 DPI)